CRANFIELD UNIVERSITY

ELEFTHERIOS ANDREADIS

DESIGN OF A LOW SPEED VANEAXIAL FAN

SCHOOL OF ENGINEERING

MPhil THESIS

CRANFIELD UNIVERSITY

SCHOOL OF ENGINEERING
DEPARTMENT OF POWER ENGINEERING AND PROPULSION

MPhil THESIS

ACADEMIC YEAR 2010-11

ELEFTHERIOS ANDREADIS

DESIGN OF A LOW SPEED VANEAXIAL FAN

SUPERVISOR: DR JOAO AMARAL TEIXEIRA

OCTOBER 2011

This thesis is submitted to fulfill the requirements for the degree of Master in Philosophy

ABSTRACT

The ventilation of industrial areas and tunnels is a safety requirement and characterizes the quality of a working environment. Low speed fans are used to achieve the required ventilation level. An attempt to design a low speed vaneaxial fan, meeting the specifications of a given fan that is already in the market takes place in this Thesis. The project was conducted with the support of the Fläkt-Woods Company and the main target is to design a ventilation fan, meeting the requirements for pressure rise, volume flow and size, of an existing model. The efficiency improvement is driven in part by the new national and international legislation concerning the operation of electrical equipment. Companies require higher efficiencies without compromising safety features of the fan and the fan capability to operate at high temperatures.

A low speed fan design procedure is established based on the available literature and design tools. The free vortex approach is employed, which provides acceptable efficiency and relatively simpler design. The design procedure can be used to design a fan given a set of customer requirements. Many software tools are used to design the fan. A Matlab code for the blade design is developed and other codes are used to establish the final fan design. The effectiveness of the design procedure is verified with CFD simulations carried out as part of this project. Three new designs that are developed with the established design procedure are presented in this Thesis. The new designs differ in the hub to tip ratio, the rotational speed and the number of the blades and the vanes. The experience acquired from the analysis of the performance of the first new design is used to improve the performance of the following designs in order to achieve the best efficiency possible. The effect of tip clearance is investigated thoroughly in the new designs because the tip clearance has a major impact on the fan performance and safe operation of the fan at high temperatures. The mechanical integrity of the fan is examined last to verify that the fan can operate in high temperature.

The target of improved efficiency (higher than 79%) is achieved in one of the fan designs attempted and it was calculated 82%. The off design performance of the new fan is satisfactory as well. This new design can be further optimized, since the modification of minor design features is in itself a methodology that can incrementally improve the efficiency of a low speed fan. The new fan can operate at high temperatures (400°C), however the safety factor at this temperature is 1.25 for combined steady mechanical and thermal loading and it can be further improved either through the use of materials with better resistance in thermal loading or with an increased tip clearance.

ACKNOWLEDGEMENTS

I would like to express my gratitude to Dr Joao Amaral Teixeira for his supervision, guidance and assistance throughout the preparation of this study.

I am particularly grateful to Professor Pericles Pilidis for his support during this project.

I would also like to thank Mr Iain Kinghorn, Technical Manager of Fläkt-Woods Company, Colchester, UK for the initiation of this project and for the useful information that he provided.

Last but not least, I would like to thank from my heart my beloved wife Lillian, who inspired and motivated me to successfully complete this MPhil.

LIST OF CONTENTS

LIST OF FIGURES

LIST OF TABLES

SYMBOLS

Air Angle	**α**
Angle Velocity	**ω**
Average Velocity	**W**
Blade Angle	**β**
Blade Height	**h**
Blade Width	**L**
Brake Horsepower	**BHP**
Camber (angle)	**θ**
Chord	**C**
Cross Sectional Area	**A**
Deflection (angle)	**ε**
Density	**ρ**
Deviation (angle)	**δ**
Efficiency	**η**
Enthalpy	**H**
Flow Coefficient	**φ**
Hub Diameter	**d**
Incidence (angle)	**i**
Lift Coefficient	$\mathbf{C_L}$
Mass Flow	**M**
Noise	**N**
Number of Blades/Vanes	**z**
Power Consumption	**PC**
Pressure Coefficient	$\mathbf{C_p}$
Radius	**r**
Relative Velocity	**V**
Rotational Velocity	**U**
Solidity	**σ**
Space	**S**
Stagger angle	**ζ**
Static Pressure	$\mathbf{P_s}$
Static Pressure	**p**
Temperature	**T**
Time	**t**
Tip Diameter	**D**
Total Pressure	$\mathbf{P_t}$
Volume Flow	**Q**
Water Column (pressure unit)	**WC**
Whirl Velocity	$\mathbf{U_w}$
Work Coefficient	**ψ**

1. INTRODUCTION

The role that ventilation fans play in modern societies is well understood by the public at large from the heat removal in personal computers to the large ventilation fans visible in road tunnels. Historically these have been the poor relation of turbomachines, basic in design, cheap to acquire and often with a poor efficiency. However an added environmental consciousness and the passing of national and international legislation are changing this landscape. The use of low efficiency designs is likely to attract penalties in the future and this will shift the way consumers look at the efficiency of ventilation fans and hence the premium they are prepared to pay for efficient machines.

For companies and designer this shift represents commercial opportunities together with technical challenges. Both can be tackled through additional research and the use of new technologies many already in use in the propulsion end of turbomachinery design practice. The drivers for design updating are not only in direct answer to the concerns about efficiency but also due to the fact that in recent years the ventilation of industrial areas and tunnels have become more stringent as safety requirements and the quality of working environments are improved.

There are various types of fans that can meet the requirements for every use. The main categories are the axial flow fans, which are commonly called “fans” and the centrifugal fans which are called “blowers”. The axial flow fans, which are the focus of this project are categorized as propeller fans (a propeller with a motor), tubeaxial fans (a propeller fan with a cylindrical housing) and vaneaxial fans (tubeaxial fans with a vane stage upstream or downstream).

The target of this project is to review and illustrate the procedures that can be employed to design axial flow industrial fans. To this end an existing vaneaxial fan is taken as the datum configuration and a design procedure to obtain an updated design with better efficiency is employed and described. The starting point for the new design is a set of specifications that matches the datum fan features (size, rotational speed) and its performance.

In some respects this work is expected to have a didactic dimension. The author has experience in the performance of turbofan engines but the study of low speed ventilation fans required the adoption of new terminology and the appreciation of factors specific to these machines, from the flow conditions marked by low Reynolds numbers, and thus inherently lossier than

its higher speed counterparts, to the economic realities that determine the design space.

For this reason the reader will find in Chapter 2 of this thesis a thorough explanation of fan terminology along with other aspects of the literature review.

The design of a fan starts from the operational requirements. It is very important for the designer to know the working environment of a fan and the specifications that the customer requires. The dimensions, the motor, the volume flow, the pressure rise are the basic characteristics should be defined at the preliminary stage of the design. In this project these features are defined, because the given fan is a machine employed in the field rather than a theoretical model.

Taking all the above into consideration, the next step is the presentation of the available design procedures which is covered in Chapter 3. There are plenty of examples in the available literature relative to the design procedure of a fan (Bleier 1998, Osborne 1977, McKenzie 1997, Lewis 1996) and an effort was made to implement features for every author in order to achieve the best result possible.

After establishing the design procedure, the design tools are presented in Chapter 4. The tools are used to create the geometry, generate the computational mesh and simulate the cases. A Matlab code was created to contribute to the design procedure. Other codes that were found in the literature were used for the generation of the blade geometry. CFD software is used to assemble the meshes, set and solve the cases and post process the results. Finite element software is used for the investigation of the mechanical integrity of the fan.

In Chapter 5 the investigation of the design procedure takes place using CFD analysis. The concept of the design method investigation using CFD is simple. The blade and geometry features which were the outcome of the selected design procedure are used to create the geometry of the fan for the simulation. After creating the geometry, CFD is used to solve the flow field and acquire the performance of the fan that came from the simulation. The final step is to investigate if the simulated performance of the fan meets the requirements that were used for the preliminary design of the fan.

The main task in this project is the simulation of the performance of the existing fan and for the new design fan, as well. The use of the computational fluid dynamics software is the key point for this stage. In Chapter 6 the simulations that were carried out are presented. The results of design point

calculation and off design cases are analyzed for 3 different design cases. The tip clearance effect is simulated and presented as well.

In Chapter 7 the mechanical integrity of the fan is examined. The effect of the combined thermal and mechanical loads to the impeller is presented. The mechanical integrity is investigated in order to verify that the fan can operate in high temperature conditions.

The conclusions of this project and the recommendations for further work are presented in Chapter 8. Designing a fan only from the customer requirements is a compromise between many factors. The experience acquired from the 3 new designs and the interesting opportunities for further work are then presented.

2. Literature review

2.1 Definitions

The description of the flow in a low speed fan and the various definitions for the flow characteristics represent an essential part of the fan design understanding. The fan design has its own terminology and the clarification of the terms is very important for the researcher. This section is dedicated to the presentation and definition of the terms that characterize the geometry of axial flow fans. A vaneaxial fan is shown in Figure 2.1.

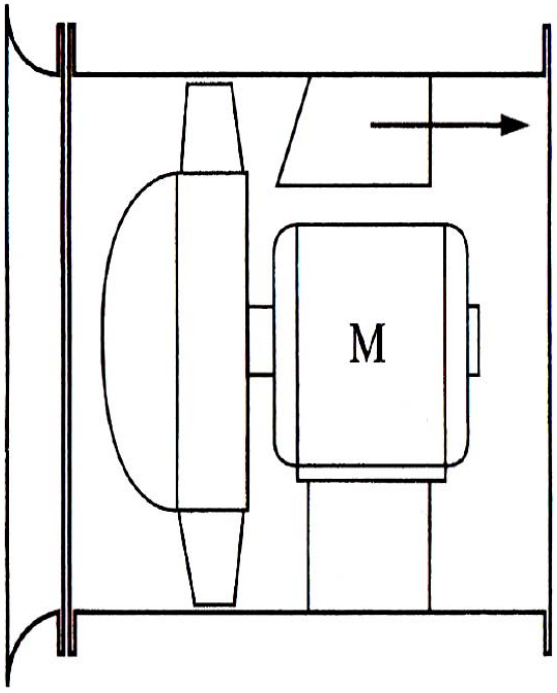

Figure 2.1 Vaneaxial Fan with outlet vanes around the motor and bellmouth inlet (Bleier,1998)

The flow in a fan is always three dimensional, however the understanding of the two dimensional flow in a fan is the first step towards the fan design. The basic terminology applies to the 2D flow, so it is more convenient to present the fan terminology with 2D representations.

The flow in a fan is visualized with 2D velocity triangles which are illustrated in Figure 2.2 and they depict the velocity vectors in a fan stage

(rotor-stator) and the relative velocity angles. From the 2D Figure 2.2 many terms can be defined.

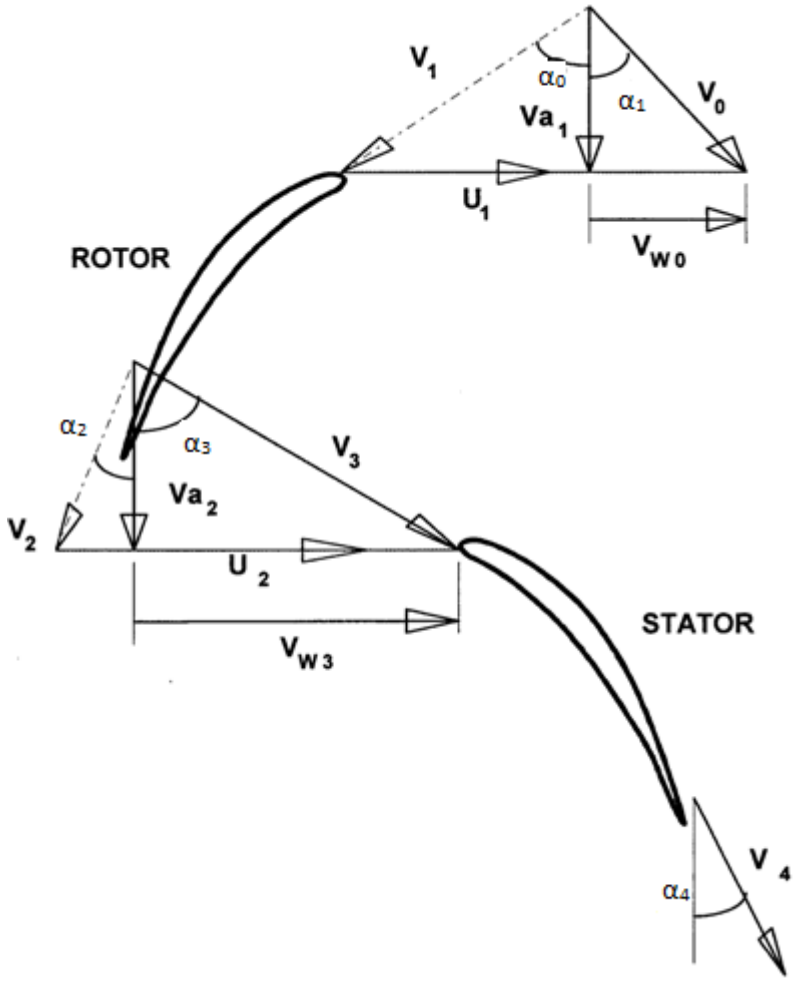

Figure 2.2 Fan stage Velocity triangles (Ramsden, 2008)

The **relative velocity V** is the velocity of the flow which enters the fan rotor with an axial velocity $\mathbf{V_a}$, relative to the moving blade which has a rotational velocity **U**.

The relative velocity at the leading edge of the rotor blade is $\mathbf{V_1}$ and at the trailing edge is $\mathbf{V_2}$. The relative velocity at the trailing edge $\mathbf{V_2}$ is different from $\mathbf{V_1}$ because of the deflection of the flow through the blade passage. The absolute velocity at the exit of the rotor blade is $\mathbf{V_3}$ which it is the vectorial sum of the $\mathbf{V_2}$ and **U** vectors**.** $\mathbf{V_4}$ is the velocity downstream of the stator at the exit of the fan. The relative velocities angles are $\boldsymbol{\alpha_1}$ and $\boldsymbol{\alpha_2}$. The angles $\boldsymbol{\alpha_0}$, $\boldsymbol{\alpha_3}$ and $\boldsymbol{\alpha_4}$ are absolute velocities angles at inlet, downstream of the rotor and downstream of the stator respectively.

The **whirl velocity U_w** or **V_w** is the tangential velocity that is added to flow by the action of the rotor. Together with the axial velocity it defines the rotor exit absolute velocity **V_3**. The whirl velocity **V_w** is a measure of the energy that the rotor blade adds to the flow. Figure 2.3 presents an alternative depiction of the triangles of velocity in an axial fan stage.

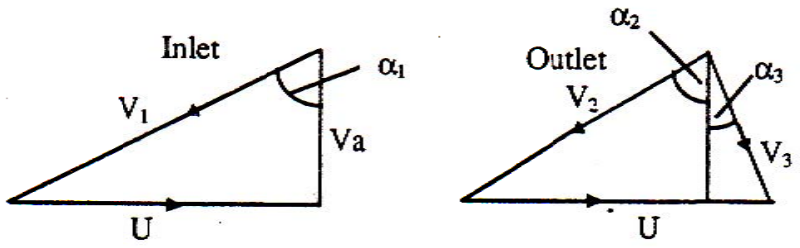

Figure 2.3 Relative Velocities – Angles in a blade (McKenzie,1997)

The **deflection** (Figure 2.4) is the angular difference between the angle of the relative velocity at the outlet of the blade **α_2** and the angle of the relative velocity at the inlet of the blade **α_1**. There is a limit to the amount of deflection that can be achieved by a blade row, which is defined by the V_2/V_1 ratio also called de Haller number. This limit is fixed by the inter blade passage diffusion. The point where the incoming flow meets the blade surface is denoted the stagnation point. The flow accelerates over the suction side of the blade because of the camber of the profile and consequently the static pressure decreases locally. In contrast the flow decelerates in the pressure side and the static pressure increases.

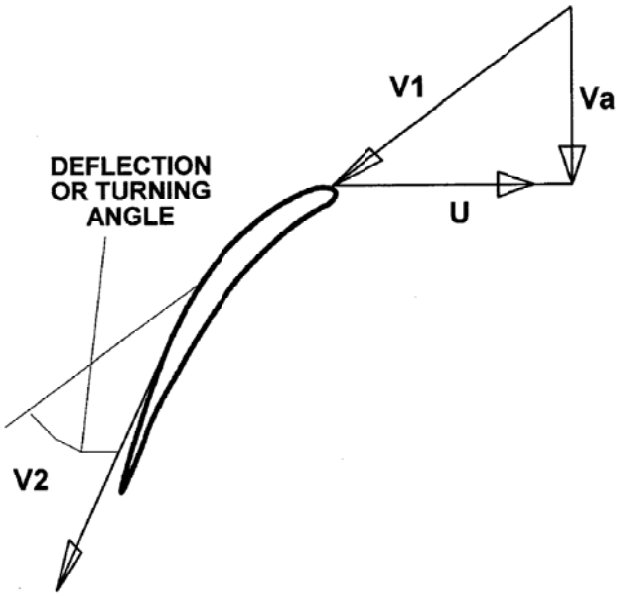

Figure 2.4 Deflection (Ramsden, 2008)

Space or Pitch is the length of the arc between two similar points in two consecutive blades (Figure 2.5).

Chord is the distance between the leading edge with the trailing edge of the blade (Figure 2.5).

The **Space (Pitch) to Chord ratio** (S/C) has a direct effect on the air turning (or deflection) and therefore on the pressure rise. Many authors use the opposite ratio, chord to space (pitch) ratio, which is commonly referred to as solidity. Closely spaced blades have a large degree of overlap and due to the influence of the adjacent blades they have a higher lift and consequently higher deflections can be achieved. On the contrary, sparsely spaced blades will have a low blade overlap and this lack of channeling implies low deflection.

Solidity (σ) is the chord to space (pitch) ratio (C/S).

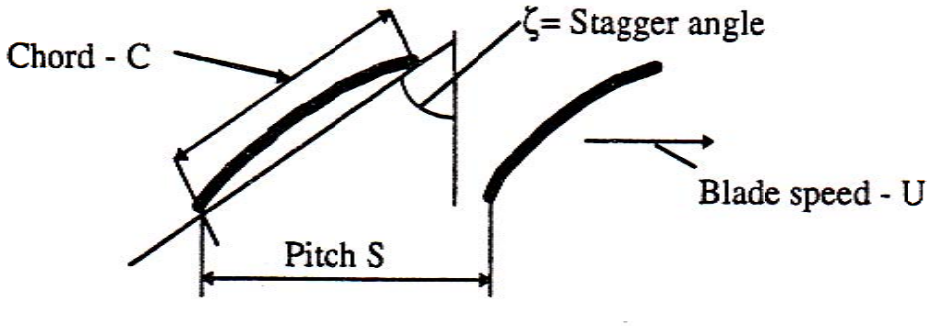

Figure 2.5 Chord, pitch and stagger angle (McKenzie, 1997)

Stagger angle (ζ) is the inclination to the axial direction of the chord, the line joining the leading and trailing edge (Figures 2.5, 2.6).

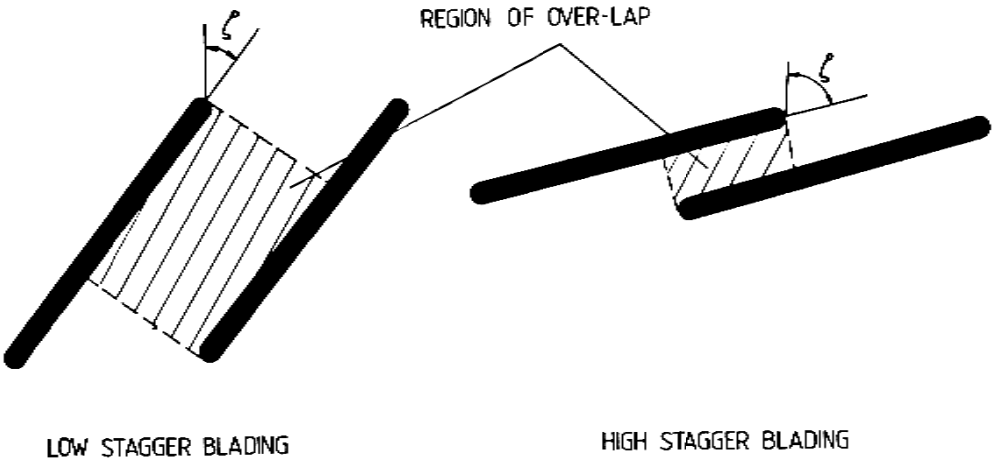

Figure 2.6 Stagger angle (Angoy, 1984)

Figure 2.7 illustrates the cascade performance for various deflection and three space to chord ratios, 0.5, 1.0 and 1.5. The nominal deflection, leftmost figure, is the deflection at 80% of the stalling deflection (maximum attainable deflection). For a given outlet angle the deflection decreases as the pitch to chord ratio increases (Lewis, 1996).

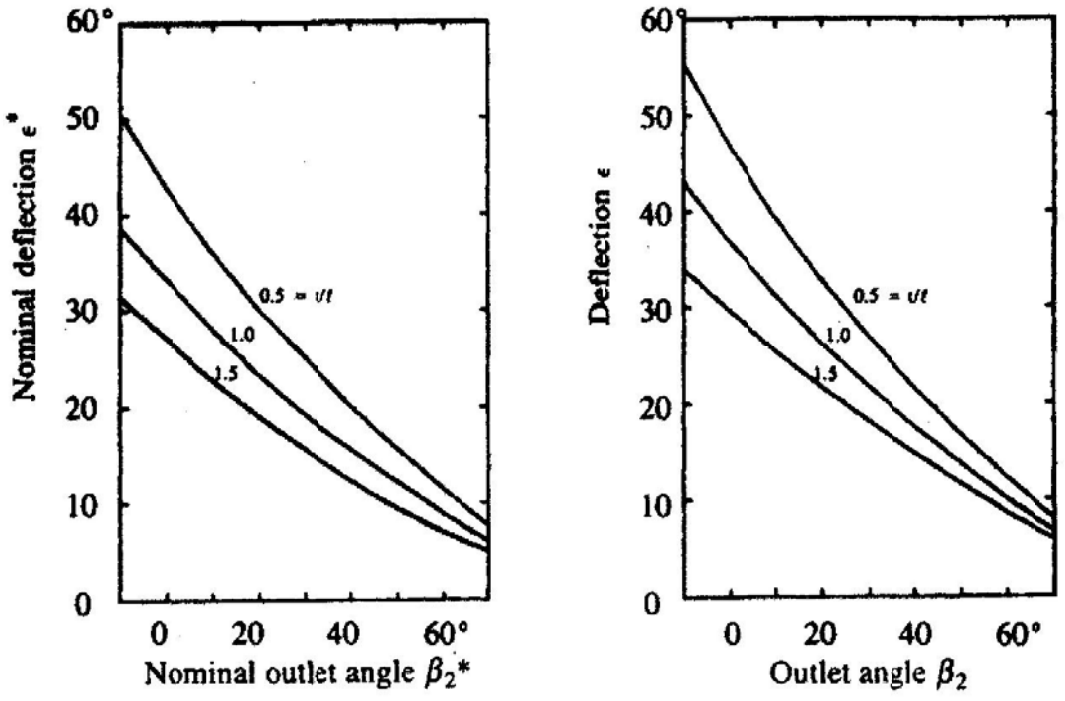

Figure 2.7 Deflection vs Outer angle (Lewis, 1996)

To obtain high pressure ratio, the stagger angle should be as high as possible. [McKenzie 1997, Osbourne 1977, Lewis 1996]. The upper limit on stagger increase is set by the blade overlap considerations. As the stagger angle increases the overlap reduces for a given space to chord ratio and this can reduce the attainable pressure rise. This can be overcome by increasing the chord, but in that case there is also a limit that comes from the diffusion due to the increased restrictions in the flow passage.

High stagger angle blades produce steep fan characteristics, though this is usually undesirable, since small movements in the operating point will produce significant changes in terms of the pressure rise and volume flow. From this point a lower rotor blade stagger, leading to fan characteristics that are flatter , would be desirable.

The outflow angle depends to a fairly small extent on the camber θ, whereas it is the stagger angle ζ which really has a big effect.

Inlet angle β_1 is the angle of the blade at the leading edge and **outlet angle β_2** is the blade angle at the trailing edge (Figure 2.8). The blade angles are related to the air angles through the incidence at the leading edge and with deviation at the trailing edge.

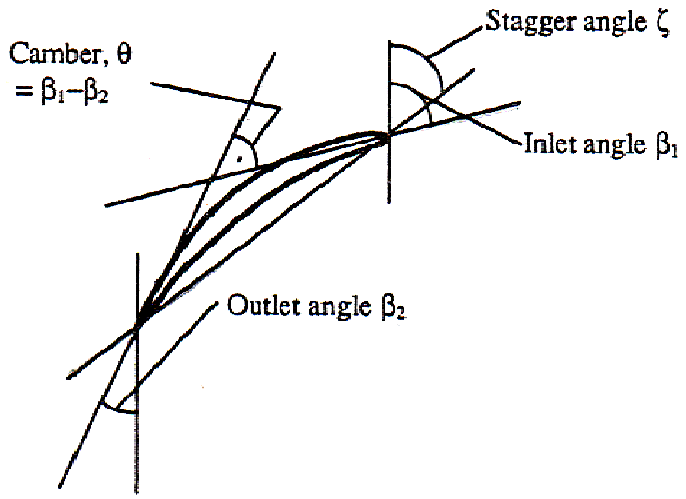

Figure 2.8 Inlet-outlet angles, camber and stagger angle (McKenzie, 1997)

Camber (θ) is the difference between the outer angle β_2 and the inlet angle β_1 and is related to the deflection of the flow (Figure 2.8).

The angle of **Incidence i**, Figure 2.9, is the difference between the inlet relative velocity angle and the blade angle at the leading.

$$i = a_1 - \beta_1 \quad (2.1)$$

The importance of the incidence angle is great, because the smooth distribution of the flow at the pressure and at the suction sides of the blade depend on the incidence

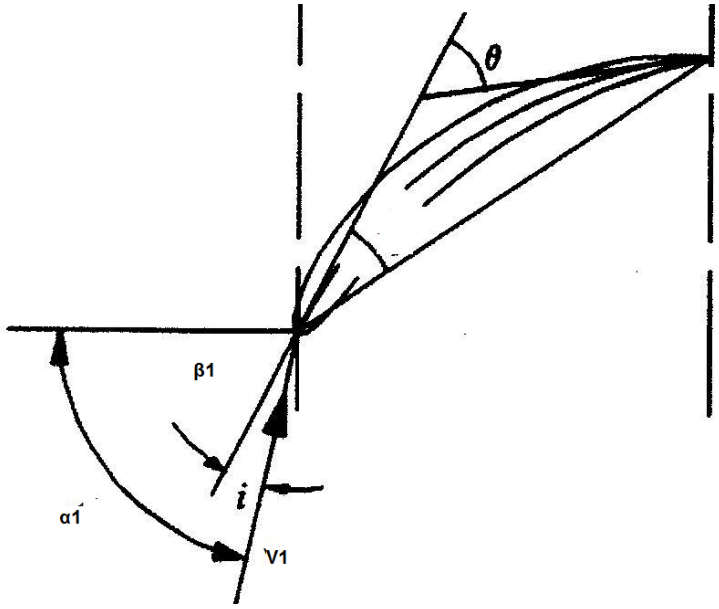

Figure 2.9 Angle of Incidence i (Ramsden, 2008)

The fluid **Deviation δ** is defined as the difference between the outlet flow angle and the angle of the blade metal at outflow, Figure 2.10. Deviation is related to the outlet of the blade in a manner similar to the incidence in relation to the inlet of the blade.$\boldsymbol{\delta = a_2 - \beta_2}$ (2.2)

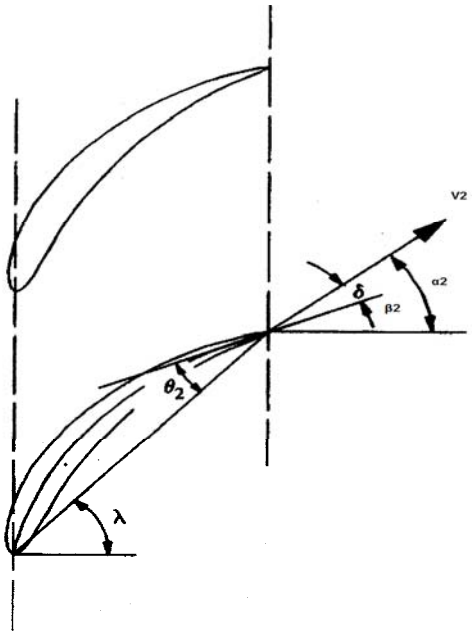

Figure 2.10 Deviation δ (Lewis, 1996)

Aspect ratio is the ratio of the mean blade span to the mean blade chord.

Hub to tip ratio is the ratio of the diameter of the hub to that of the tip of the blade. Because the location of the tip is sometimes ambiguous (the stator tip may be on the hub) this is often referred to as the hub to casing ratio.

The **tip clearance** is the margin between the tip of the blade and the casing (shroud). It has a crucial effect on the blade performance. In blade design the tip clearance is scaled with the blade height, but this doesn't take into account the blade chord.

The **diffusion factor** relates the relative velocity and the whirl velocity with the space to chord ratio and is defined from the following equation

$$D_f = 1 - \frac{V_2}{V_1} + \frac{\Delta U_w}{2 * \sigma * V_1} \quad (2.3)$$

where **σ** is the solidity. The diffusion factor is suggested to be 0.45 to obtain a reasonable blade design. A value higher than 0.6 yields separation and is thereby not recommended. Having established all the velocities, the solidity can be calculated in a straightforward manner (Strohmeyer, 2009).

Efficiency (Osborne, 1977) Fan efficiency is the ratio of the output power to the mechanical input power. The total efficiency is the ratio of the total air power to the measured fan input power and the static efficiency is the static air power to the measured fan input power.

The measured fan input power is defined in every case as the power which is absorbed by the impeller or by the entire fan (to include the losses in bearings, transmission, etc)

Reaction is the ratio of the static pressure rise at the rotor divided by the total stage pressure rise. The reaction distribution usually varies across the radii.

Fan Total pressure is the difference between the total pressures at the Fan Outlet and Inlet (Osborne, 1997)

Fan Static Pressure is the Fan Total Pressure minus the Fan Velocity Pressure. The Fan Static Pressure is not the rise in static pressure across the fan, but it is defined by the Bernoulli equation. (Osborne, 1997)

Fan Velocity Pressure is the velocity pressure corresponding to the average velocity at the fan outlet (found by dividing the volume flow of the air by the area of the fan discharge orifice) (Osborne, 1997)

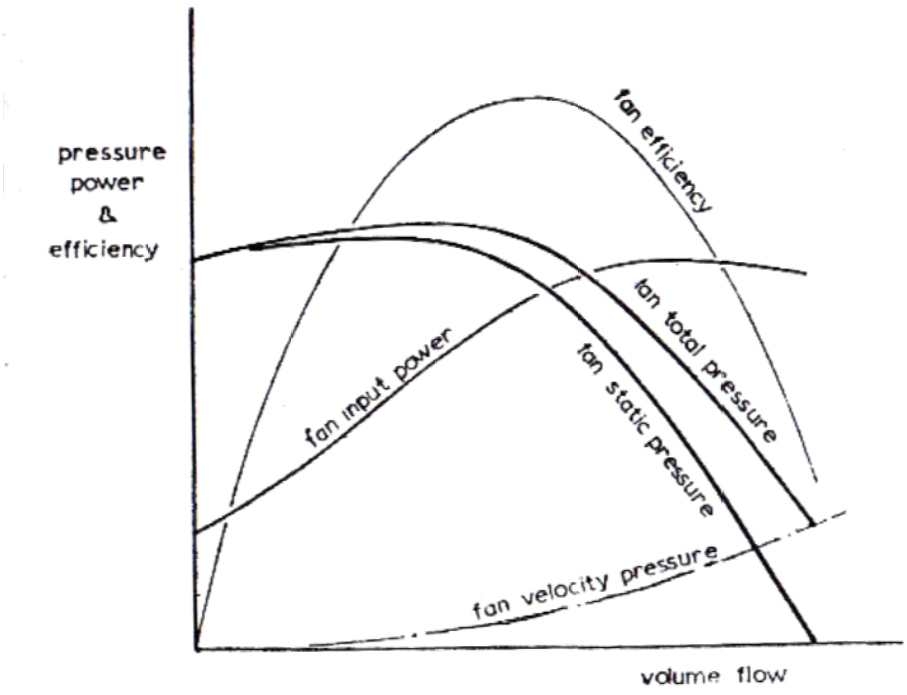

Figure 2.11 Performance characteristics of a fan (Osborne, 1977)

The Total Pressure is the sum of the static pressure and the velocity pressure according to Bernoulli's equation for incompressible flow:

$P_t=P_s+1/2*\rho*V^2$ (2.4)

At zero volume flow the Fan total pressure is equal with the Fan static pressure, because the fan velocity pressure is zero. In contrast when the fan works with open inlet and outlet, the fan total pressure is equal with the fan velocity pressure, because the fan static pressure is zero. As the volume flow decreases the fan total pressure increases and consequently the fan static pressure increases until a peak.

The highest efficiency is not achieved at the highest static pressure point, but in a slight higher volume flow because of the highest rate of increase of the fan input power.

These relationships are shown diagrammatically in Figure 2.11. The maximum efficiency does not occur at the point of highest total pressure, but in a lower total pressure point.

Air power is the result of the pressure rise multiplied by the volume flow. This occurs considering that work is done when a volume of air is moved in a distance l, in a pipe of constant area A and with constant pressure p. The work is then Δp*A*l and the power is (Δp*A*l)/t. The product (A*l)/t is the volume flow Q so the air power is Δp*Q.

The air power can be total or static, depending on the kind of pressure that is used in the above equation.

2.2. Fan Laws

The main quantities that characterize the performance of a fan are the volume flow, the pressure rise and the power consumption.

The performance of a fan that operates in a specific condition is governed by a set of variables. These can be employed to describe the performance of a related fan design operating in another condition, using the so called fan laws. The fan laws are derived from the consideration of dimensional analysis relationships. The variables used in the fan laws can be the size, the rotational speed and the density of the gas. So, by applying the fan laws the volume flow Q, the static pressure rise SP and the power consumption in two different fans can be related with the variables that govern the two fans.

In case there is a requirement for converting the performance of a fan to a different rotational speed the following laws are applicable (Figure 2.12). The dashed lines depict the performance of a 1750rpm fan and the normal lines the performance of a 2625 rpm fan.

The Volume Flow is proportional to the fan speed (2.5) and the Static Pressure is proportional to the square of the fan speed (2.6)

$$\frac{Q_2}{Q_1} \propto \frac{rpm_2}{rpm_1} \quad (2.5) \qquad \frac{P_{s2}}{P_{s1}} \propto \left(\frac{rpm_2}{rpm_1}\right)^2 \quad (2.6)$$

Total Pressure and velocity pressure also vary as the square of the fan speed

The Power consumption PC is proportional to the cube of the fan speed (2.7) and the noise N varies according to formula (2.8)

$$\frac{PC_2}{PC_1} \propto \left(\frac{rpm_2}{rpm_1}\right)^3 \quad (2.7) \qquad N_2 - N_1 \propto 50 * \log_{10}\frac{rpm_2}{rpm_1} \quad (2.8)$$

The efficiency remains the same and has the same trend for different volume flow range. This trend was expected because the power consumption and Static Pressure are vary both proportionally with the square of rotational

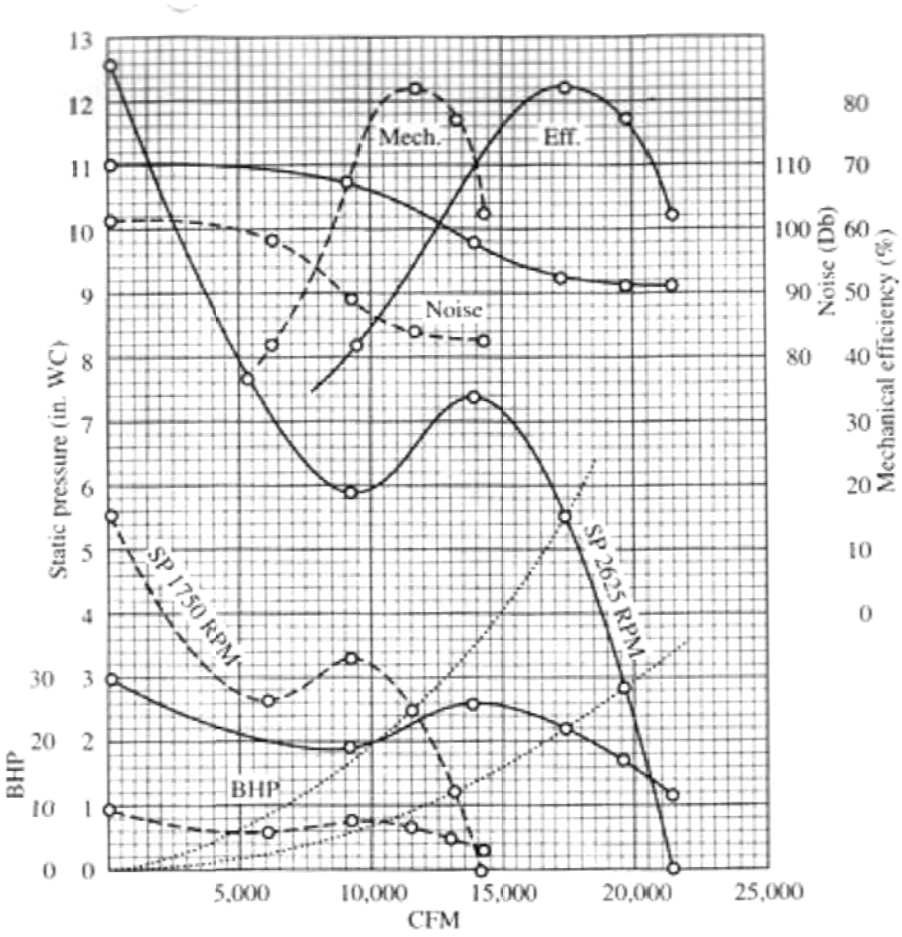

Figure 2.12 Same Fans with different rotational speeds (Bleier,1998)

The second case is the variation of the fan size. The size of the fan is defined by the tip diameter D. The fan laws are applicable in this case assuming the geometric proportionality of the fans (same number of blades, same other size ratios, same blade angles). The effect of fan size on the performance of the fan is illustrated in Figure 2.13. The dashed lines depict the performance of a 1750rpm fan and the normal lines the performance of a 2625 rpm fan. The dashed lines depict the performance of a 27in fan and the normal lines the performance of a 40.5in fan.

The Volume Flow is proportional to cube of the size

$$\frac{Q_2}{Q_1} \propto \left(\frac{D_2}{D_1}\right)^3 \quad (2.9)$$

The Static Pressure is proportional to the square of the fan speed (2.10) and the Power consumption is proportional to the fifth power of the fan speed (2.11)

$$\frac{P_{s2}}{P_{s1}} \propto \left(\frac{D_2}{D_1}\right)^2 \quad (2.10) \qquad \frac{PC_2}{PC_1} \propto \left(\frac{D_2}{D_1}\right)^5 \quad (2.11)$$

The noise varies according to the following formula

$$N_2 - N_1 \propto 50 * \log_{10}\frac{D_2}{D_1} \quad (2.12)$$

The efficiency remains almost the same. There is a minor increase (<1%) for large fans (Bleier, 1998)

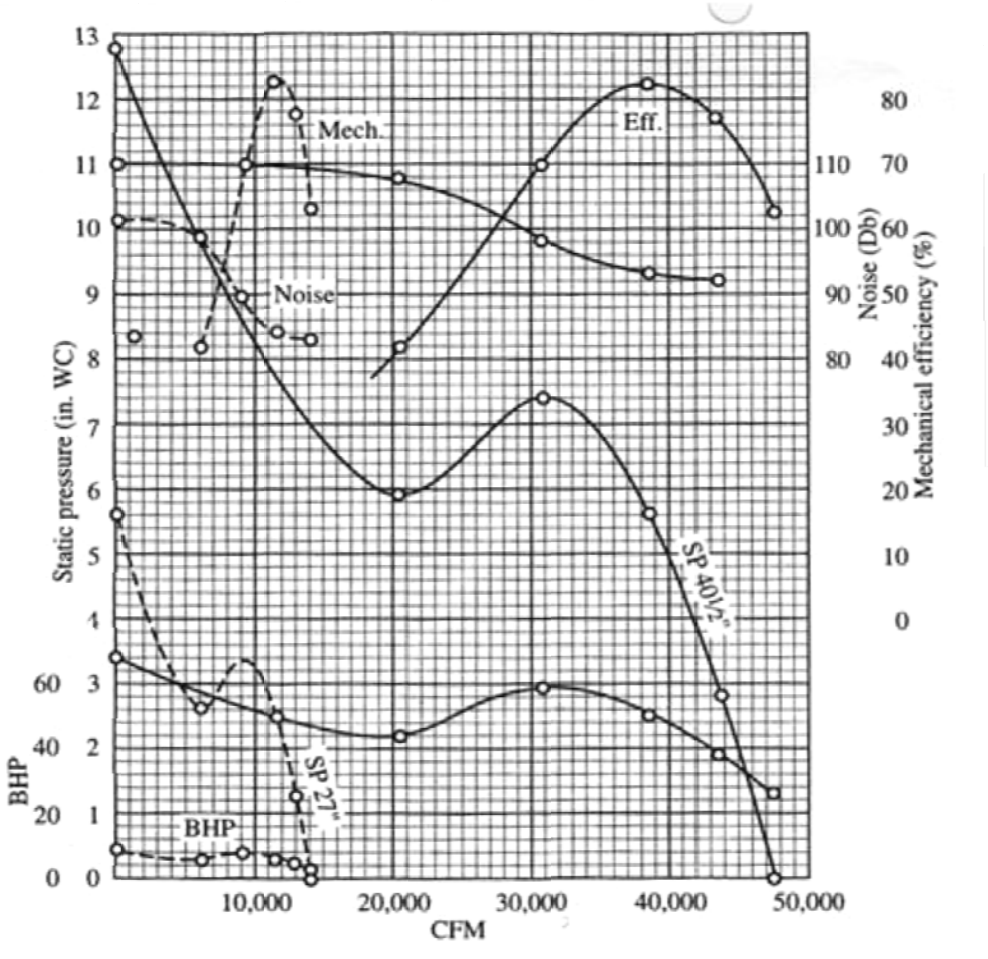

Figure 2.13 Similar Fans with different sizes (tip diameters 27'' and 40.5'') (Bleier)

The efficiency curve and the static pressure curve in the smaller fan are more steep, so the range of operation is smaller than in the large fan. This is due to the fact that in a smaller fan the maximum volume flow is about 4

times lower than the maximum volume flow in a larger fan, while the static pressure rise is about 2.5 times lower.

The power consumption increase in the large fan is much higher than the static pressure rise increase, because the larger fan has to move quadruple volume of air and achieve 2.5 times more static pressure. The power consumption is proportional to the product of the static pressure rise and the volume.

The third variable that affects the fan performance is the air or gas density. The fan may operate in various altitudes or the working fluid may have different density than air.

In this case the Volume Flow will remain the same: $\frac{Q_2}{Q_1} = 1$ (2.13)

Static pressure will vary directly as the density ρ: $\frac{P_{s2}}{P_{s1}} \propto \frac{\rho_2}{\rho_1}$ (2.14)

Power consumption will vary directly as the density ρ:$\frac{PC_2}{PC_1} \propto \frac{\rho_2}{\rho_1}$ (2.15)

It is interesting to investigate the effect in the performance in a case where two variables change at the same time as illustrated in Figure 2.14. The above mentioned set of rules can then be combined to give the predicted performance. In the case of the simultaneous change of rotational speed and size the fan laws application has the following results:

$$\frac{Q_2}{Q_1} \propto \left(\frac{D_2}{D_1}\right)^3 * \frac{rpm_2}{rpm_1} \quad (2.16)$$

$$\frac{P_{s2}}{P_{s1}} \propto \left(\frac{D_2}{D_1}\right)^2 * \left(\frac{rpm_2}{rpm_1}\right)^2 \quad (2.17)$$

$$\frac{PC_2}{PC_1} \propto \left(\frac{D_2}{D_1}\right)^5 * \left(\frac{rpm_2}{rpm_1}\right)^3 \quad (2.18)$$

The following table refers to an example where there is variation of size and rotational speed with reciprocal ratios

$$\frac{D_1}{D_2} \propto \frac{rpm_2}{rpm_1} \quad (2.19)$$

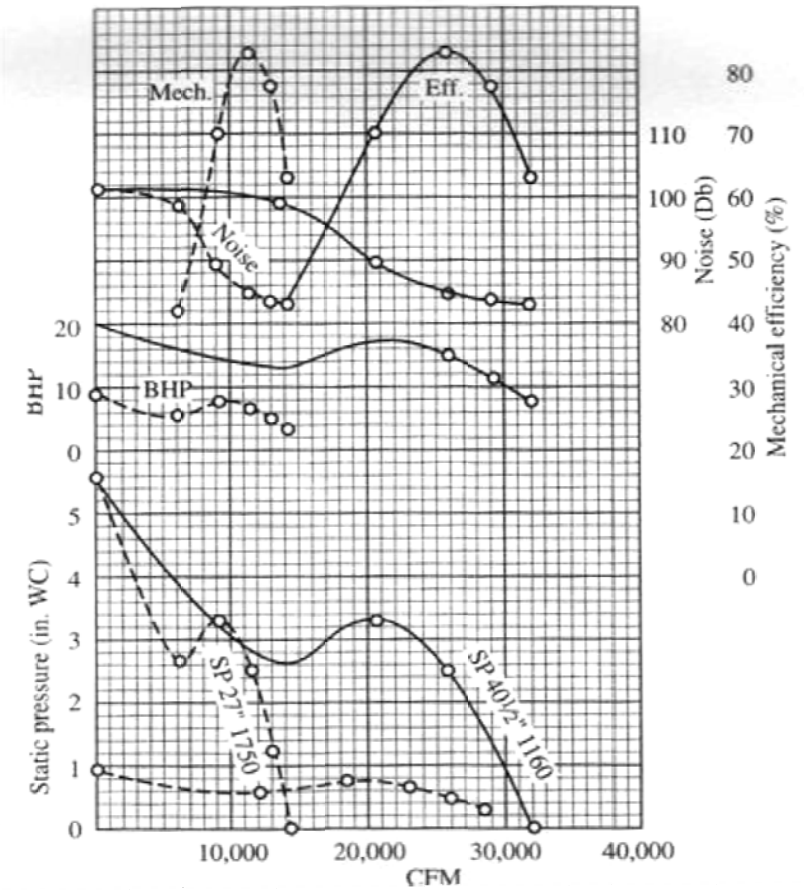

Figure 2.14 Similar Fans with different tip diameters and rotational speed (Bleier,1998)

The important observation in Figure 2.14 is that the static pressure remains the same and the efficiency as well. So by increasing the size and by decreasing the rotational speed by the same percentage the volume flow rises more than the static pressure which remains the same and this results in a flatter pressure curve. On the other hand the efficiency and the noise level remain almost the same.

Other things that can be noticed are as follows

a. The larger fan has flatter static pressure curve because the the conversion factor for the static pressure is smaller than the one of the volume flow

b. The efficiency curve in the larger fan is flatter as well

2.3 Flow Coefficient Φ and Work Coefficient Ψ

There are numerous fans in the market and the assessment or the comparison of their performance is difficult when the common performance

variables (size, static pressure, rotational speed) are used. The initial design of a fan also requires a data base where the performance of a number of fans can be meaningfully compared. If, for example, the performance of two fans regarding the static pressure and the volume flow has to be compared, the performance has to be converted to take into account the relative sizes and the rotational speeds of the two fans.

For this reason dimensionless coefficients can be employed. For the fans design, the main dimensionless coefficients are the flow coefficient φ and the work coefficient ψ. These coefficients are derived from the air volume and the pressure rise at the point of maximum efficiency and with standard working fluid (standard density) at the mid span.

The Flow or Volume Coefficient φ relates the volume flow Q with the size of the fan D and with the rotational speed U. Through this coefficient the capacity of the fan to move the air can be categorized. The definition of the Flow Coefficient φ is (Osborne 1977, Bleier 1998, Eck 1973):

$$\varphi = \frac{Q}{\left(\pi * \frac{D^2}{4}\right) * U^2} \quad (2.20)$$

Where Q is the volume flow, D the outer diameter, U=ω*r

Another definition for φ which is also more convenient is the following

$$\varphi^* = \frac{V_a}{U} \quad (2.21)$$

With some manipulation it follows that $\varphi^* = \frac{\varphi}{1-\nu^2}$ (2.22)

Where $\nu = \frac{d}{D}$ which is the hub to tip ratio

The quantity φ* is denoted as φ by some authors (McKenzie 1997, Ramsden 2008, Lewis 1996). The coefficient φ gives the order of magnitude of the size of the fan.

The Work or Pressure Coefficient ψ relates the pressure rise in the fan with the dynamic pressure of the peripheral velocity. The magnitude of this coefficient typifies the pressure rise capability of the fan. The definition for ψ for incompressible flow is

$$\psi = \frac{\Delta P}{\frac{1}{2} * \rho * U^2} \quad (2.23)$$

where ρ is the density

The ΔP may be the total pressure rise or most commonly the static pressure rise and this is the useful ΔP and not the design ΔP (Osborne, 1977).

Figures 2.15 and 2.16 illustrate actual values of φ and ψ from fans that are found in the market. These values can be the starting point for a new fan design.

Design source	ν	ϕ	ψ	η	
A1	0·33	0·198	0·044	78%	upstream guide vanes
A2	0·33	0·180	0·086	79%	
A3	0·47	0·230	0·16	84%	
A4	0·7	0·365	0·50	77%	
B	0·5	0·25	0·30	85%	
C1	0·45	0·277	0·38	86%	downstream guide vanes
C2	0·5	0·268	0·52	85%	
D1	0·5	0·244	0·155	78%	no guide vanes
D2	0·25	0·17	0·11	84%	
E	0·55	0·145	0·25	86%	downstream guide vanes
F	0·55	0·225	0·24	79%	
G	0·50	0·203	0·49	75%	contra-rotating

Figure 2.15 Values for φ and ψ from actual fans (Osborne, 1977)

The work coefficient for high speed cases thus for compressible flows is defined as the Stagnation Enthalpy rise over the rotational speed squared (Lewis 1996, McKenzie 1977)

$$\psi = \frac{\Delta H}{U^2} \quad (2.24)$$

Example no.	Type of fan	Hub-tip ratio	Blade width (in)	Flow coefficient ϕ	Pressure coefficient ψ
1a	VAF	0.52		0.243	0.195
1b	VAF	0.68		0.256	0.316
1c	Axial-centrifugal			0.200	0.520
2a	FC centrifugal			0.742	1.99
2b	FC centrifugal			0.742	2.00
2c	BI centrifugal			0.186	0.984
2d	RT centrifugal			0.217	1.211
3a	VAF	0.62		0.374	0.274
3b	Axial-centrifugal			0.222	0.644
3c	Airfoil centrifugal			0.222	0.792
4a	FC centrifugal			0.690	1.95
4b	Cross-flow		11	0.381	1.50

Figure 2.16 Values for φ and ψ from actual fans (Bleier, 1998)

It is interesting to investigate how the efficiency is related with the dimensionless coefficients φ, ψ and for this particular case there are available what are known as Smith charts (Lewis, 1996). In these charts, another dimensionless coefficient is incorporated, the de Haller number which as seen is defined as the ratio of the outlet relative velocity to the inlet relative velocity

$$dH = V_2/V_1 \quad (2.25)$$

The de Haller number is a measure of the diffusion of the blade passage and it must be higher than 0.7 in order to avoid large separation losses (Ramsden, 2008)

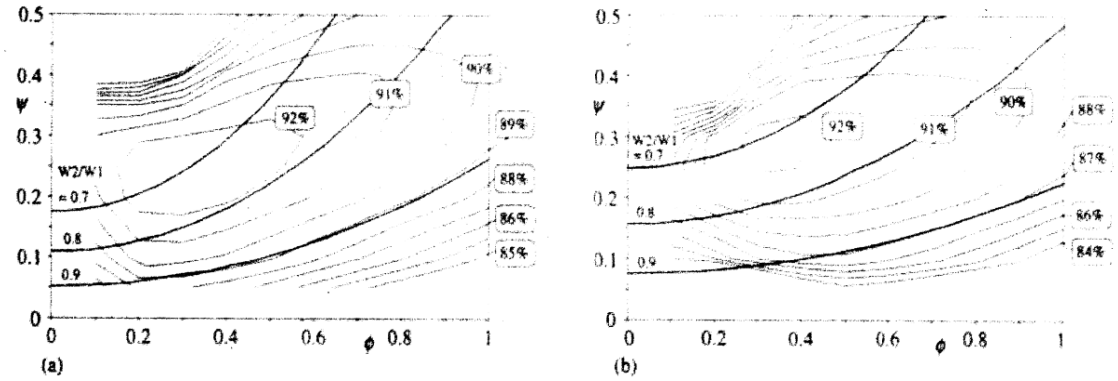

Figure 2.17 Smith Charts for (a) 50% reaction (b) 70% reaction stage (Lewis, 1996)

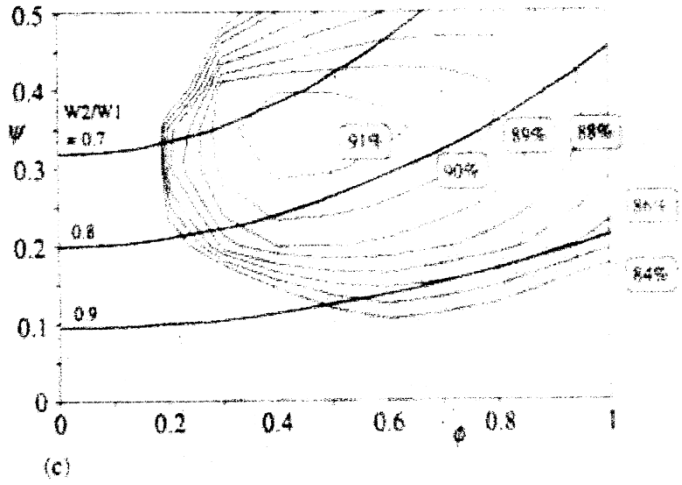

Figure 2.18 Smith Charts for a 90% reaction stage (Lewis, 1996)

Smith charts are illustrated in Figure 2.17 and Figure 2.18. Every point in the charts represents the maximum efficiency that can be achieved for a pair of φ and ψ, taking also into account the de Haller number.

The object of this study is a vaneaxial fan, which is a fan stage where the stators are placed downstream of the rotor. After reviewing the literature the main conclusion regarding the range of the φ and ψ parameters for this particular vaneaxial machine is the following:

Flow coefficient φ: 0.2-0.3

Work coefficient ψ: 0.2-0.4

Other important conclusions concerning the effect of the dimensionless coefficients to the fan design, according to (Eck, 1973), are:

a. When the product φ*ψ is maximum the fan has the maximum capacity with minimum size, which gives the cheapest design
b. The maximum value of ψ gives the minimum noise generation
c. The higher the φ the larger the capacity of the fan - The higher the ψ the higher the pressure rise

2.4 Axial Flow Fans

An axial fan may be defined as a fan where the flow of the air is basically parallel to the axis of the rotor throughout its transit through the machine. The main difference between a fan and a compressor is that the purpose of a fan is to move air while the purpose of a compressor is the

increase of pressure. The role of low pressure axial fans therefore is the moving of large volumes of air at a relatively low speed and with a modest pressure rise.

These machines find great applicability over a wide range of engineering applications. Mechanical ventilation uses fans so that control over air movement is obtained and the environmental conditions in a given space are not subjected to the uncertainties of the natural ventilation systems. In many applications it is essential to control the contamination such as in industrial environments or tunnels as illustrated in Figure 2.19.

Figure 2.19 Tunnel Ventilation (www.roadtraffic-technology.com)

Another application of axial flow fans is thermal management and an example for this is the cooling of electronic components, Figure 2.20. This is one of the main concerns for the achievement of the higher packaging densities which are required by the general trend of microminiaturization.

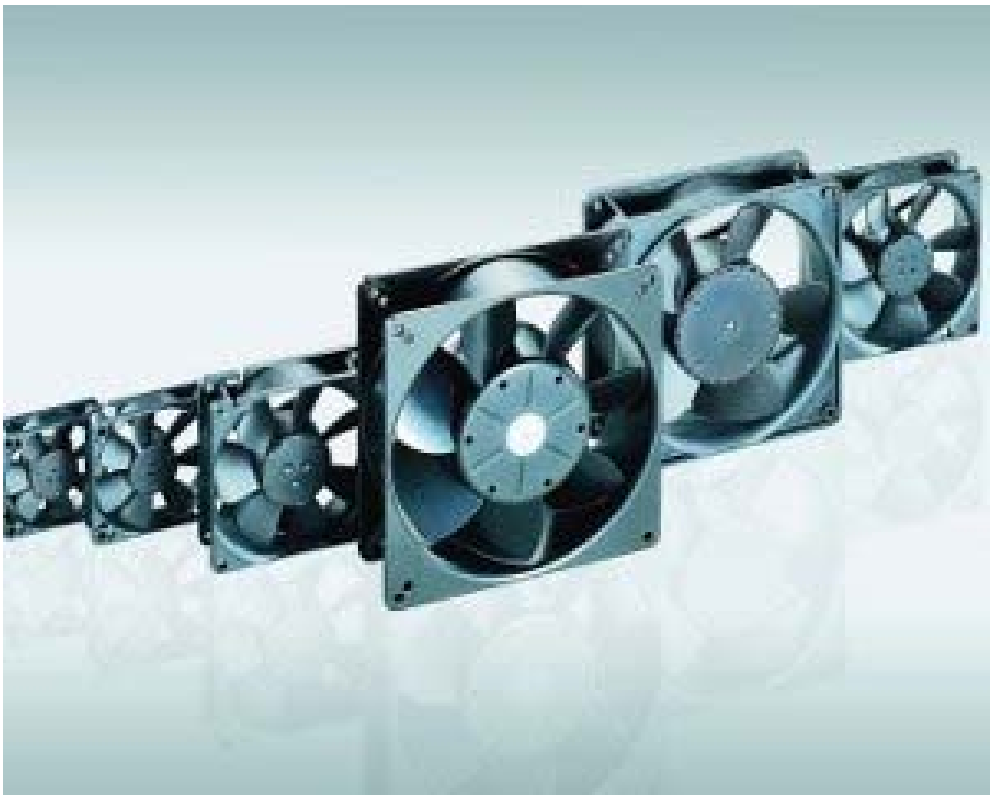

Figure 2.20 Electronics cooling fans (www.qmed.com)

A fan is a machine used to produce a continuous flow of air by aerodynamic action. Fan engineering requires a good knowledge of fan types (centrifugal, axial, and mixed) together with the theory of their operation and design, and of the fan laws, fan testing, fan systems, fan mechanics (materials strength) and fan selection.

The selection of a fan for air-conditioning or ventilation applications involves choosing the most inexpensive combination of size, arrangement and type while providing stable operation. The main advantages of axial flow fans are their high efficiency, compactness and simplicity of installation. However, the pressure development along an axial fan is considerably lower than a centrifugal fan for a given impeller diameter.

The fan selection for a particular application is usually concerned with its characteristic curve which defines a relation between pressure and volume or mass flow. For incompressible flow due to the low developed pressure rise, the characteristic curve of a small axial fan, for standard atmospheric conditions, can be expressed as pressure difference against mass flow rate at a given rotational speed as illustrated in Figure 2.21.

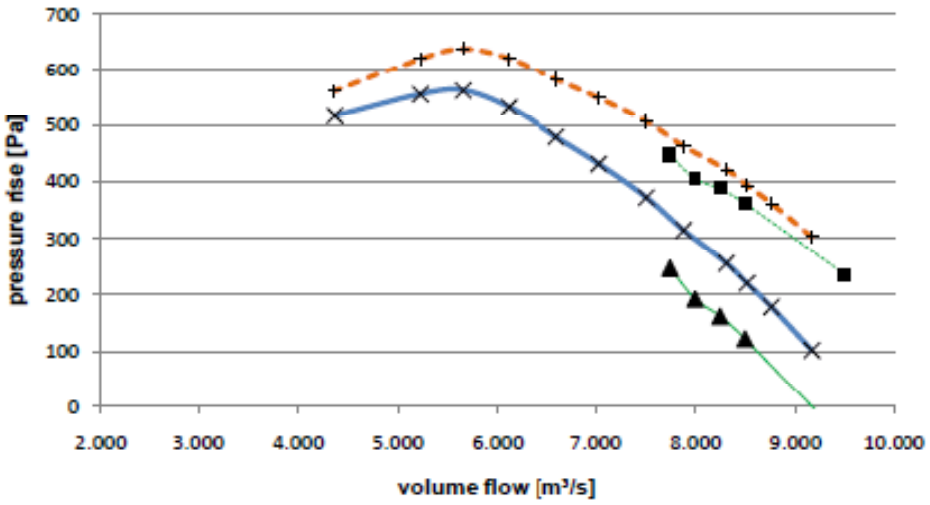

Figure 2.21 Characteristic line of a low speed fan (Strohmeyer, 2009)

In the simplest form of an axial fan, the air approaches the rotating component of the fan (impeller) with a given axial velocity. The work done on the fluid by the impeller torque adds a rotational component to the velocity. As a result the absolute velocity at the exit is higher than the axial velocity, thus some of the total pressure that was developed by the fan does not appear as useful total pressure.

There are 3 main types of axial fans: the propeller fan of Figure 2.22, the tubeaxial fan of Figure 2.23 and the vaneaxial fan of Figure 2.24.

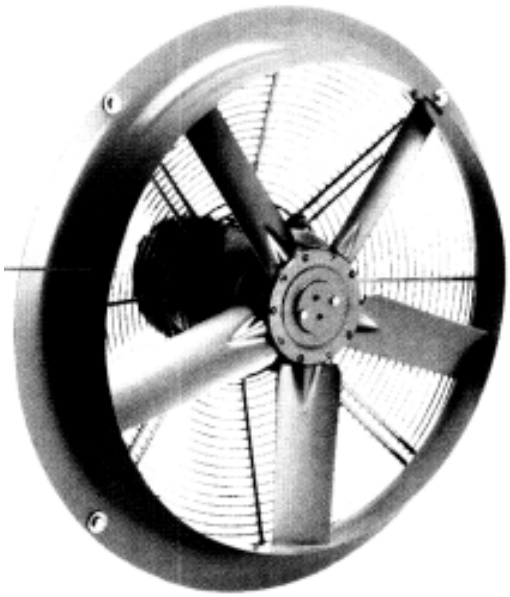

Figure 2.22 Propeller fan (www.canadablower.com)

Figure 2.23 Tubeaxial fan (www.cincinnatifan.com)

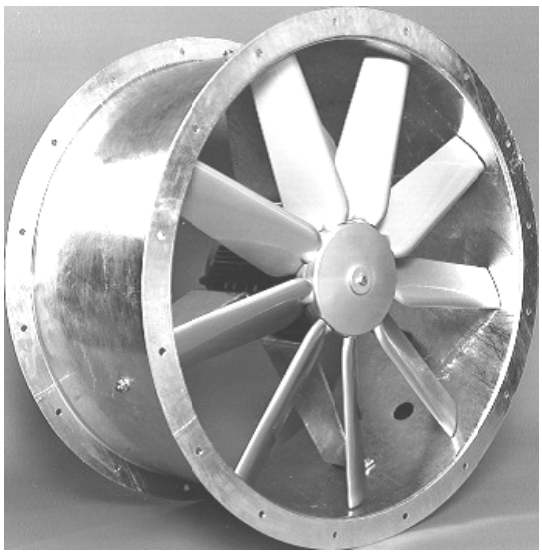

Figure 2.24 Vaneaxial fan (www.flaktwoods.com)

The propeller fan is used when the lower cost is the more important factor of the design. Often they do not have aerofoil blades and their efficiencies are quite low.

The tubeaxial fans is a propeller fan with a cylindrical housing (shroud). It has more sophisticated design, increased static pressure and efficiency and a hub to tip ratio range from 0.3 to 0.5 (Bleier, 1998)

When there is a requirement for higher pressure and higher efficiency guide vanes are added to the fan and in that case the fan is called vaneaxial fan. In fans where the loss of useful pressure is high (outlet velocity angle

greater than 15 degrees, McKenzie 1997, Osborne 1977) guide vanes are added to the design in order to remove the rotational component of the velocity and convert some of the dynamic pressure into useful static pressure. The vaneaxial fans have higher hub to tip ratio than the tubeaxial fans. The hub to tip ratio for vaneaxial fans ranges from 0.5 to 0.8 (Bleier, 1998)

The guide vanes can be located on the outlet side or on the inlet side of the fan blades. In the case of inlet vanes the static pressure is produced only from the fan blades; the contribution of the inlet guide vanes is the preparation of the flow for the fan blades as shown in Figure 2.25.

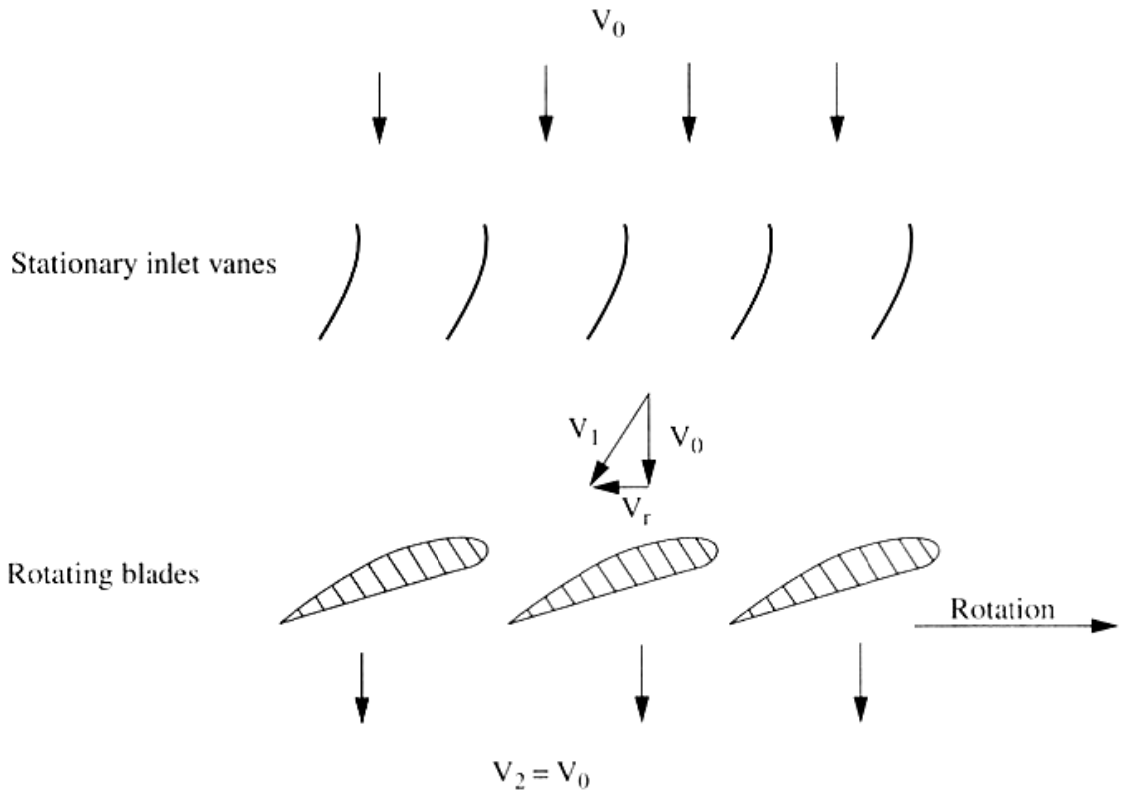

Figure 2.25 Vaneaxial fan with inlet vanes (Bleier, 1998)

In the case of downstream guide vanes a percentage of the static pressure is produced at the fan blades and another percentage from the vanes as shown in Figure 2.26.

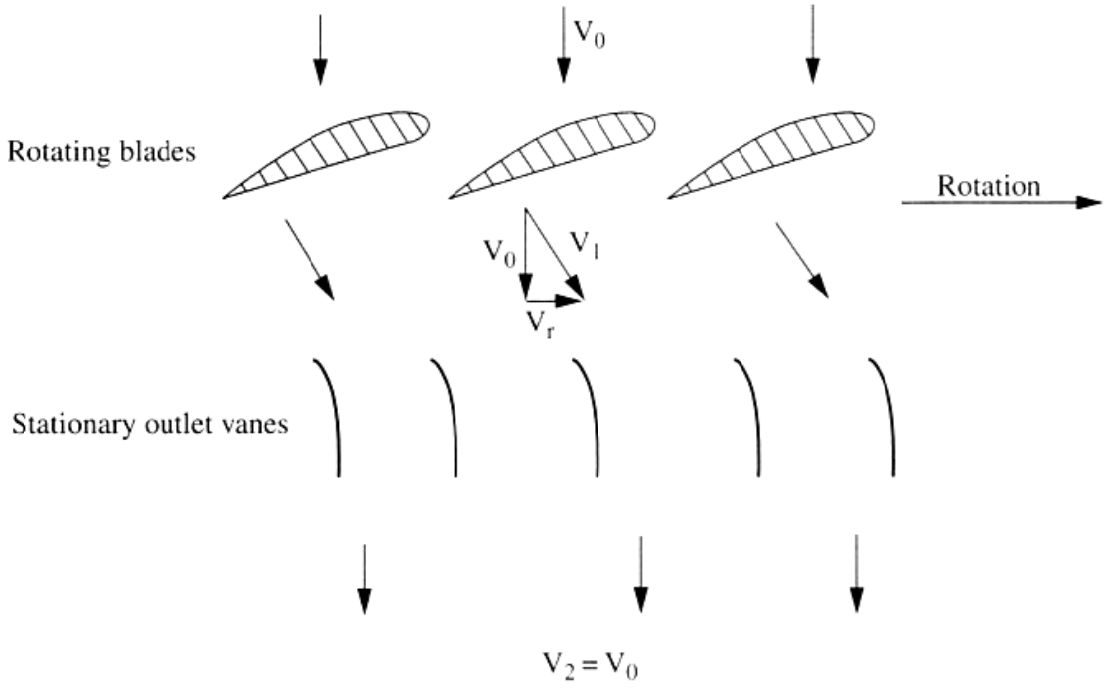

Figure 2.26 Vaneaxial fan with outlet vanes (Bleier, 1998)

The guide vanes provide an increase in the static pressure and the efficiency of a vaneaxial fan comparing with an impeller fan or a tubeaxial fan. In most applications the outlet vanes are preferable than the inlet vanes. In specific cases where the motor is installed at the front of the fan for better accessibility, the inlet guide vanes are the better solution.

However, inlet guide vanes have important disadvantages in performance comparing with the outlet vanes, especially in high static pressures (Bleier, 1998) as follows:

a. The shape of the inlet vanes is more critical, than the downstream guide vanes

b. The opposite spin that the inlet vanes give to the flow result higher noise

c. The inlet vanes are staggered in a permanent position so they can provide the necessary initial inlet angle only in the design point conditions. Their efficiency is decreasing in of design cases while the noise increases

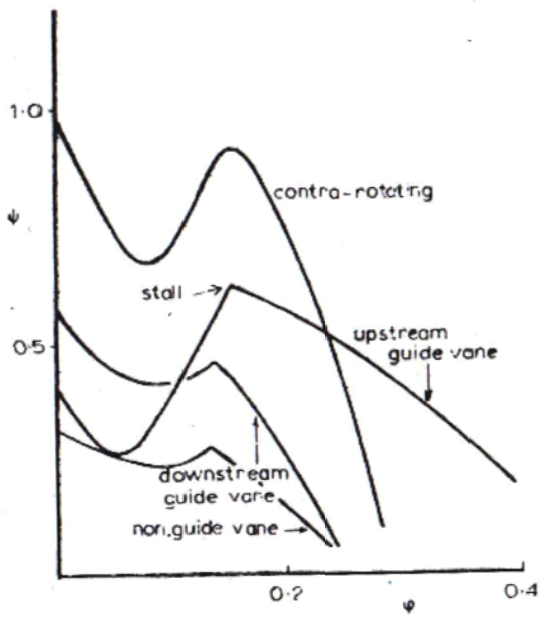

Figure 2.27 Various type axial fan performance (Osborne, 1977)

In Figure 2.27 the performance of a fan is illustrated in terms of the dimensionless pressure flow characteristic ψ and the dimensionless volume flow characteristic φ for all types of axial fans. In Figure 2.28 the performance of a vaneaxial fan is illustrated in terms of static pressure and volume flow.

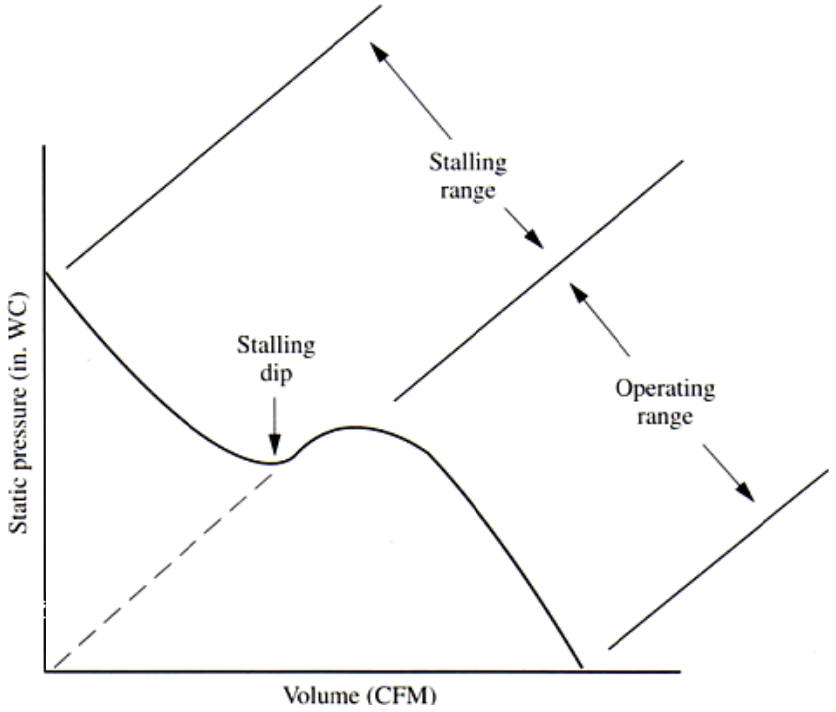

Figure 2.28 Performance curve of a vaneaxial fan (Bleier, 1998)

The performance curve starts from the point of free delivery (static pressure=0). If the flow restrictions increase in the environment or ducting system where the fan operates, the static pressure increases and the volume flow decreases. This is due to the fact that with increasing flow restrictions, the volume flow will decrease and the axial velocity will decrease. The inlet angle of the relative velocity will increase (same rotational speed and lower axial velocity) and the angle of attack will increase and as a result the static pressure will increase (operating range).

However this will happen until the maximum useful angle of attack when the peak of static pressure is reached. After that point, the angle of attack will increase above the stall point of the blade, the flow will not be able to follow the contour of the blade, separation will occur and the static pressure will finally decrease simultaneously with the volume flow (stall dip region).

After the stalling dip region it would be expected that the lift coefficient will decrease until the point of zero flow and zero static pressure is reached (dashed line). However, the fan continues its operation albeit with low efficiency and high noise. When the fan operates in a stalled condition the flow is to some extent thrown outwards by centrifugal force and in this way static pressure is produced until the point of zero flow.

3. Preliminary Fan Design Method

3.1 Introduction

Various aerodynamic techniques have been employed for the design of low speed fans. The most powerful design methods are the three dimensional methods which are available due to the advance in computational aerodynamics. However, the application of these advanced methods to industrial fans is only justified for special cases (Smith, 1989)

The use of the two dimensional airfoil characteristics is generally adequate for the design of an industrial fan. The design of an industrial fan based on the 2-D airfoil characteristics is very well documented in literature. For a preliminary design of an industrial fan the 2-D approach will result in a fan design with acceptable performance.

The purpose of a fan is to move a required volume of air and at the same time to overcome the resistance of the area by providing the necessary pressure rise. The volume flow Q and the pressure rise ΔP are the main design parameters for a fan and it is common to categorize fans according to the volume flow (size) and pressure rise.

3.2 Method Selection

The preliminary design of an axial fan can be approached in two main ways:

a. Treating the fan as a series of isolated airfoils

b. Regarding it as a rotating cascade

The choice of the method depends on the space to chord ratio of the fan; the ratio of annulus area to the blade area. The space to chord ratio depends on the loading, so relatively early in the design procedure the appropriate method becomes apparent.

In the isolated aerofoil approach each blade is considered as a series of two-dimensional airfoil sections. The lift and drag forces that act upon them are resolved into the torque and thrust planes respectively and the integration of them from root to tip gives the shaft torque and static pressure rise across the rotor disc. Knowledge of the local lift and drag forces, which are derived

from the local air velocity relative to the blade, is required for the calculation of the static pressure rise. The designer controls the velocity and pressure distribution within the annulus to maintain radial equilibrium.

The main limitation to the isolated aerofoil approach is the distance between the blades. When the blades are sufficiently close to each other, there is a divergence between the theoretical and actual values of the lift forces, because their pressure fields interact and seriously restrict the development of the full lift forces.

This issues can be corrected using empirical rules that derive from experiments, however the effect of these empirical corrections deteriorate as the distance between the blades decreases. According to Bass 1987, for solidity values greater than 0.7 the isolated airfoil method is not recommended. For closer spacing an alternative approach is needed and unless facilities are available for a more elaborate computation of the flow field and the aerofoil surface pressures recourse must be had to the cascade method.

According to the cascade method the row of blades is regarded as a row of rotating diffusing passages and the deflection imparted to the flow is considered rather than the lift forces on the individual blades, although the latter can be expressed in terms of inlet and outlet flow angles. Total pressure loss corresponds to blade drag and the deviation of the flow at the outlet from the condition of tangency to the camber line is analogous to the lift slope of an airfoil (Bass, 1987).

Experiments showed that the lift that an airfoil produces as an isolated airfoil is not the same with the lift that is produced from the same airfoil as a part of a cascade. Dixon, 1998 defines as k as the ratio of the lift of the blade is cascade to the lift of the blade isolated. The variation of k with the space to chord ratio for different stagger angles is depicted in Figure 3.1. For lower space to chord ratios (less space between blades) and especially for high stagger angles k is high and the designer should be careful with the design assumptions. The effect of closely spaced blades is difficult to predict in an analytical solution, however the result will be obvious in a CFD simulation.

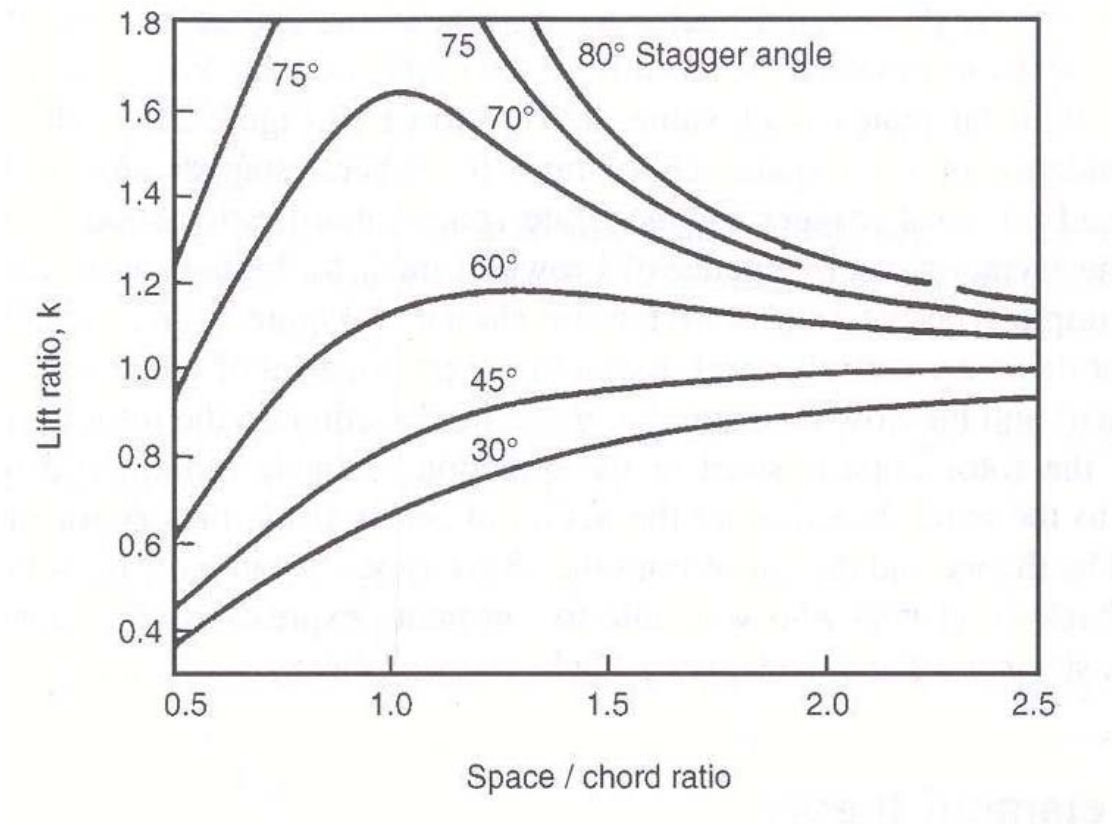

Figure 3.1 Lift ratio, k in variation with space to chord ratio (Dixon,1998)

In general and according to Turner, 1966 conventional compressor stages are designed by the cascade method, while high stagger low solidity ducted fans are designed on modified isolated aerofoil theory.

3.3 Radial equilibrium

In an axial fan the flow must be maintained in equilibrium between the radial static pressure gradient and centrifugal field. As a result, the choice of the work distribution along the blade is influenced.

A vortex is a mass of fluid that rotates. This phenomenon occurs in axial fans in order to balance the forces, because of the pressure difference and the rotating speed.

Usually the preliminary design starts by calculating the behavior of a blade at mid radius. The behavior at the mid radius of the fan represents the total behavior of the blade, but still the conditions across the radii have to be established. The aerodynamic loading at each radius must be carefully

designed, because the variation of performance at each radius can cause difficulties in the choice of the blade geometry and the blade profile.

The first step is to define the aerodynamic performance as one moves along the radii. There are several assumptions that can be made and from these assumptions different design philosophies arise.

3.3.1 Free Vortex Design

The free vortex is the simplest design and offers the best efficiency possible. In a free vortex condition the axial velocity is constant across the radii while the swirl velocity is inversely proportional to the radii. That means that as one moves from the hub to the tip the swirl velocity is lower in order to keep the contribution of pressure rise constant from tip to root. This is associated with constant axial velocity across the annulus and the result is that no downstream energy losses from the redistribution of kinetic energy occur.

The free vortex pattern is like that of the water draining in a bath tub, where the rotational velocity near the plug hole is high but reduces in magnitude as the radius away from the drain increases.

The first assumption that can be made is that the total energy remains the same the same across the radii. The total energy is expressed by the Bernoulli's equation for incompressible flow along a streamline:

$P_t = P_s + \frac{1}{2} * \rho * u^2 = \text{constant}$ (3.1)

This equation can be manipulated to the more convenient form:

$U_w * r = \text{constant}$, (3.2) where U_w is the whirl velocity

The above equation confirms the previous assertions regarding the fact that the axial velocity remains constant across the radii while the swirl velocity is inversely proportional to the radii. This characterizes the "free vortex" design. The difference in the flow between a free vortex design and a non free vortex design is illustrated in Figure 3.2.

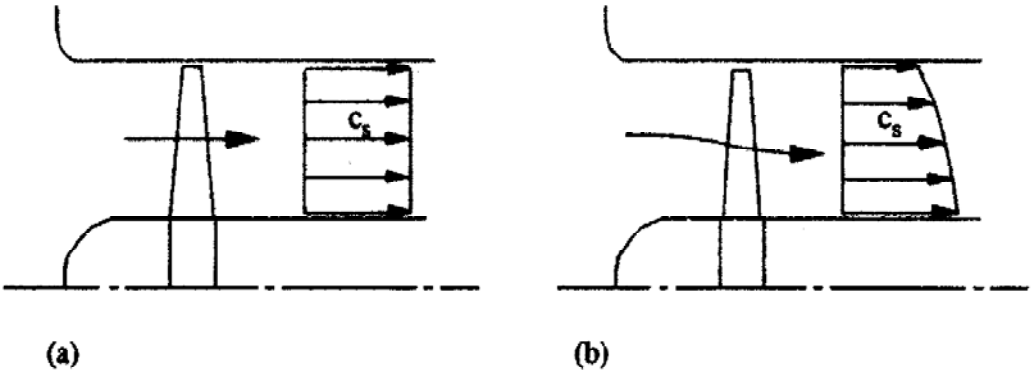

Figure 3.2 (a) free vortex axial fan (b) non free vortex axial fan (Lewis,1996)

An important and practical advantage of the free vortex design is that it is stable and simplifies the fan design whenever it can be adopted.

A major disadvantage however is that a free vortex design implies high root loading. Since the hub velocity is much less than the tip velocity, this difference must be compensated for through a high twisting of the blade at root in order to maintain the same pressure rise contribution across the whole span. As a very approximate indication a free vortex approach is unlikely to be satisfactory for hub/tip ratios less than about 0.3 although for very lightly loaded fans a smaller value may be possible. Its use in extreme cases results in very large root chords and highly twisted blades in this region according to Bass, 1987. Examples of the preliminary design of a fan blade employing a free vortex methodology can be found in Lewis,1996.

Where conditions require it, very considerable work grading from root to tip can be employed giving much reduced root loading and a much more manageable design but care is required to maintain the radial equilibrium mentioned above. Values of root/tip work loading of 2.0 or more have been successfully achieved using the flow deflections of the cascade approach combined with an assumption of a free vortex swirl distribution

Bass, 1987 states that in many cases the design can be based in the free vortex swirl distribution while at the same time considerable work grading from root to tip can be employed in order to improve the design.

3.3.2 Non Free Vortex Design

Besides the free vortex design, radial equilibrium can also be achieved with either constant swirl velocity, forced vortex or the mixed vortex designs.

In the constant swirl design approach the swirl velocity is kept constant across the span:

$U_w = K$, (3.3) where K is a constant

In the forced vortex design the swirl velocity is proportional to the radius:

$U_w = K*r$ (3.4)

The mixed vortex design in turn is a combination of free vortex and forced vortex:

$U_w = K*r + K/r$ (3.5)

Examples for the above mentioned radial equilibrium approaches may be found in Lewis, 1996.

3.4 Hub to tip ratio definition

According to the procedure that is described in Bleier's handbook, (Bleier, 1998) the input data for the design of a fan are the Volume Flow Q, the Static Pressure P_s, the Fan Diameter D and the rotational speed rpm. These requirements are specified by the customer in any case.

The hub diameter can be calculated from the following equation

$$d_{min} = (\frac{19000}{rpm}) * \sqrt{Ps} \quad (3.6)$$

or from Figure 3.3

In Figure 3.3 the hub diameter can be found if the Static Pressure and the Rotational speed are set.

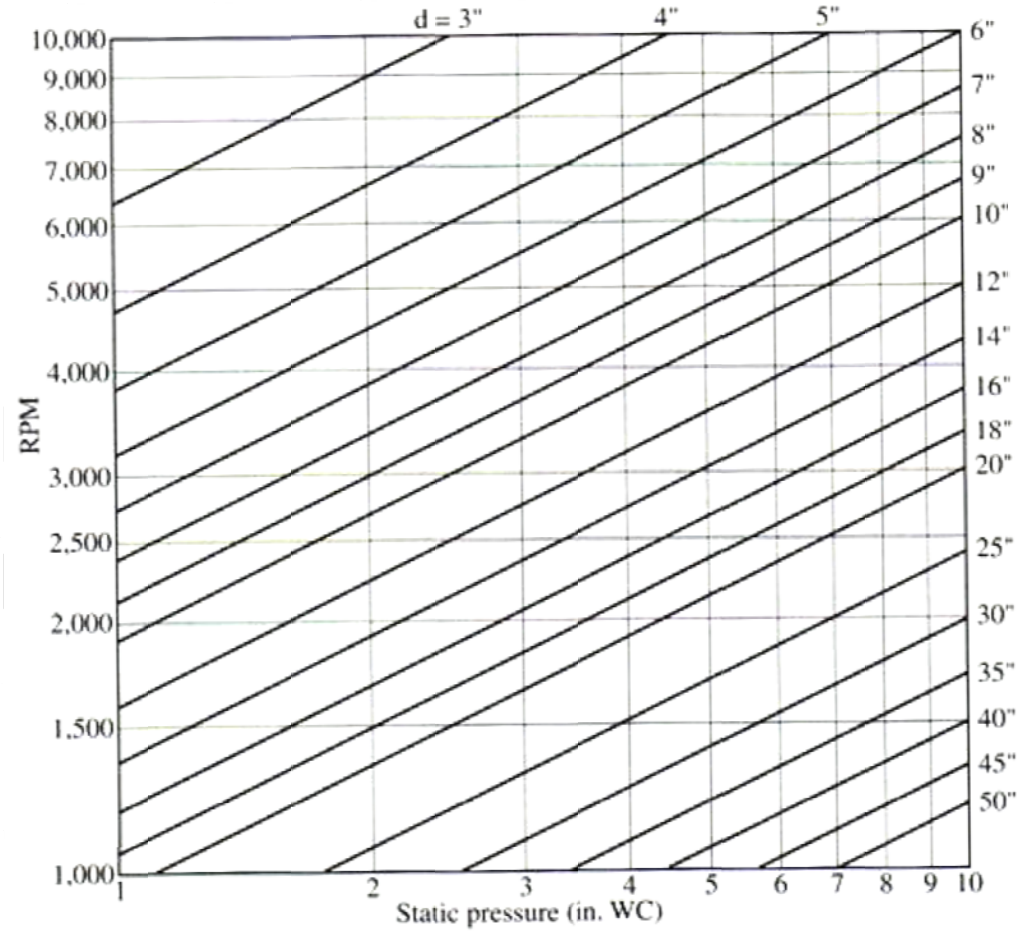

Figure 3.3 Hub Diameter calculation (Bleier, 1998)

The hub diameter is a critical parameter, because a smaller hub diameter could invite the occurrence of turbulence and reverse flow near the hub, which can lead to stall.

Furthermore as McKenzie, 1997 states the size of the fan annulus area is important because the lower the fan annulus velocity, the lower the losses due to the diffusion of the annulus velocity in the duct.

McKenzie defines the hub to tip ratio by plotting the values of $\Delta H/Va^2$ and Va/U at the diagram in Figure 3.4. The values of $\Delta H/Va^2$ and Va/U can be calculated after assuming a hub to tip ratio. This is an iterative procedure until a satisfactory value of Pressure Coefficient Cp is achieved.

$Cp=1-(V_2/V_1)^2$ where V_2/V_1 is the de Haller number. The de Haller number cannot be more than 0.7, otherwise separation will occur at the trailing edge area. As a result the maximum Cp that is acceptable is 0.5

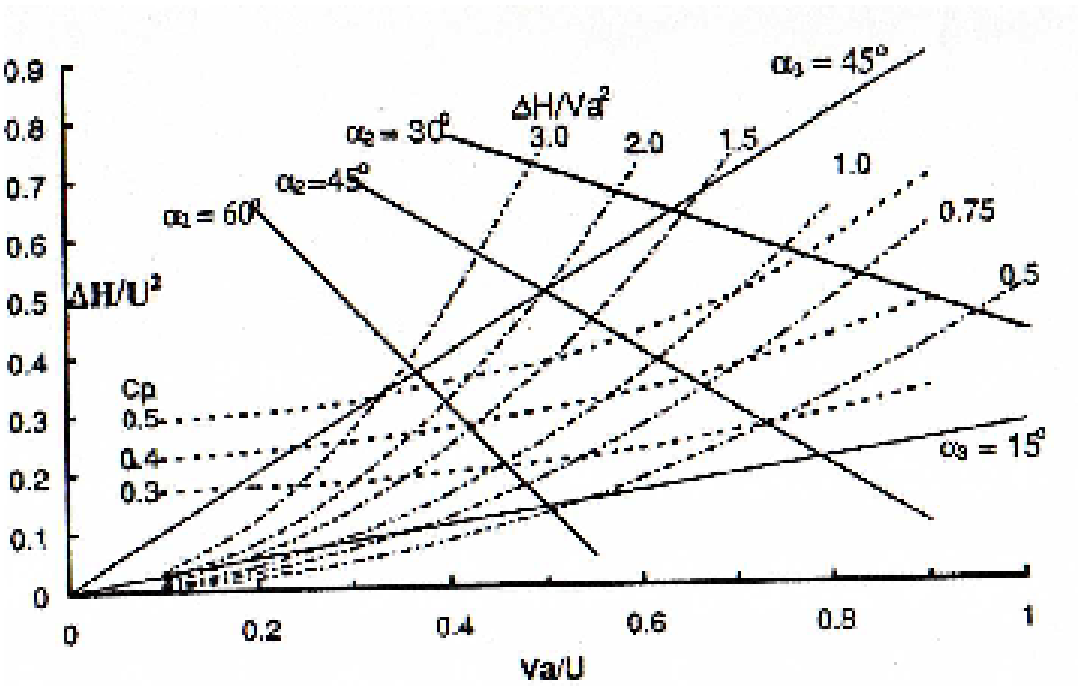

Figure 3.4 Work coefficient vs flow coefficient diagram (McKenzie,1997)

Osbourne, 1979 on the other hand uses established values of φ and ψ that were mentioned in Figure 2.15 to obtain the hub to tip ratio.

According to Bleier, 1997 the hub to tip ratio for Vaneaxial fans varies from 0.5 to 0.8.

3.5 Airfoil selection

The choice of aerofoil for low pressure fans is not critical and in practice often depends largely on the availability of enough aerodynamic data to cover the range of working conditions encountered by the different radial stations along the blade (Bass, 1987). Provided that the operating lift/drag ratios are at least 50, a readily achievable target, the section efficiency is not very sensitive to small changes in drag.

The C4 airfoil is chosen from McKenzie,1997 for the preliminary design of a fan. Bleier, 1997 used a NACA 65 profile for his preliminary design of an axial fan.

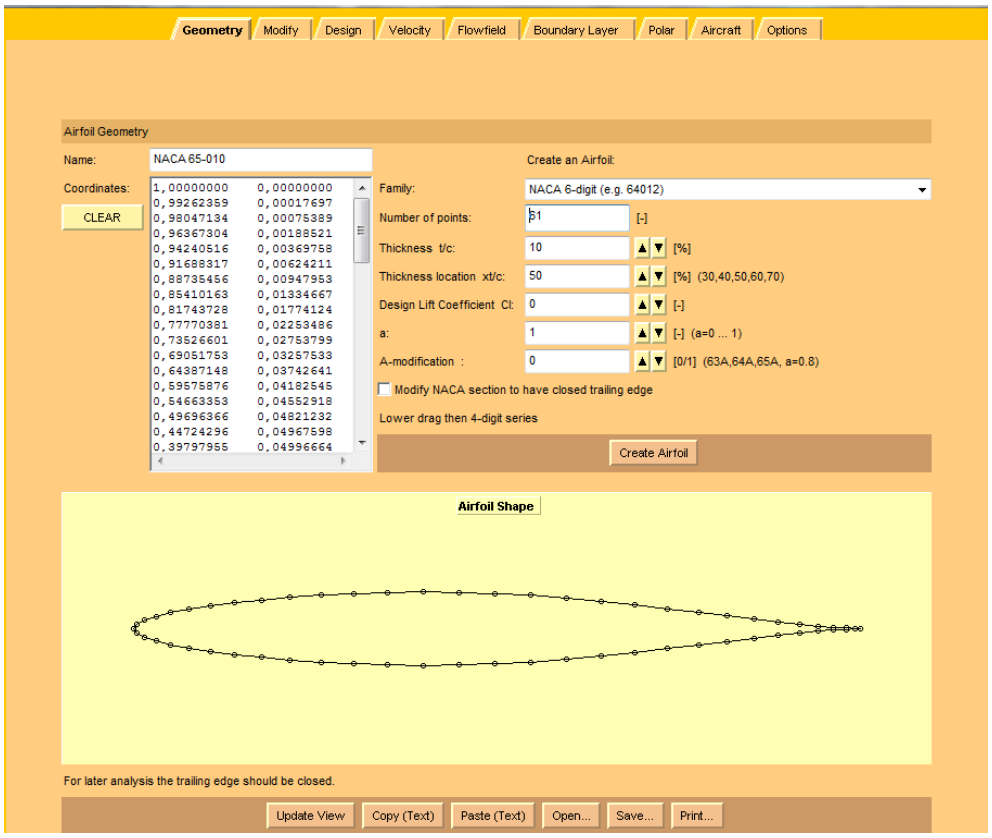

Figure 3.5 NACA 65010 airfoil [http://www.mh-aerotools.de/airfoils/javafoil.htm]

A NACA 65 airfoil profile is illustrated in Figure 3.5. The knowledge of an airfoil profile coordinates and the aerodynamic characteristics of an airfoil are necessary for the selection of the airfoil. A very useful application for the creation of various airfoils and the airfoil analysis may be found in the following website http://www.mh-aerotools.de/airfoils/javafoil.htm.

3.6 Blade Geometry

Best efficiencies for vaneaxial fans are obtained with airfoils as cross sections of blades. These airfoils have high lift to drag ratios. Additionally for a good efficiency the airflow of an axial fan should be evenly distributed over the working face of the fan wheel which means that a free vortex design is preferred.

The velocity of the rotating blade increases with the radius. This can be compensated for by twisting the blade resulting in larger blade angles near the hub and smaller blade angles near the tip.

The airfoil blades are manufactured from aluminum or steel castings and they are usually twisted and tapered. There are several advantages and disadvantages in a tapered airfoil according to Bleier, 1998:

1. Wide chord at the tip: high pressure, high efficiency and quiet operation, but cause of considerable motor overload at the point of no delivery but fans with such blades have a deeper stalling drop

2. Medium chord at the tip: this reduces the maximum static pressure and the no delivery overload

3. Narrow chord at the tip: non overloading brake horsepower characteristic, flatter pressure curve and efficiency slightly lower, but acceptable.

McKenzie, 1997 considers that the tip should not exceed the hub chord by more than 20% for centrifugal loading reasons. In his preliminary design example of an industrial fan, the tip chord is 2/3 of the hub chord to ensure a reasonable size of the airfoil and a modest thickness to chord ratio. Osborne,1977 suggests a tip chord that is 75% of the hub chord in order to achieve a solidity of unity for a specific number of blades.

3.7 Blade design

The air angles can be calculated from the velocity triangles of Figure 2.2 and the equations resultant from the free vortex design method. The blade angles derive after the consideration of the incidence and the deviation is taken into account. According to McKenzie, 1988 the peak efficiency can be achieved when the angle of incidence lies between $+5^{o}$ to -10^{o} as it is illustrated in Figure 3.6.

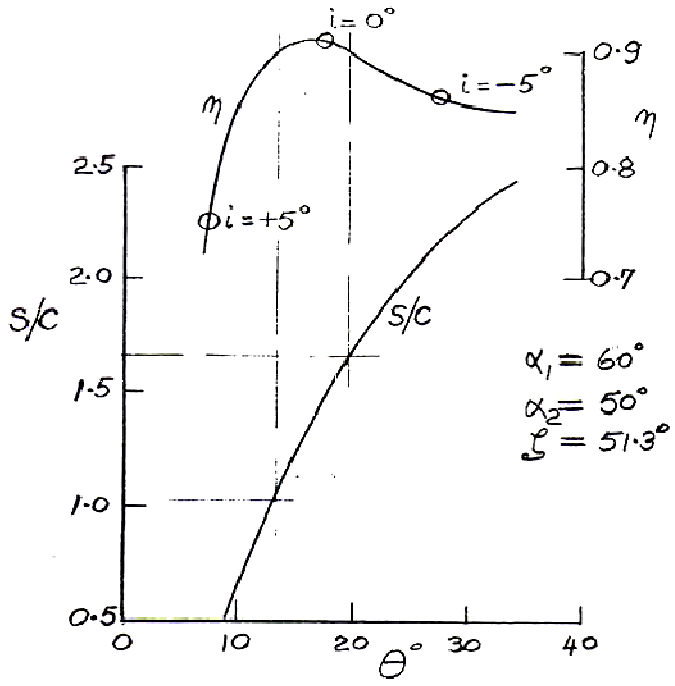

Figure 3.6 Blade geometry for fixed air angles (McKenzie, 1988)

A trial and error procedure is used by McKenzie, 1997 to find the most appropriate incidence. The variation of incidence affects the space to chord ratio which has to be between a range of values in order to give the desired efficiency as it is shown in Figure 3.7.

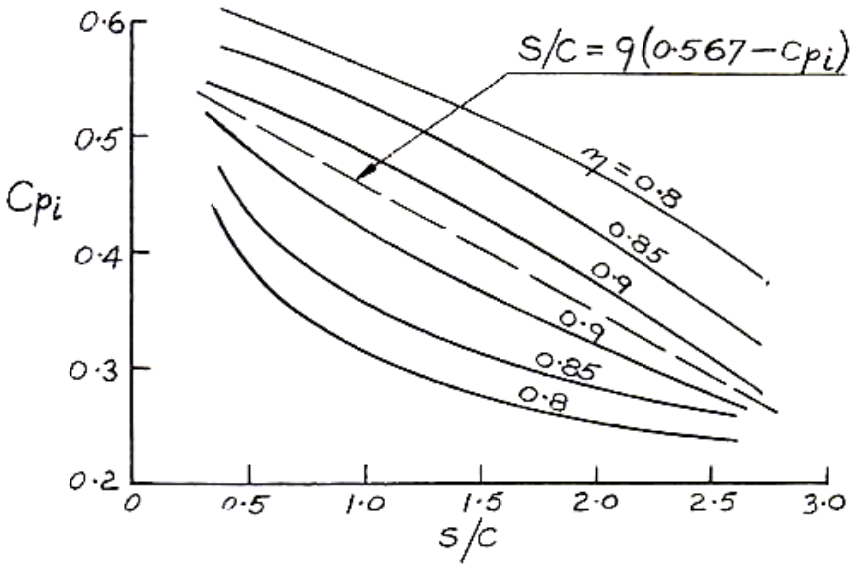

Figure 3.7 Efficiency contours (McKenzie, 1997)

The following equations are used for the calculation of the blade angles. An analytical example may be found on McKenzie, 1997

$a_1=\text{atan}(U/V_a)$ (3.7)

$\tan a_2=\tan(a_1)-\Delta H/U*V_a$ (3.8)

$\tan a_3=U/V_a-\tan a_2$ (3.9)

$Cp_i\,(\text{rotor})=1-(\cos a_3)^2$ (3.10)

$S/C\ (\text{rotor}) = n_{blades}*(0{,}567-Cp)$ (3.11)

$\tan a_m= (\tan a_1+\tan a_2)/2$ (3.12)

$\tan \zeta = \tan a_m -0.15$ for low staggers or $\tan \zeta = \tan a_m -0.213$ for high staggers (3.13)

$\theta= (0{,}5-0{,}31*(S/C)^{(1/3)}$ (3.14)

$\beta_2=\beta_1-\theta$ (3.15)

deviation $\delta=\alpha_2-\beta_2$ (3.16)

deflection $e =a_1-a_2$ (3.17)

$\underline{i = \alpha_1- \beta_1}$ (3.18)

$\theta=2(\beta_1-\zeta)$ (3.19)

$\underline{S/C=\delta/(1.1+0.31\theta)^3}$ (3.20)

The equations for incidence and space to chord ratio are underlined to show the relation between these two design features. McKenzie, 1997 found that the maximum efficiency occurs when the mean angle and the stagger angle are related according to the equation $\tan \zeta = \tan a_m -0.15$ or $\tan \zeta = \tan a_m -0.213$. This is the result of the experiments that were made on cascades with C4 airfoil blades. For a different basic airfoil, the stagger angle is correlated with the mean air angle with a modified equation.

From the above mentioned procedure it is clear that the airfoil profile in every section from hub to tip will be different. In McKenzie's example C4 is the base profile, but in every section the camber and the stagger can be different in order to maintain the principle of the free vortex design which is ensures the same amount of pressure rise for every section.

Bleier, 1997 follows a similar procedure. The velocities and the air angles are calculated for every section and then the base airfoil is modified

accordingly in order to give the desirable static pressure rise. The equation that is used to calculate the lift coefficient of every section is the following:

$Ps = 6{,}6456 * 10^{-3} * z_B * C_L * l * W$ (Bleier,1998) (3.21)

P_s : Static Pressure rise in Pascals

z_B : Number of blades

C_L : Lift coefficient of the airfoil at the specific radius

L : Blade width

W : Average relative velocity of the flow (m/s)

From the above equation the C_L can be calculated and from the C_L the necessary modification can be made to the base profile. It is obvious that the designer should have available the necessary data for the aerodynamic characteristics of an airfoil. From the C_L, the angle of attack can be found and finally the blade angle can be calculated. Figure 3.8 illustrates a C_L vs angle of attack diagram which can be used to obtain the angle of attack for a given lift coefficient.

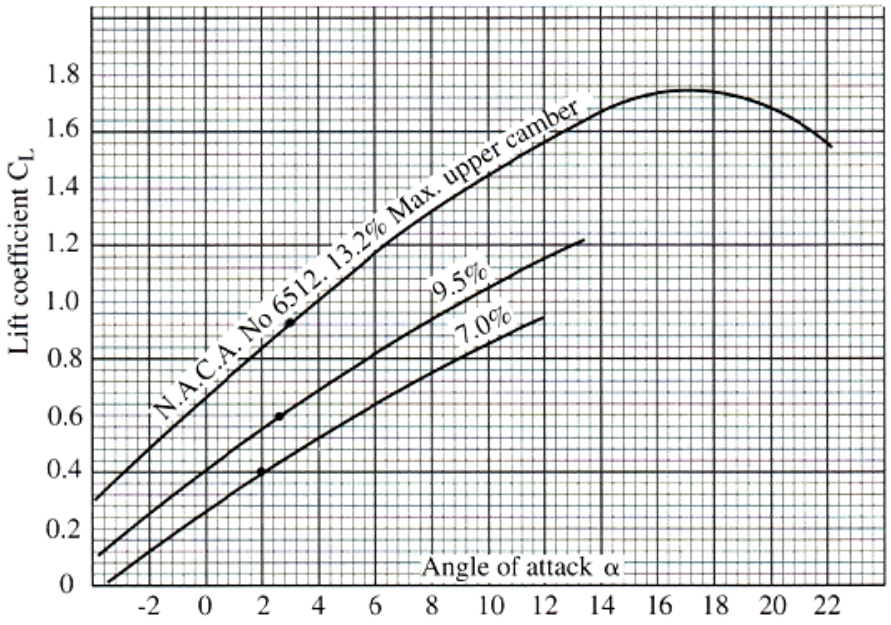

Figure 3.8 Lift coefficient variation with angle of attack for a 4-digit NACA airfoil (Bleier, 1998)

A similar approach is suggested by Osborne, 1977. After the calculation of the velocities and the air angles, the solidity is selected and from solidity the C_L can be found using the following equation which derives from the radial equilibrium and the free vortex design.

$$\frac{1}{2} * \frac{c}{s} * C_L * u_m = u_w \quad (3.22)$$

where $\frac{c}{s}$ is the solidity and u_m is the mean velocity $(V_1 + V_2)/2$

From the $C_{L,}$ the angle of attack can be found and finally the blade angle can be calculated.

The procedure to calculate the vane angles is similar.

3.8 Number of blades

The number of blades is a compromise between many design features; the blade chord, the space to chord ratio, aspect ratio, noise level and turbulence. A certain design can be modified be changing the number of blades and their width (chord) to achieve the same pressure rise.

High number of blades with small chord result in a loss in efficiency and higher noise. Low number of blades with large chord result in a better efficiency, but the hub will be too wide and bulky. A good practical number of blades for vaneaxial fans is 5-12 according to Bleier, 1998 and the designer can select the number of blades from this range.

The number of blades according to McKenzie, 1997 is the result of the combination of the calculated space to chord ratio and the value of the aspect ratio that is selected by the designer. An aspect ratio of 1.5 is recommended by McKenzie, 1997 for the preliminary design of an industrial fan. Osbourne, 1977 selects 9 blades for his preliminary design, within the Bleier's range 5-12.

The number of blades for a preliminary design of a fan depends on the experience of the designer. The decision procedure starts from a set of assumptions (aspect ratio, number of blades, blade chord, and solidity) while the other design features can be calculated based on that initial set of assumptions. If the result is not satisfactory the procedure can be revisited.

3.9 Number of Guide vanes

According to Bleier, 1998 there are two practical rules for the stator guide vanes:

a. The number of guide vanes should be greater than the blades, because they should be closer to each other in order to reduce the danger of blocking the flow because of the overlapping.

b. The number of rotor blades and the number of stator blades should have no common divisor, otherwise two blades can pass simultaneously two vanes which result an increase in the noise level. When two blades can pass simultaneously two vanes wakes are created and 2 disturbances are produced per one revolution (2^{nd} engine order excitation) and these disturbances create noise. The failure is not very possible, because the speed is relatively low.

McKenzie calculates the number of vanes after assuming a vane chord. The value of the vane chord should be inside the range of the maximum blade chord and the minimum blade chord. The chord is then trimmed in order to give an integer and prime (preferably) number of vanes.

The shape of outlet vanes has not great importance. They can have an airfoil shape or a uniform thickness with the proper curvature (cheaper). The vanes have in most cases constant thickness (Bleier, 1998)

3.10 Influence of hub to tip ratio

Vaneaxial fans have converging tail pipes and expanding diffusers for static regain. The hub diameter is higher in vaneaxial fans comparing with tubeaxial fans, in order to maintain good performance. A smaller hub diameter might result in the occurrence of turbulence and possible reversed air flow near the hub (stalling).

The Static Pressure increases with the square of the hub diameter and for a constant tip diameter with the square of the hub to tip ratio.

In Figure 3.9 the effect of hub to tip ratio to the static pressure rise is illustrated which is a result of Bleier's, 1997 experiments in a 29 inch fan with same number of blades (5), same rotational speed (1750rpm), same angle (16) but different hub to tip ratios (52% and 68%).

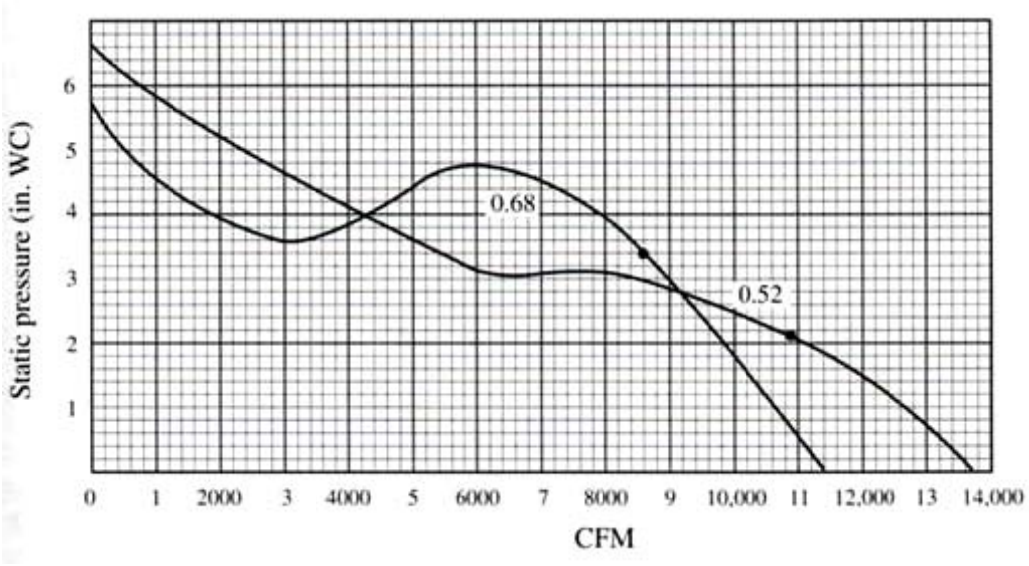

Figure 3.9 Volume Comparison of 29in vaneaxial fan (5 blades, 11 vanes) with hub to tip ratios 52% and 68% (Bleier, 1998)

The effect of hub to tip ratio can be summarized according to Bleier, 1998 as follows

a. The fan with higher hub to tip ratio produces higher maximum static pressure rise.

b. According to the fan laws the static pressure rise ratio should have been proportional to the hub to tip ratio. The static pressure rise is slightly lower because in the second fan the blade tip is slightly narrower ($(0.68/0.52)^2$ X 3.05=5.22 and the maximum is 4.75)

c. The static pressure value where we have the maximum efficiency is not the predicted one, once again because of the narrower tip blade ($(0.68/0.52)^2$ X 2.1=3.6 and the maximum efficiency occurs at is 3.4)

d. The first fan delivers higher volume but in lower static pressure. The Volume Flow Q variation with Static Pressure P_s line is more flat than the line of the second fan

e. The decrease in the static pressure (stalling dip) is much higher in the second fan. Fans with higher hub to tip ratio have higher stalling dips

3.11 Influence of blade angle

The higher the blade angle the higher the volume flow (larger blade passage), the higher the pressure, the higher the energy consumption for the same rotational speed. In Figure 3.10 illustrates the different performance curves of volume flow variation with static pressure for same size and same speed vaneaxial fans with different blade angles. The blades are single thickness blades (not airfoils) and there is a 12^{o} twisting from hub to tip.

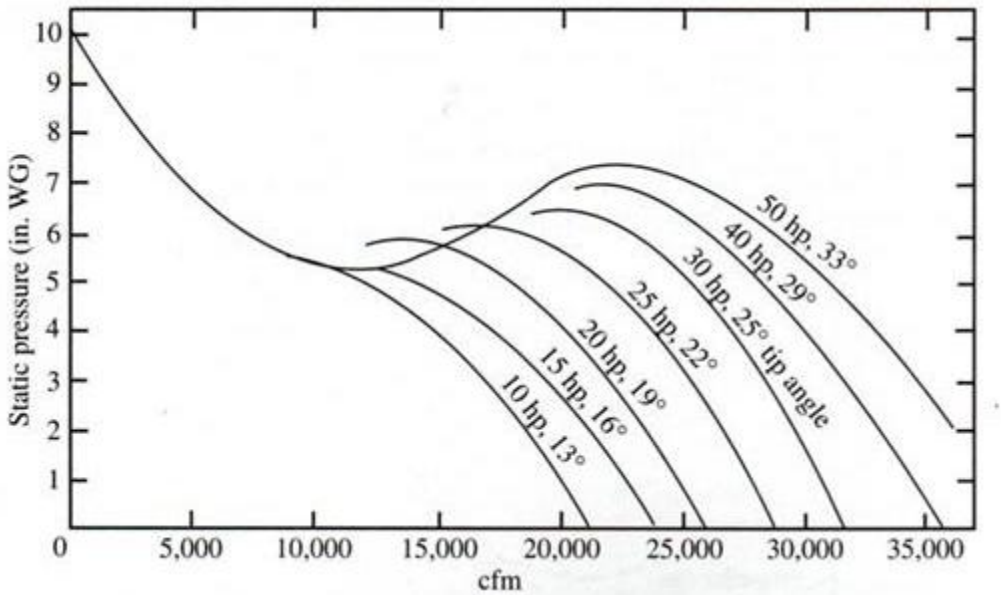

Figure 3.10 Influence of Blade angle (36in, 1750 rpm, 13-33 angles) (Bleier, 1998)

3.12 Influence of tip clearance

The tip clearance is an important feature of an axial fan. The main advantage of an increased tip clearance is the safety margin that it offers in a hostile working environment (high temperature). The main disadvantage is the deterioration of the fan performance. According to Bleier, 1998, an increase in the tip clearance has the following effects:

a. Volume flow decreases slightly
b. Maximum Static Pressure decreases considerably
c. Power consumption decreases, but not as much as the pressure
d. Mechanical efficiency decreases considerably
e. Small increase in the noise level at the free delivery

A smaller tip clearance results in optimum performance in all respects. The effect of tip clearance is summarized in Figure 3.11.

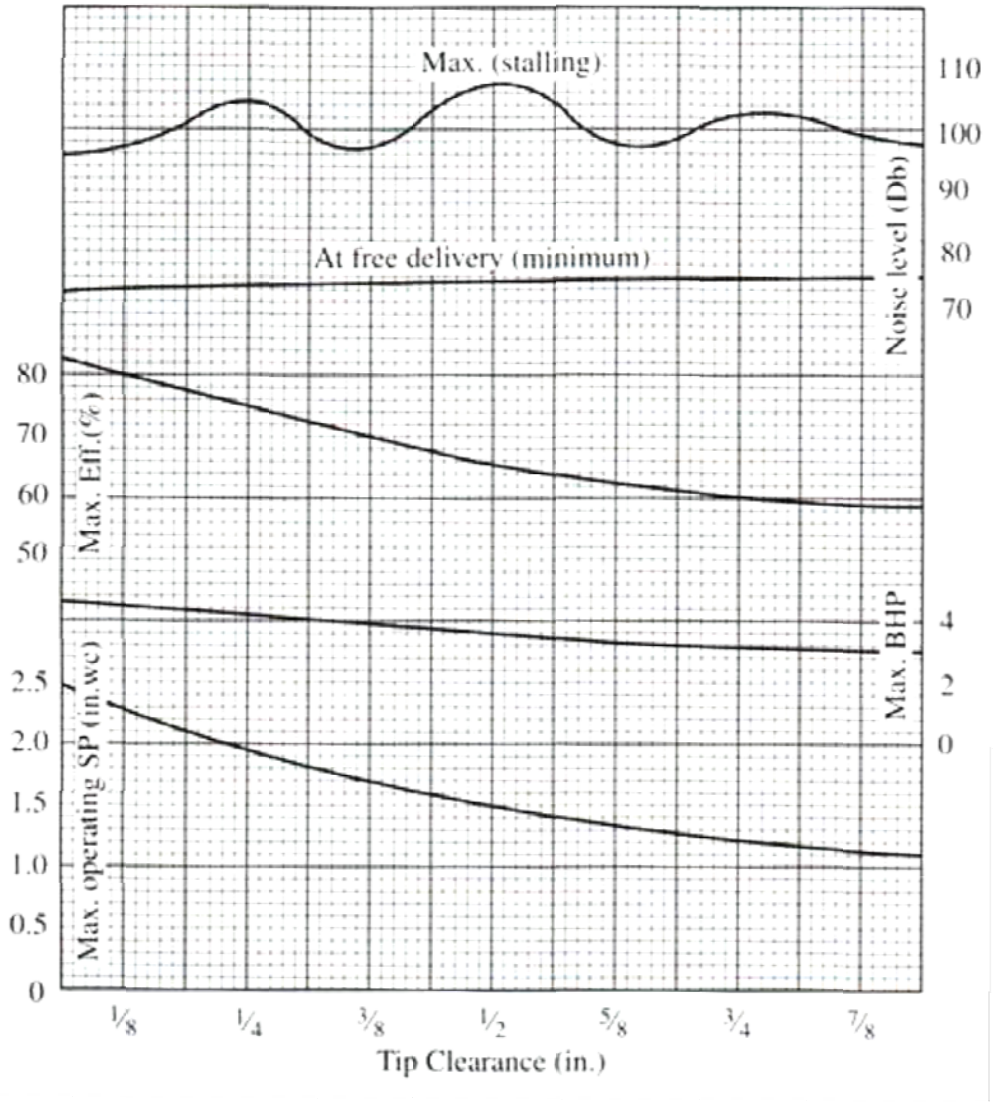

Figure 3.11 Summary of the influence of the tip clearance, (Bleier, 1998)

3.13 Three dimensional effects

The previous analysis assumes that the flow over the blades is two dimensional and that the loading distribution can be obtained from root to tip. However, in an actual fan there are factors that were not taken into account during the 2-D analysis. At the blade root, an aerodynamically difficult situation arises in which the skewed boundary layer of the hub is swept into the corner formed by the convex surface of the blade and the hub wall giving rise to an area of stalled flow in this corner. A similar situation exists at the

blade tip. The situation is further complicated by the presence of a high centrifugal field to which the boundary layer at rest or moving slowly relative to the blade is subjected.

The influence of rotation on a rotating aerofoil with two dimensional characteristics is great if the extremely high radial acceleration is included in the calculations. Furthermore according to Bass, 1987 the stall initiates at an incidence that is lower than what is expected notionally while the 3-D effects of the tip clearance reduce the expected performance notably as is illustrated in Figure 3.12.

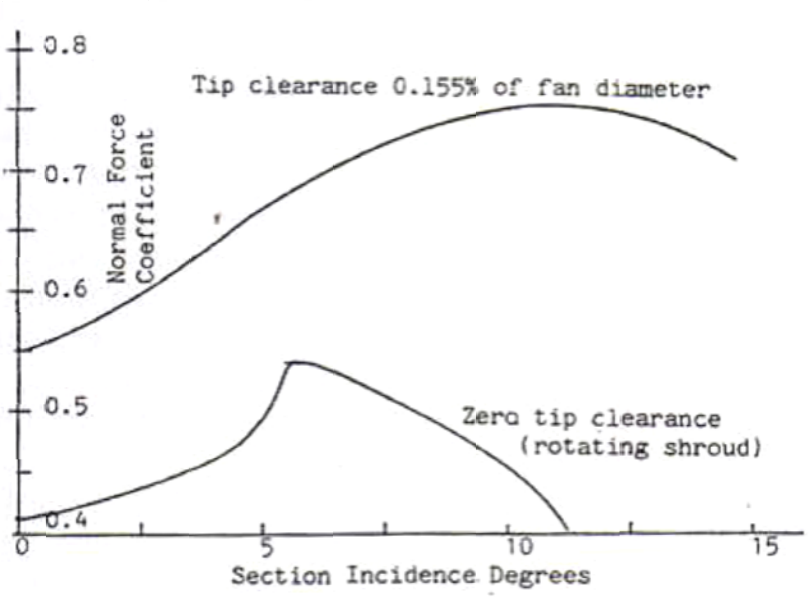

Figure 3.12 Effect of tip clearance on the characteristics of the blade tip section, (Bass, 1987)

Bass, 1987 states that in a situation where a considerable number of large continuously operating fans is required, small changes in efficiency can represent significant costs. Even in this case, providing that the loading conditions are not too severe, high efficiencies are attainable by the careful application of relatively simple design measures.

3.14 Losses

The fan operation requires the supply of energy for the acceleration of the fluid and energy to overcome forces that resist the fluid flow.

The total energy that is supplied to the fluid can be expressed in terms of volume flow Q and pressure loss Δp, because pressure is energy per unit volume of fluid. The pressure loss is evident at each change of direction of the flow, change in section area, obstruction.

The fan losses are due according to Cumpsty, 2003 to skin friction, flow separation, secondary flows and energy dissipation at the system's discharge. Due to the fluid friction within the real stage, some of the ordered kinetic energy entering the blade rows is dissipated as heat during the diffusion process, which is practically loss of useful energy. The skin friction arises from the flow "scrubbing" against flow surfaces. Separation and the secondary flows can occur through bends or discontinuities (blade edges, tip, duct misalignments, sudden enlargements of the duct etc).

Lewis, 1996 defined a loss coefficient for the rotor as well as for the stator, in order to standardize the calculation of losses. The loss coefficients are functions of flow coefficient φ, the work coefficient ψ, the Reynolds number Re, the stage reaction and the inlet Mach number (Lewis, 1996). McKenzie, 1997 defines a loss coefficient as well and he associates the loss coefficient with the incidence, Figure 3.13. At high incidence the flow cannot follow the geometry of the convex side of the blade and separation occurs. At large negative incidence the flow reaches very high velocities and can become choked.

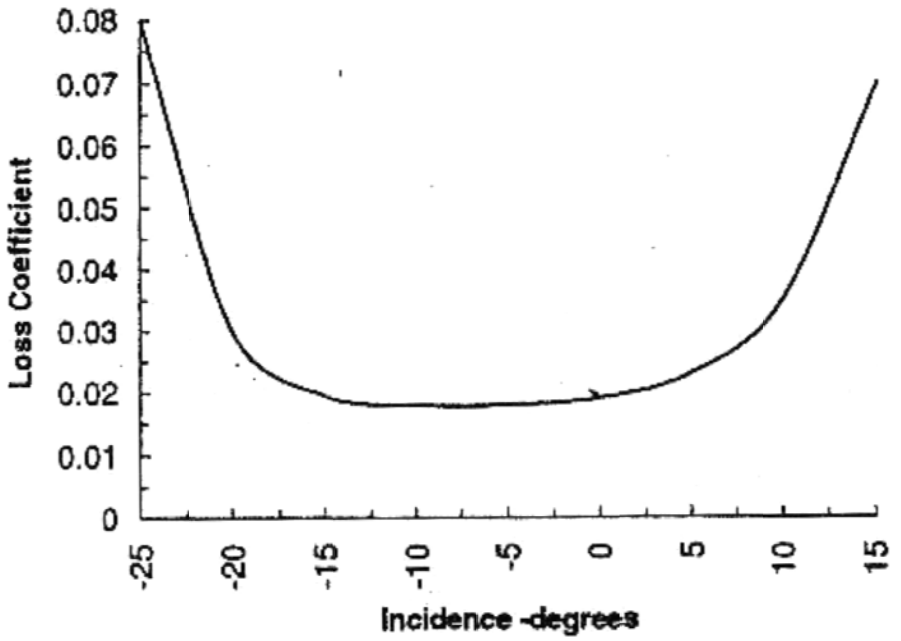

Figure 3.13 Loss coefficient variation with incidence (McKenzie, 1997)

4. Fan Design Tools

4.1 Introduction

The theoretical calculation of the fan is the first approach towards the preliminary fan design. The theory, the equations and the method that were mentioned in the literature review (Chapter 2) and in the design procedures (Chapter 3) are employed to generate a fan geometry and hence from the fan geometry to a simulation model for the CFD calculations. Furthermore, the preliminary design of a fan requires the performing of a number of tasks. In this project these steps are the following:

1. Definition of the geometry; calculation of the design parameters according to the specifications for the fan
2. Creation of the geometry; processing of the design data in order to create the rotor and the stator geometry
3. Computational domain(s) creation
4. Meshing of the computational domain(s)
5. Assembly of the subdomains, physics and boundary condition set up
6. Setting up and simulate the case
7. Results processing

Many design tools are required for the completion of the above mentioned tasks. In this chapter the design tools that were used for this project will be presented.

4.2 MATLAB codes

For the calculation of the design parameters the main software that is used is MATLAB.

The McKenzie procedure that was described in a previous chapter was implemented in an EXCEL spreadsheet. All the equations and the solution flow were written in the EXCEL spreadsheet, so that the effect of varying several parameters in the design could be investigated. An attempt was made to convert this excel spreadsheet into a more sophisticated and automated MATLAB code, but there was no time available within the schedule of the

present work; however it can be a future task. In this excel spreadsheet the user can change the design parameters of the case in every step of the procedure according to his experience and the level of familiarization that he has with the fan design in order to achieve the desirable result.

4.2.1 MATLAB code for Osborne method

The Osborne, 1977 method for a preliminary fan design was encoded with MATLAB and the result is quite interesting. This code can be used for the study of Osborne procedure for a preliminary fan design. The initial design factors of this code are the dimensions of the fan, the rotational speed, the duty and the efficiency. One of the limitations of this code is that there are no calculations for the stator, because there is no such analysis in the Osborne procedure. One step further could be the implementation of the stator's design in this code. The results are the pressure rise (total and static), velocity vectors, blade angles at the hub and at the tip and the blade geometry in a text file that was named "profile.curve" file.

Nevertheless there are four output diagrams as well. The first of them compare the flow and work coefficient of the current design with the flow and work coefficients of existing designs (Figure 4.1).

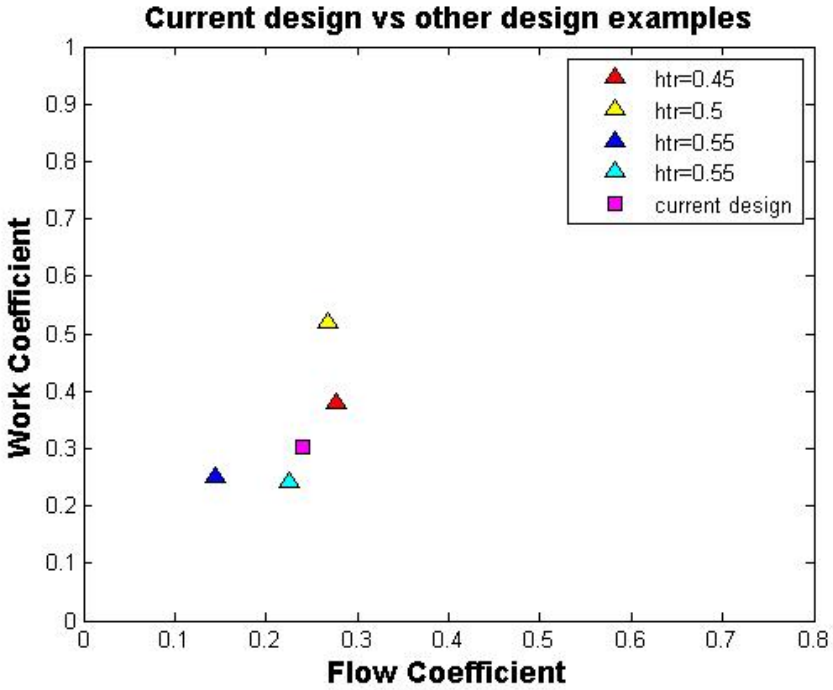

Figure 4.1 Comparison of work and flow coefficient of the new design with the existing designs

The second diagram (Figure 4.2) illustrates the cascade performance for a typical deflection at the rotor's hub. This diagram can be utilized in order to find the upper and lower limit for the space to chord ratio for a certain set of deflection and outer angle.

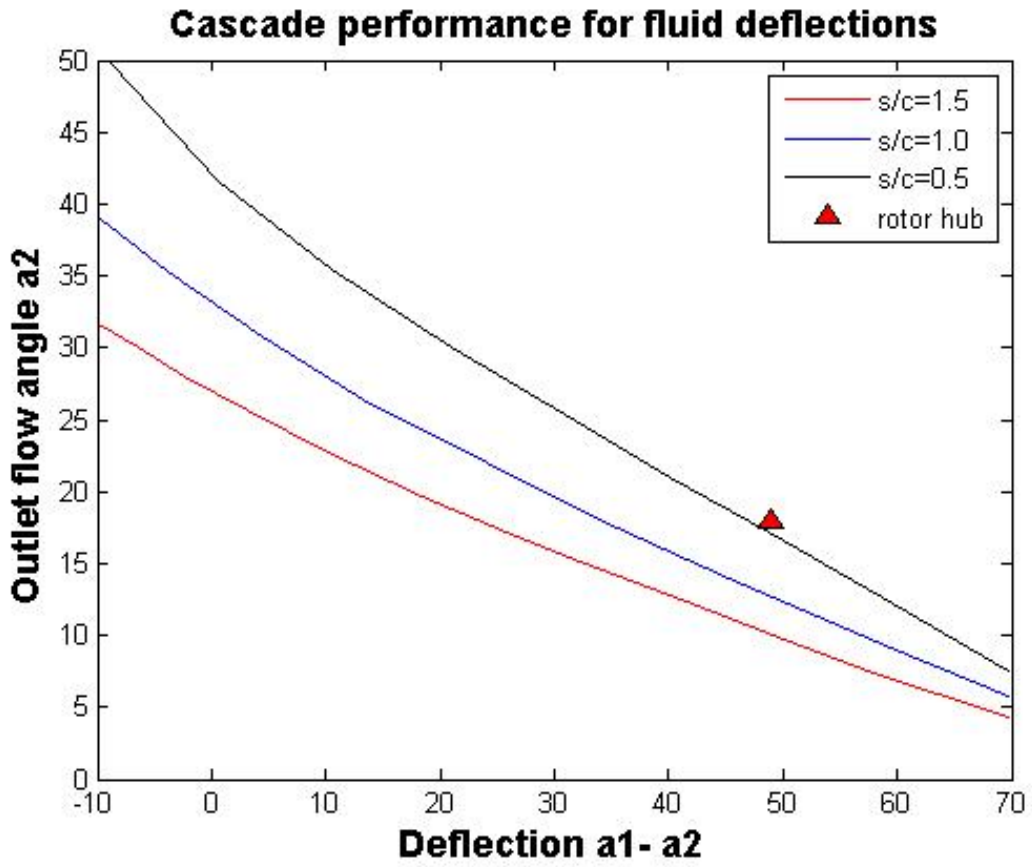

Figure 4.2 Deflection in variation with the Outer flow angle for the hub rotor

The last output diagram (Figure 4.3) depicts all the sections of the blades stacked, in order to help the designer decide if the computed geometry corresponds to an acceptable design.

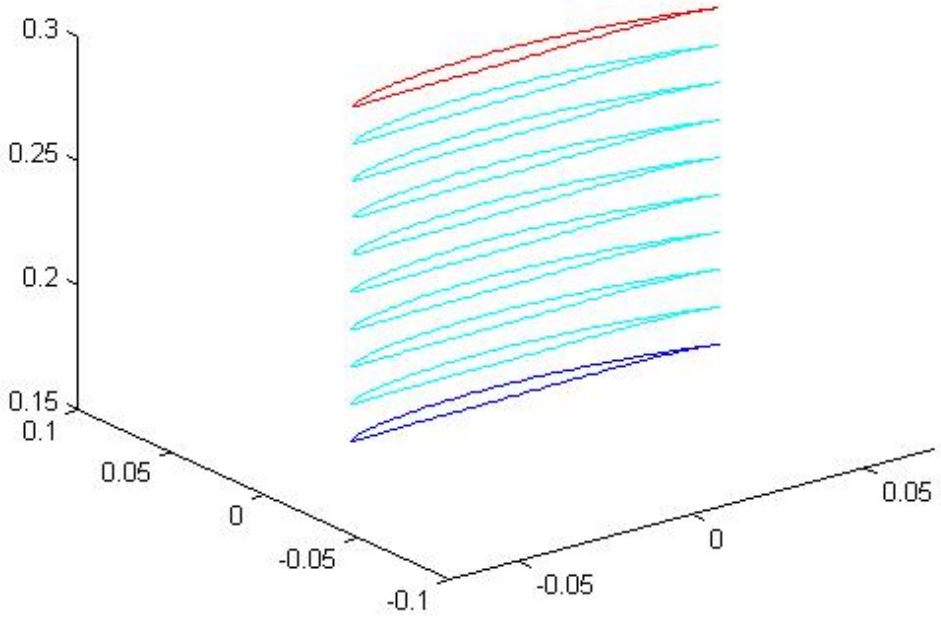

Figure 4.3 3-D plot of blade sections (output from MATLAB code)

4.2.2 MATLAB code for blade geometry

The definition of the blade and vane geometry is the most important task in fan design. Another MATLAB code was created to process the design data and provide the necessary geometry for the rotor and the stator. Although there is available software that can create blade geometry (Lewis for example), this code was created to suit the specific design outputs of McKenzie's preliminary design method. Generally, this code can create the blade geometry when specific data is imported.

The inputs for this code are the stagger angle, the camber angle and the chord of every section of the blade and the basic airfoil profile which is used for the particular design (uncambered). The code implements these features in every section of the blade and stacks all the sections into the center of gravity. The output is a text file (profile.curve) that can be used for the later stages. Another important output, as it is shown in Figure 4.4, which is a 3D plot with the final sections of the blade, which again helps the designer to decide if the geometry produced is an acceptable design.

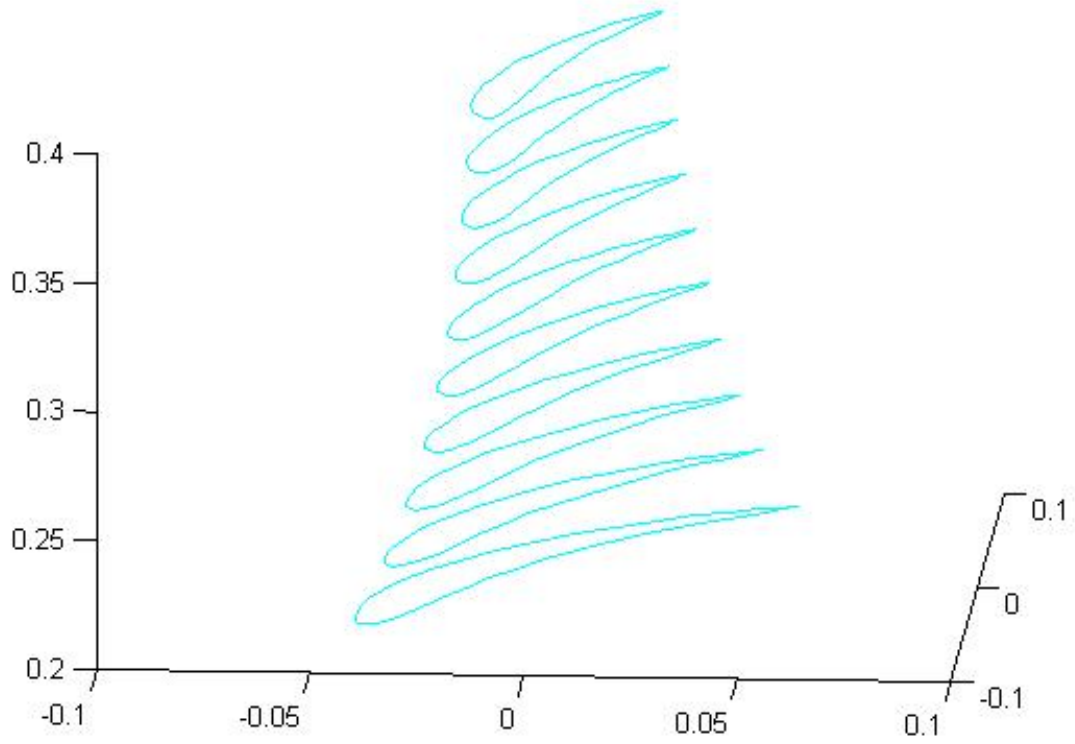

Figure 4.4 3D plot of blade sections (output from MATLAB code)

4.3 Lewis software

Another tool that was used for the creation of the blade geometry, which is an alternative to the above mentioned MATLAB code, is a code that was developed by Lewis, 1996. The program for the section profile generation is called STACK and it can only be used in a DOS environment. For this purpose it is required to use a DOS emulator program (like DOSBOX or equivalent).

The inputs for this software is the camber angle, the position of maximum camber, the stagger angle, the chord, the profile thickness and the maximum thickness position. There is a limited selection of airfoil profiles that can be used, but there is an option to use a user defined profile. For this project the inputs were the results from the McKenzie's low fidelity 1-D simulation procedure that was presented in the previous Chapter 3. Figure 4.5 depicts the Graphical user interface of STACK code.

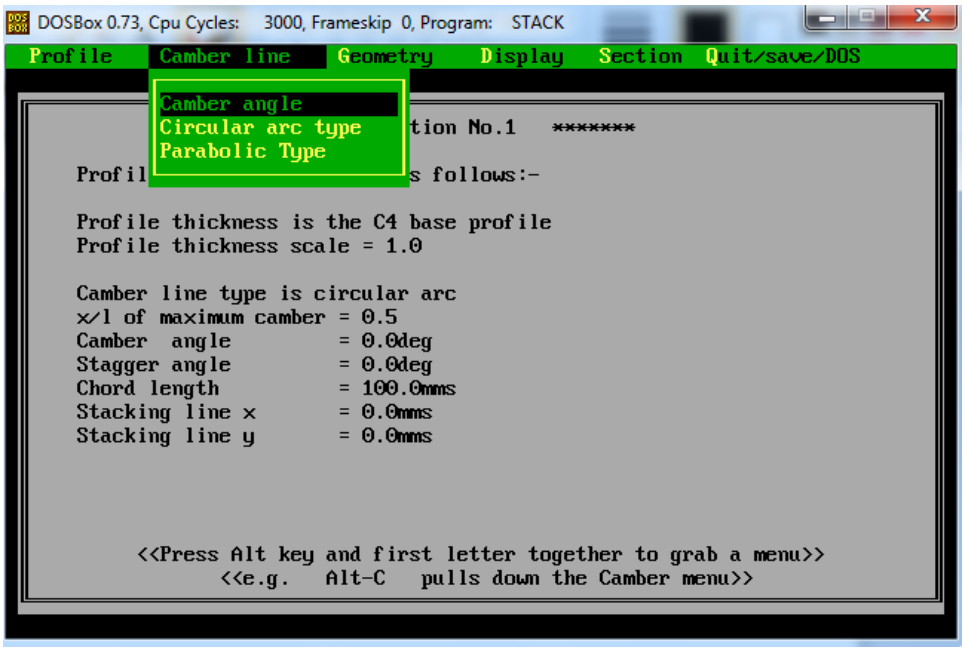

Figure 4.5 GUI of program STACK

The output of STACK is a file with the 2-D (x,y) coordinates of the blade or the vane for each section. In these results is very easy to add the third coordinate z, which is the radii of every profile. Figure 4.6 illustrates the two dimensional graphical representation of 4 blade sections stacked at the center of gravity of each section.

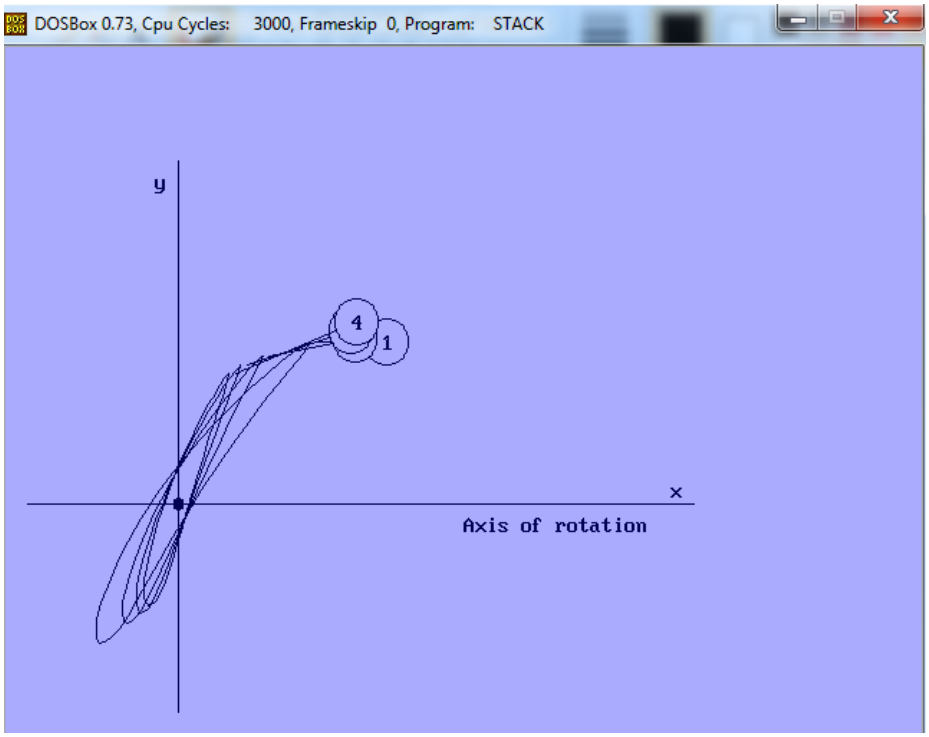

Figure 4.6 2D display of the 4 blade profiles (STACK program)

The STACK code has a few disadvantages that make its use limited:

a. The maximum number of sections is 11, although this number is enough for preliminary design

b. There are limited available airfoil profiles.

c. The results are 2-D, however, as it was explained above, the third coordinate can easily be added using EXCEL.

d. The base coordinates of the available profiles are not many and the profiles especially at the leading and the trailing edges were not perfect. The final points that define the profile of every section are 41 which is a relatively small number of points.

The above mentioned limitations didn't affect the coordinates generation and the blades that were designed using STACK code had acceptable shapes for a preliminary design. STACK was used successfully for the profile creation in many design cases of this project.

4.4 ANSYS Turbogrid

ANSYS TurboGrid is a powerful tool that is focused on rotating machinery analysis. Its main purpose is the mesh creation, while preserving the underlying geometry. These meshes, which are separate files, are used in the ANSYS workflow to solve blade passage flow cases. The main input for this software is the blade geometry which is made up of three files: the "profile.curve", the "hub.curve" and the "shroud.curve". These three files provide the coordinates that define the geometry of the blade, the hub and the shroud respectively.

The user can select the basic features of the mesh and then trim it in order to achieve the most appropriate mesh for a particular case. Figure 4.7 illustrates a stator vane that was created from the coordinates files that were loaded

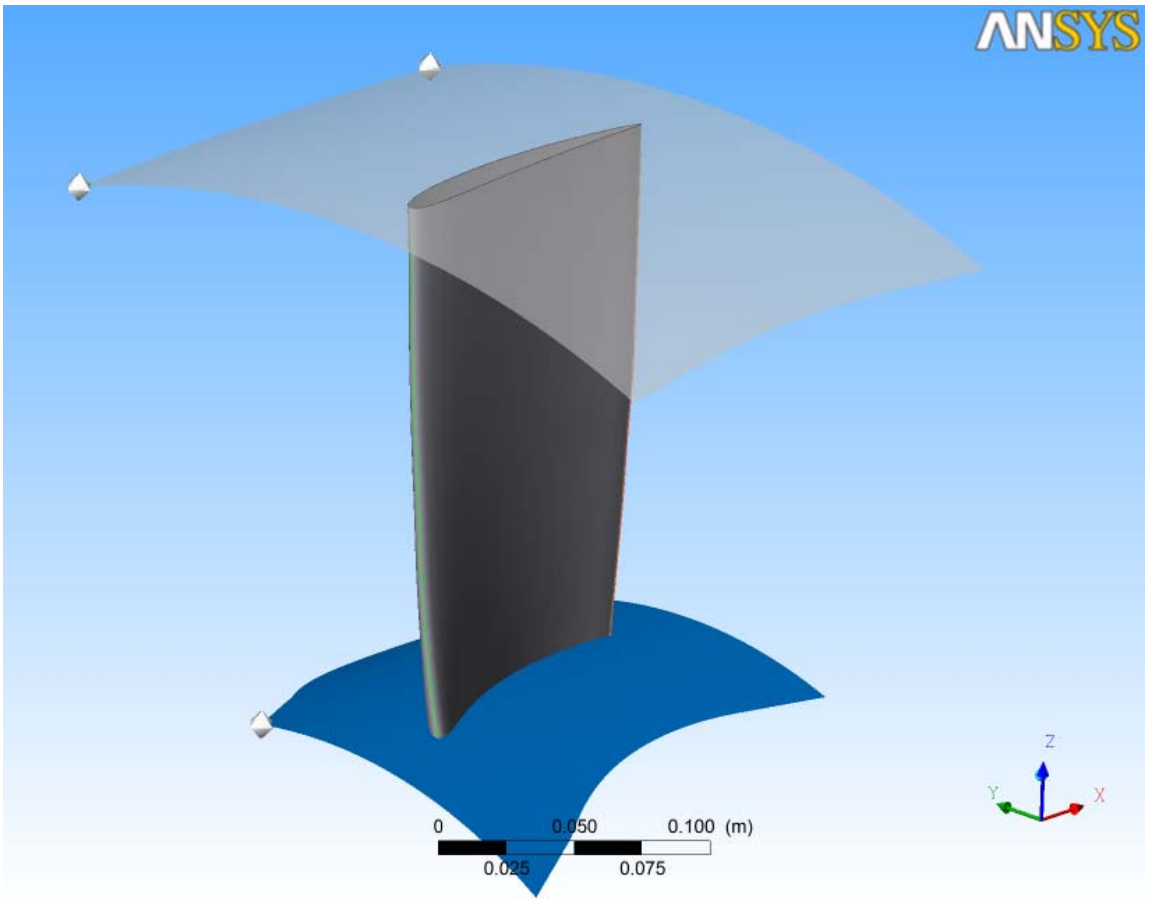

Figure 4.7 Stator vane in ANSYS Turbogrid

4.5 GAMBIT

GAMBIT is also a meshing tool; however the geometry must be created in GAMBIT before the meshing. Its purpose is the geometry (not CAD geometry) and the mesh creation of surfaces and bodies. Domains without rotating parts can be easily designed and meshed with GAMBIT. GAMBIT is used to create geometry and meshes for CFD calculations with FLUENT, which is not developed particularly for rotating components, although rotating machinery cases can be solved with FLUENT. The non rotating domains do not require the complexity of Turbogrid, so they can be created using GAMBIT. GAMBIT needs practice and guidance in order to acquire quick results, but generally it is friendly user software. GAMBIT was used for the geometry and mesh creation of the domain that is illustrated in Figure 4.8.

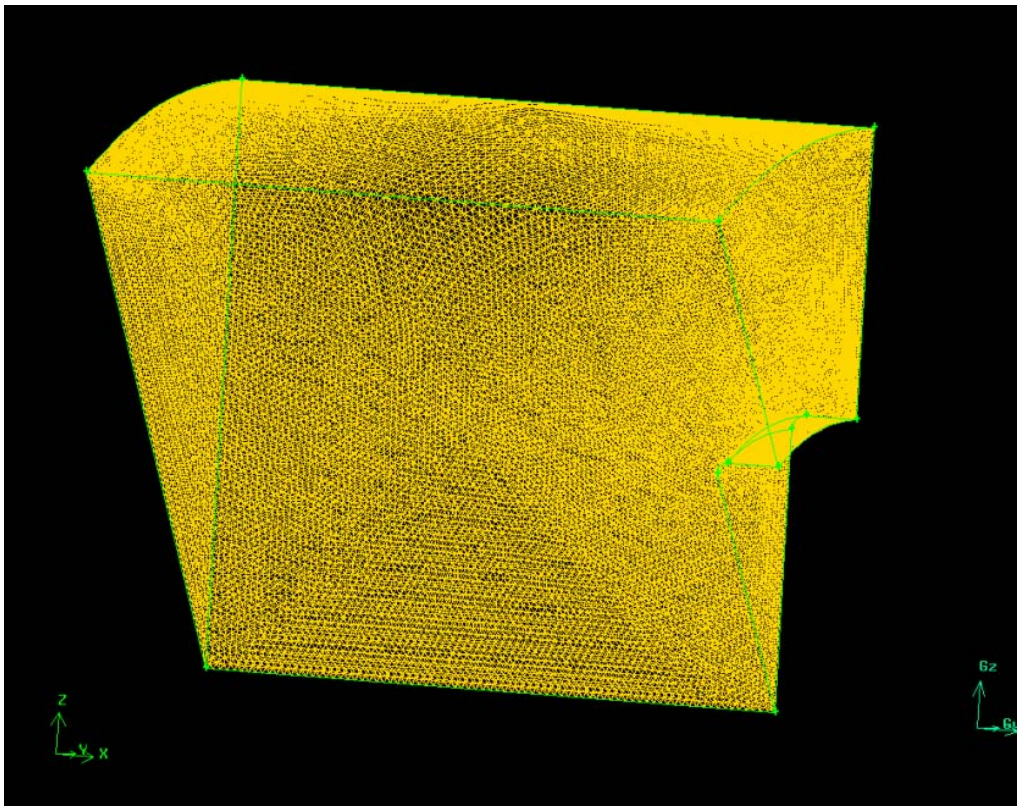

Figure 4.8 Induct domain in GAMBIT

GAMBIT development stopped after ANSYS bought FLUENT. There are no newer versions and updates for this software. Alternative software for meshing is ANSYS Meshing and ICEM.

4.6 ANSYS CFX-Pre

ANSYS CFX-Pre is the physics and solution parameters definition pre-processor for ANSYS CFX-Solver. The meshes are imported into CFX-Pre after being produced in various mesh generators and the physical models are selected for the CFD simulation. The file that is produced is the input file for the CFX-Solver. ANSYS CFX-Pre is used to assembly the domains, set the physics and the boundary conditions and finally set the case before the solver. CFX Pre is a powerful tool which can help the user to create a simulation model relatively quickly by using a specific option for turbomachinery cases. The practice and the guidance are mandatory for the user in order to acquire the necessary experience. Figure 4.9 illustrates a four domain assembly where the boundary conditions are set.

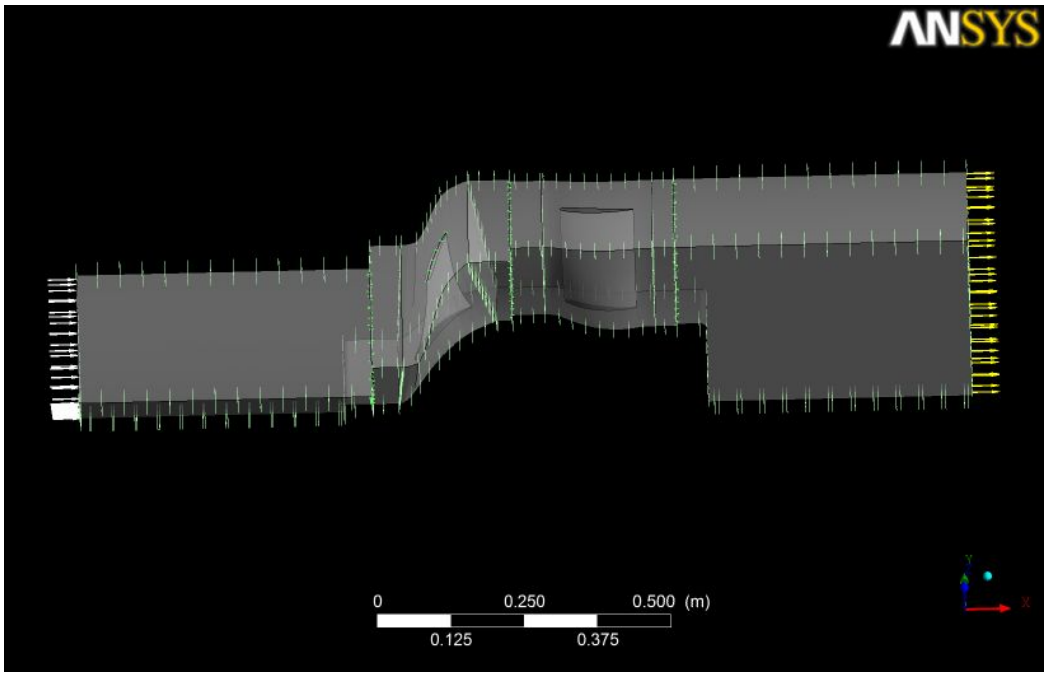

Figure 4.9 Flow domains in ANSYS CFX-Pre

4.7 ANSYS CFX-Solver

CFX-Solver is the CFD solver and allows the user to control the CFX-Solver interactively and view information about the emerging solution. CFX-Solver can be operated from a command line as an alternative and this can be particularly useful for batch mode operations CFX-Solver uses the output of the CFX-Pre.

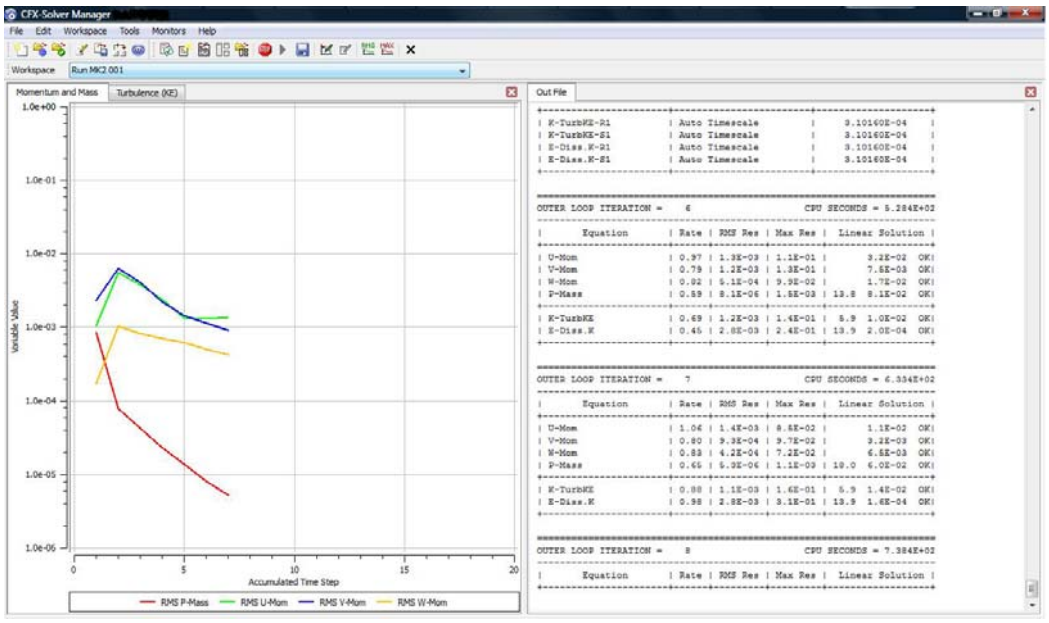

Figure 4.10 GUI of ANSYS CFX-Solver

4.8 ANSYS CFX-Post

CFD-Post is designed to allow easy visualization and quantitative analysis of the results of the CFD simulations. It has a graphical user interface that includes a viewer panel in which all graphical output from CFD-Post is plotted. In CFX-Post there is a “Turbo” option in the same manner as it is found in CFX-Pre. The turbo workspace improves and speeds up post-processing for turbomachinery simulations. The analysis of the results requires extensive experience by the user and of course guidance in order to spot the good and the weak point of the design and find the ways to improve or to implement changes to the fan.

The following Figure 4.11 illustrates the blade to blade view of the relative velocity flow field of a fan stage. The visualization of the flow helps the designer to identify any problems in the design or to confirm a successful design.

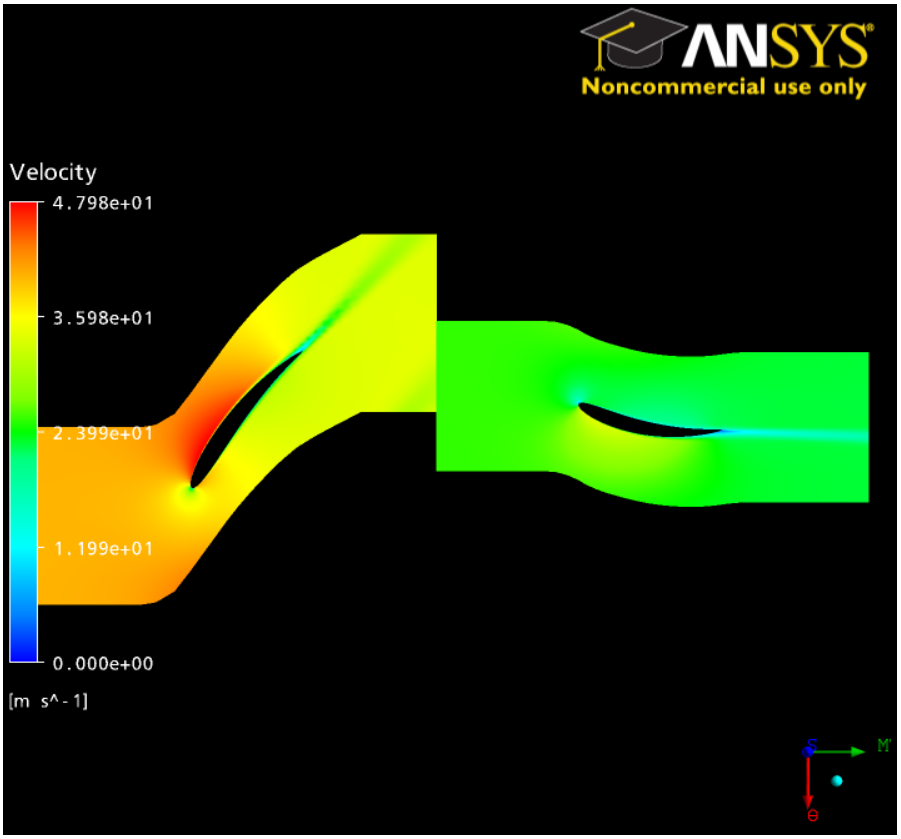

Figure 4.11 Blade to Blade view of the relative velocity field

The chart of Figure 4.12 depicts the pressure distribution over the pressure and suction sides of the blade. The nearly automated production of

such plots simplifies considerable the analysis task.and contributes to the speeding up of the design cycle.

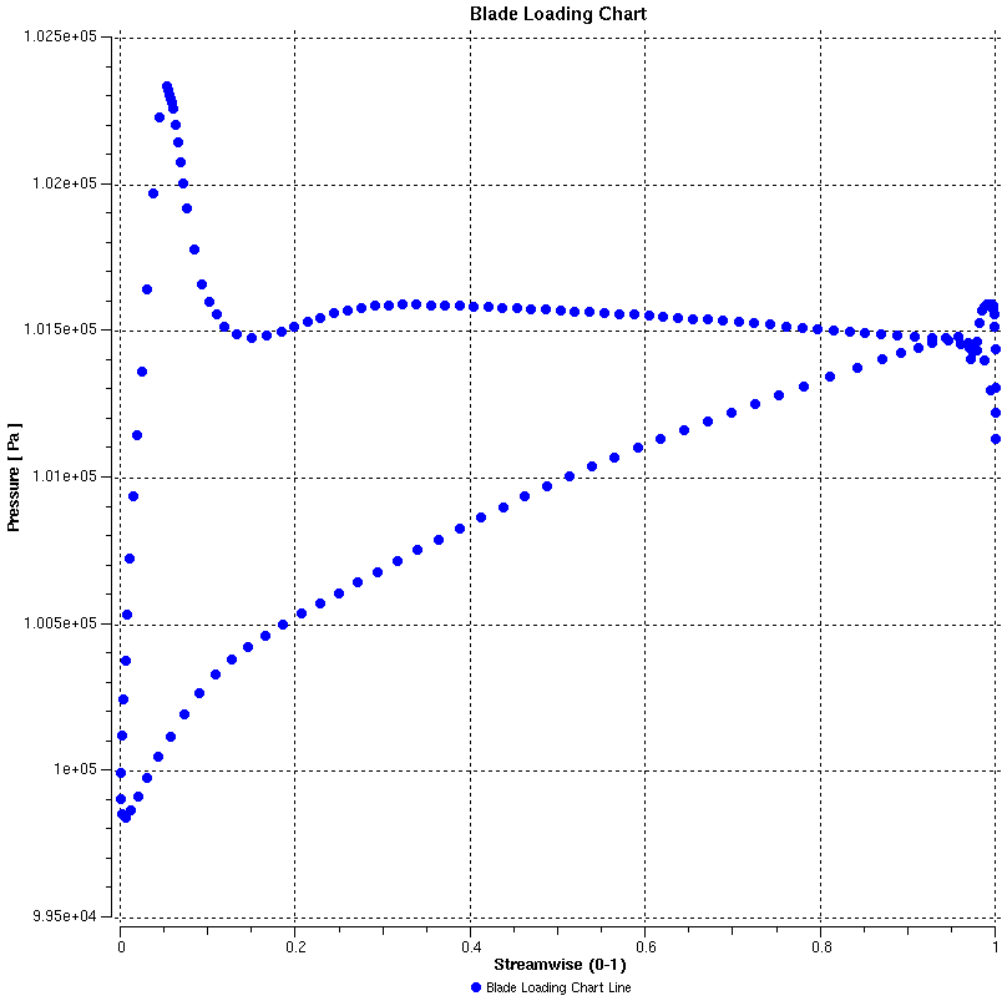

Figure 4.12 Pressure distribution across the blade (pressure/suction side)

4.9 Other MATLAB codes

The tools that were used for this project are presented in this chapter. During the course of this project a few more MATLAB codes relative to fan design were developed.

The first code can calculate the air angles in a vaneaxial fan and produce useful diagrams in order to understand the performance of a cascade. The following Figures are the results of the first program run for a vaneaxial fan with hub to tip ratio = 0.68, φ=0.25 and ψ=0.31.

Figure 4.13 shows the pitch to chord ratio across the radii for the rotor and the stator. The variation of the pitch to chord ratio is high in the rotor and as a result the blade has to be tapered. A tapered blade has a smaller chord as one moves from hub to tip. In contrast there is a small variation of the pitch to chord ratio at the stator.

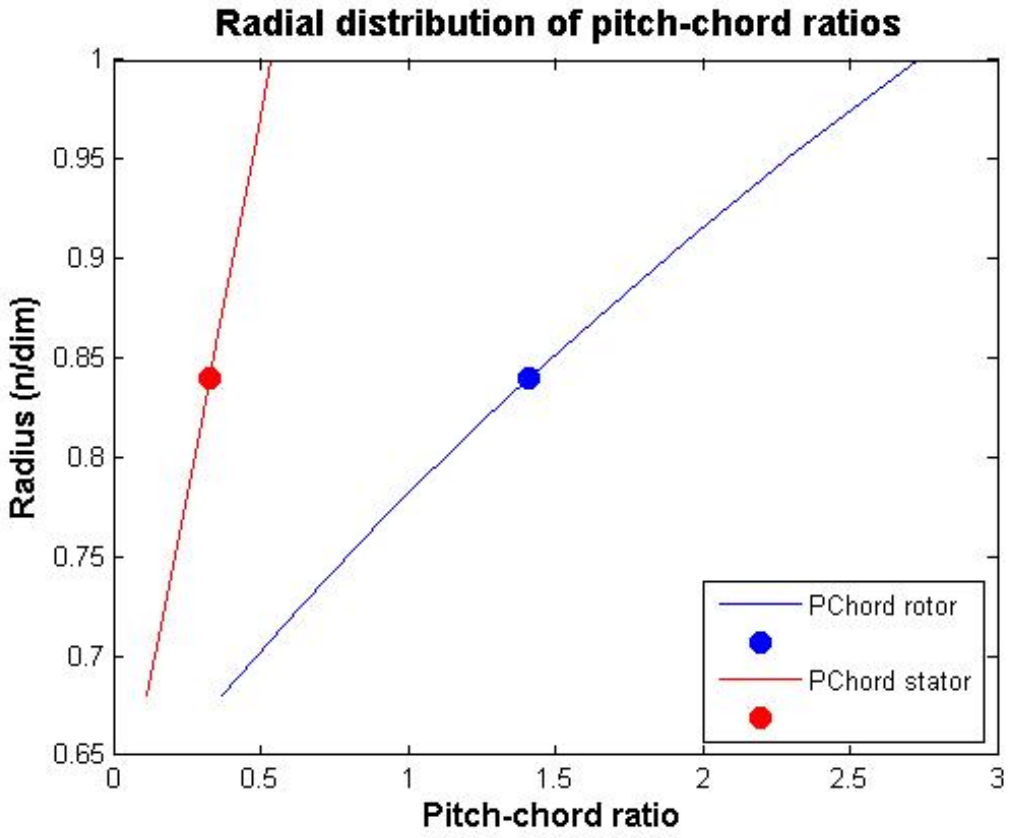

Figure 4.13 Variation of pitch to chord ratio across the radii

In Figure 4.14 the relative velocities angles are illustrated and the swirl velocity angle at the exit of the blade as well. The variation of the air angles (beta1, beta2) across the radii is in a good range according to Figure 2.4. The swirl angle at the exit of the blade is quite high and this proves that the use of downstream vanes improve the efficiency, because they convert the swirl velocity to static pressure rise.

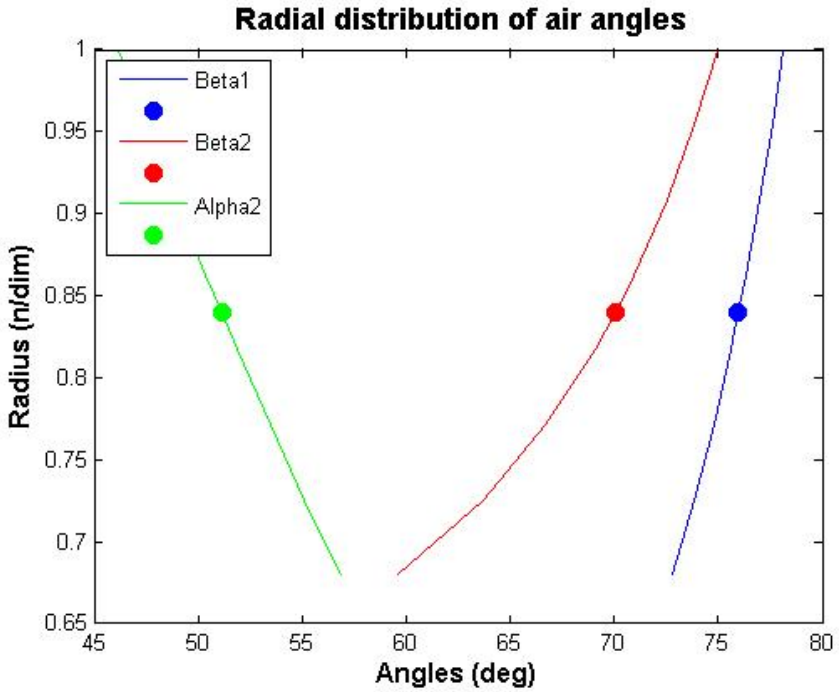

Figure 4.14 Variation of relative velocity angles across the radii

Figure 4.15 depicts the variation of the reaction across the radii is illustrated. The range of reaction is from 0.76 at the hub to 0.89 at the tip. The reaction range are inside the literature limits 0.7-0.9 (McKenzie, 1997).

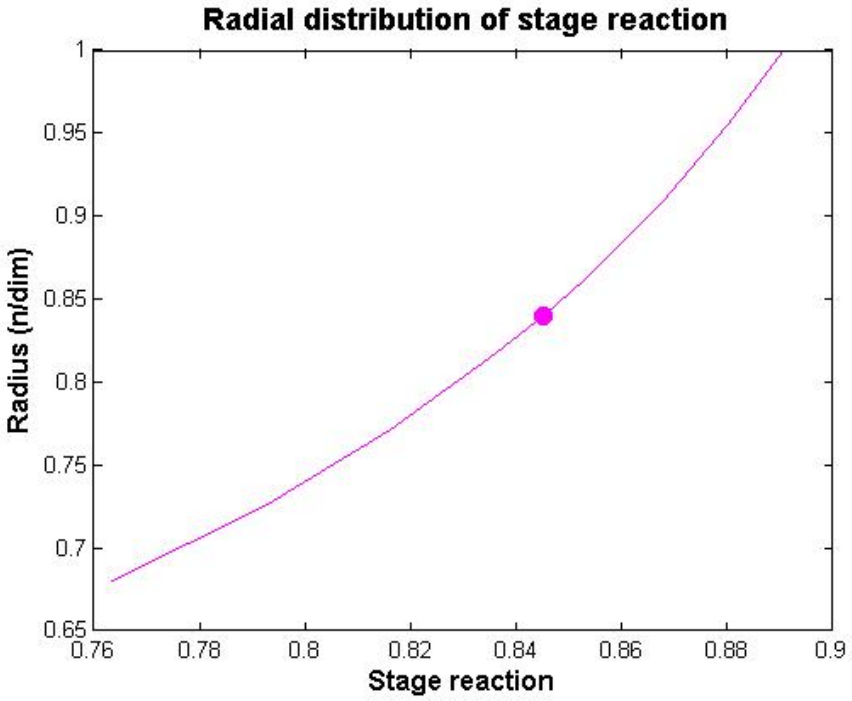

Figure 4.15 Variation of stage reaction across the radii

Figure 4.16 shows the distribution of the flow and work coefficients across the radii. Both values decrease as we move from hub to tip.

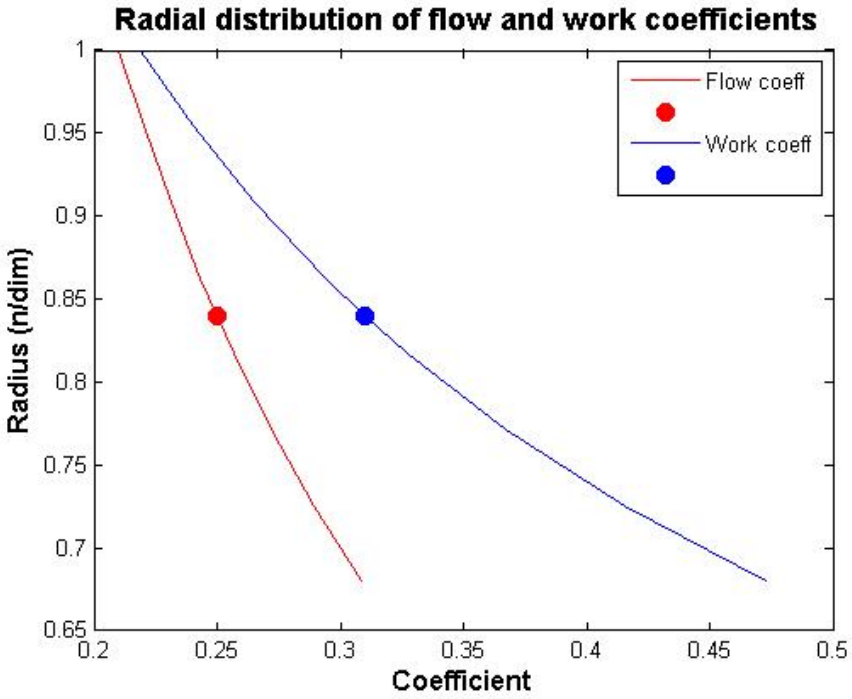

Figure 4.16 Variation of work and flow coefficient across the radii

One more output of this MATLAB code is also a table with values for the design variables. The input data appear first and then the variation of the coefficients and reaction across the radii.

Another MATLAB code was created in order to help in the creation of the profile coordinates for the NACA65 airfoil series. The inputs of this code are the camber and the maximum position of the camber and the output is a file with the coordinates of the profile.

A similar MATLAB code was also developed for the extraction of the lift and drag coefficient of every airfoil for different Reynolds numbers. The inputs are the camber, the position of the maximum camber and the Reynolds number and the output is the Cl and the Cd and the angle of attack respectively.

4.10 ANSYS-Mechanical

The mechanical integrity of the new designs is examined using the Static-Structural module of ANSYS. The geometry can be created or imported

and then meshed. The boundary condition and the loading conditions which can be thermal or mechanical gradients are set. The outputs of the software are the deformation and the stress field which are very useful in order to estimate the mechanical integrity of the fan. The visualization of the results that is illustrated in Figure 4.17 is another important feature of the software, because the designer can review the results more efficiently.

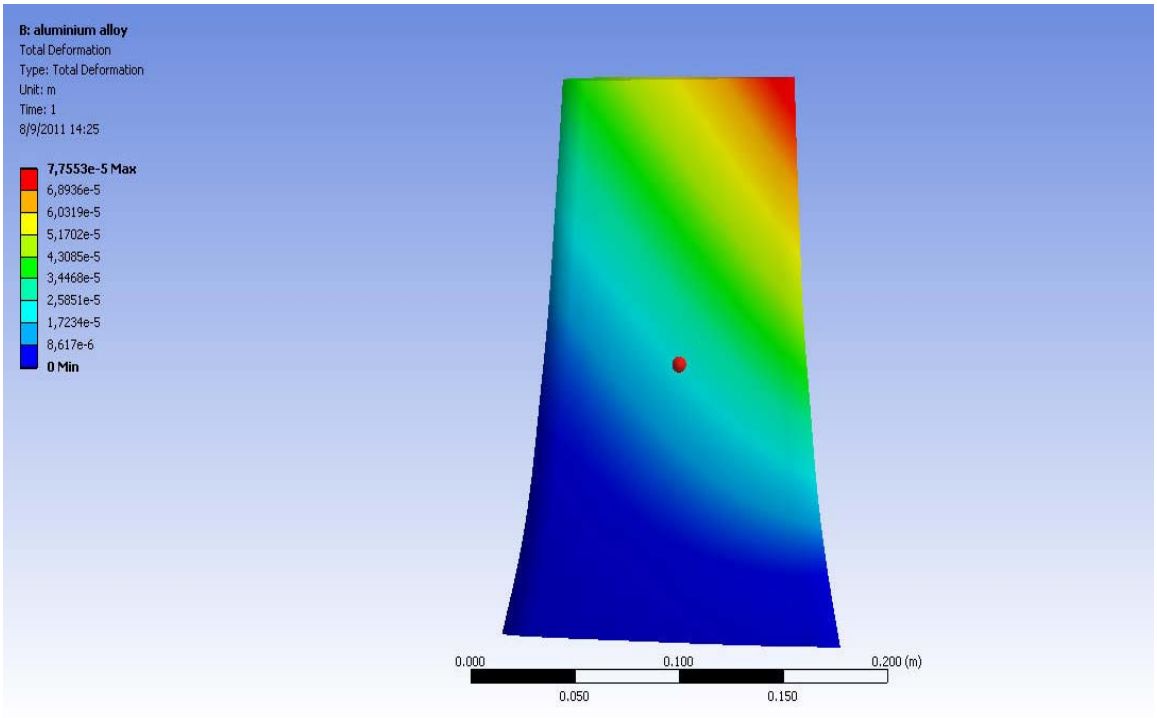

Figure 4.17 Blade deformation for normal operating conditions for aluminum 6061-T6

5. McKenzie's Method Validation

5.1 Introduction

In this Chapter an attempt is made to simulate the performance of a fan that was designed according to McKenzie's method. The target is then to compare McKenzie's method results with the output of a CFD analysis.

As it was mentioned in the Chapter 3 the McKenzie method is the most appropriate method for the design of the new fan. The preliminary design of an industrial fan is presented by McKenzie, 1997.

The preliminary design of an industrial vaneaxial fan is analyzed step by step and the target of this analysis is to evaluate the results using CFD. According to McKenzie's example the design procedure starts with the specifications of volume flow, pressure drop, size and rotational speed and the outcome of the process is the blade and geometry features of the vaneaxial fan.

The concept of the method comparison using CFD is simple. The blade and geometry features which were the outcome of McKenzie's preliminary design will be used to create the geometry of the fan for the high fidelity 3-D simulation. After creating the geometry, CFD can be used to solve the flow field and acquire the performance of the fan that came from the high fidelity 3-D simulation. The final step is to investigate if the high fidelity 3-D simulated performance of the fan meets the requirements that were used for the preliminary design of the fan.

The results of this investigation will show how reliable is McKenzie method and if a fan can be designed efficiently according to this method. When it comes to the final conclusion it is going to be taken into account that McKenzie's procedure refers to a preliminary fan design and it is not a final design. Many simplifications and assumptions were made during the procedure which affected the performance of the fan.

5.2 McKenzie's example

The specifications are usually requirements of the client. The inputs for this example are the following:

1. Volume flow : 5 m^3/s

2. System Duct diameter : 0.75m
3. Duct System pressure drop : 500Pa
4. Fan rotational speed : 1500rpm

Many assumptions need to be made in order to obtain a proper solution for the preliminary fan design:

1. Diffusion efficiency : 80%
2. Static pressure recovery : 80%
3. Total to total pressure rise efficiency : 85%
4. Tip clearance : 2% of blade span

A few more considerations and assumptions were made during the procedure in order to improve the design like the approximation of the number of the blades and the vanes, the taper of the blade etc.

The final result was the design features of the fan which are the rotor blade geometry and the stator vane geometry. In particular these features are the following:

1. Hub to Tip ratio
2. Number of Blades/Vanes
3. Airfoil specifications
4. Blade metal angles
5. Camber angle for every profile
6. Stagger angle for every profile
7. Chord length for every profile

All the above geometry features are necessary in order to build the model of the vaneaxial fan.

5.3 Geometry creation

The definition of the geometry was the first step for the problem set up. The next step is the creation of the geometry of the flow region and the whole the computational domain for the CFD calculations.

The geometry of the blade and the vane was created using the Lewis program STACK that was described in Chapter Design tools. The inputs for this software is the camber angle, the position of maximum camber, the stagger angle, the chord, the profile thickness and the maximum thickness

position of 4 profiles from hub to tip. All these data were the results of preliminary design in McKenzie's example. The airfoil that was used was the C4. Figure 5.1 illustrates the 4 section of McKenzie's blade that are stacked in their center of gravity

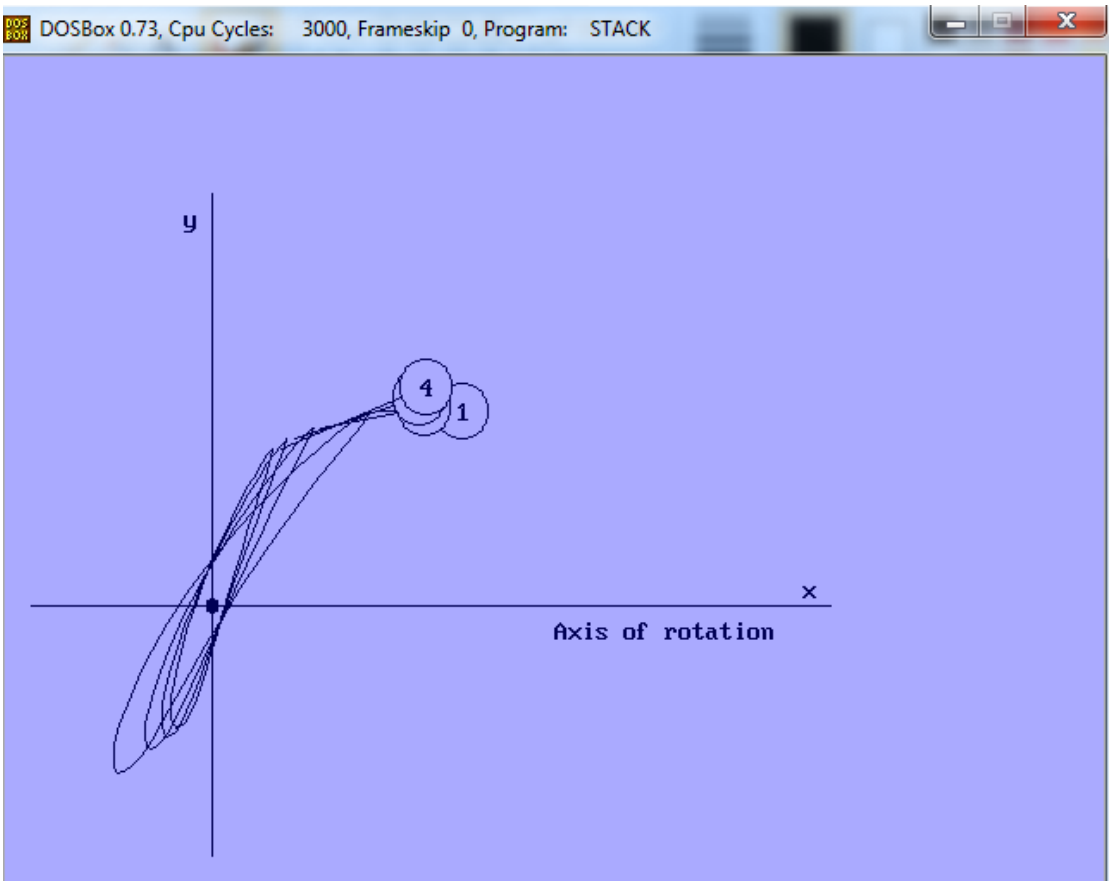

Figure 5.1 2D display of the 4 blade profiles (STACK program)

The output of STACK is a text file with the 2D coordinates (X, Y) of the 4 profiles from hub to tip. The third dimension Z, which is the span, was added to create the 3D design of the blade and the vane. Two more text files were written one for the hub and the other for the shroud.

The final output of this procedure was the definition of the coordinates of the blade, the vane and their hubs and shrouds with 6 text files (3 for the blade and 3 for the vane). A small modification of these text files was made in order to have the appropriate format for the next step.

The same coordinates came up using the MATLAB code that was described in Chapter 4. The output of the MATLAB code is visualized in figure 5.2 For this case it was the data from Lewis software that was used.

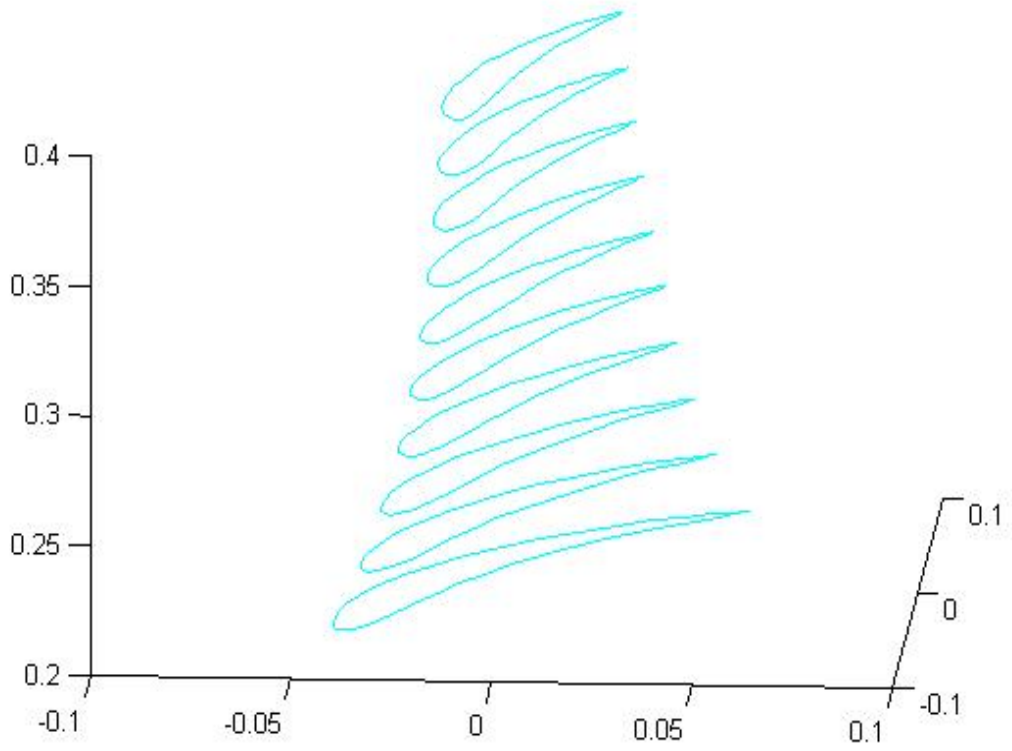

Figure 5.2 3D plot of the blade using MATLAB code

It is important to mention that the final design has one domain for the rotor and one domain for the stator, which means that no domains for the inlet and the outlet were defined separately. In McKenzie's example there was no reference for the existence of an inlet domain or an outlet domain, so the design for the CFD calculations has two main domains. Although no separate domains were defined for inlet and outlet, Turbogrid creates a small domain for the inlet and the outlet in order to be easier to set the boundaries and the properties at inlet and outlet.

The next step is the creation of the blade and vane and their domain. ANSYS Turbogrid is the software that was used to accomplish this task. For the creation of the blade and the blade domain the 3 text file were imported in Turbogrid. The bspline option was selected for the curve type and the surface type. The number of the blades was entered manually in Turbogrid and a few more parameters were adjusted properly. The tip clearance which consists a very important parameter was set in Turbogrid as well. The blade is illustrated in figure 5.3 along with the hub and the shroud.

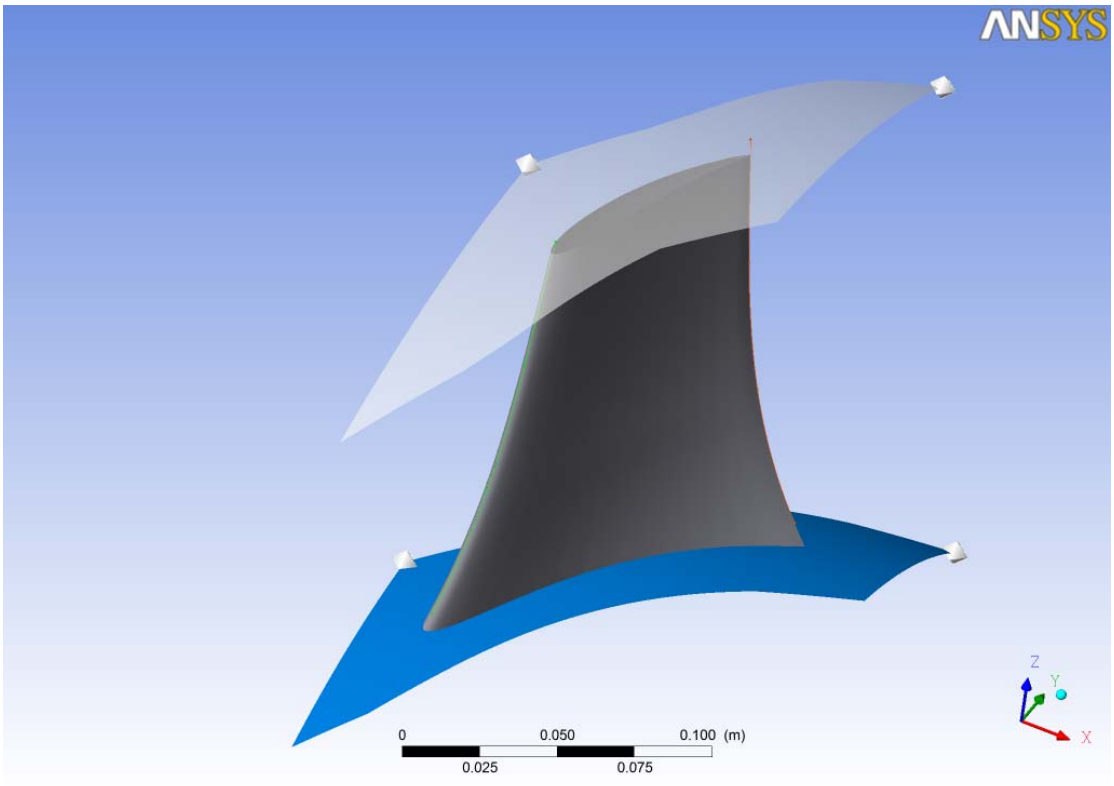

Figure 5.3 Representation of the blade, the hub and the shroud in Turbogrid

5.4 Meshing

ANSYS Turbogrid was used for the meshing of the domains as well. During the pre-process stage the grid generation constitutes one of the most important steps after creation of the geometry. It is required to subdivide the flow domain into smaller subdomains which are not overlapping each other. The flow physics are solved within the domain geometry that has been created. The result is the generation of the mesh which is made from small cells.

The method for the topology definition of the grid was the H/J/C/L-Grid and an O-Grid was included with a width factor of 0.5. For the tip topology the H-Grid Not matching was selected. For the first approach, a fine mesh size was selected with a target of 200.000 nodes and the option normalized was selected for the near wall size specification. The impact of the size of the mesh was later investigated to prove the independence of the result from the size of the mesh. The stator domain mesh in Turbogrid is depicted in figure 5.4

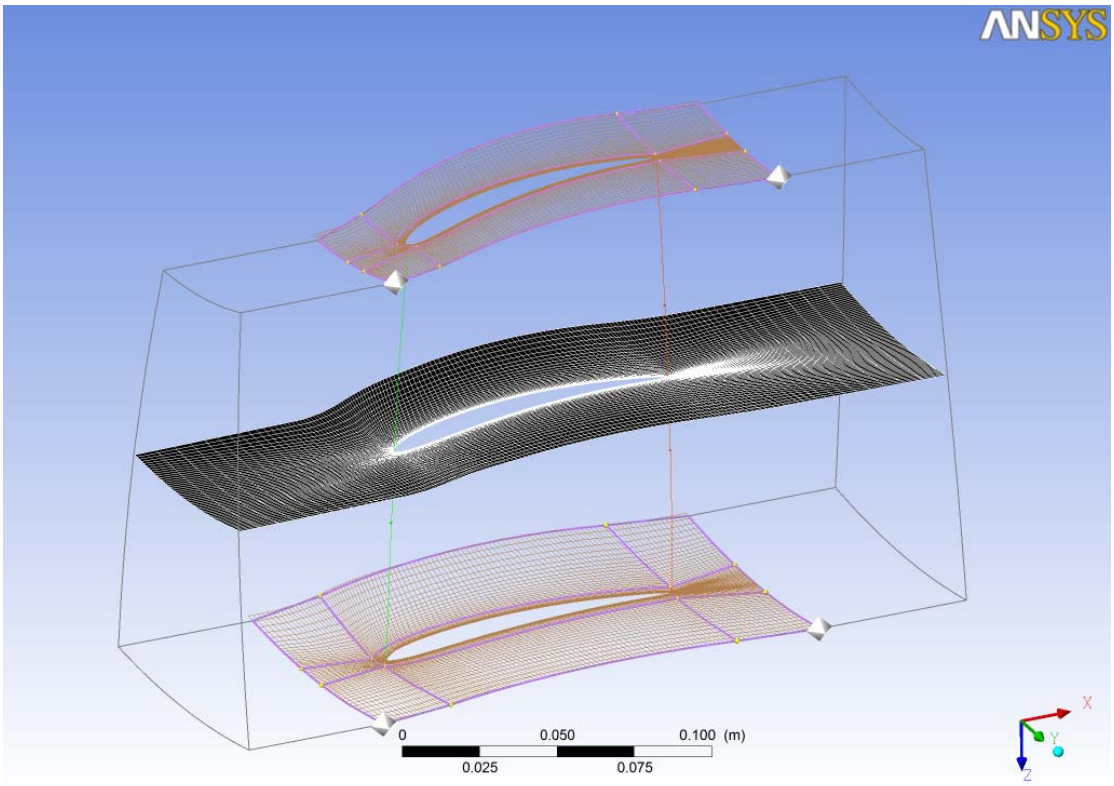

Figure 5.4 Representation of the stator vane mesh

5.5 Physics and Fluid properties - Boundary Conditions

The two domains (rotor domain and stator domain) were imported to ANSYS CFX-Pre in order to continue the solution of the fluid flow by defining the physics and the boundary conditions. The option "turbo mode" was selected for the set up, which is a special mode, allowing users to set up turbomachinery simulations. One of the main advantages of turbo mode is the automatic setup of the boundary regions and conditions.

The physics selection is the first step to set up the case. The simulation is a viscous steady state simulation. There is no heat transfer and the viscous model that was selected is the k-epsilon model. The k-e turbulence model offers a good compromise between numerical effort and computational accuracy and uses always standard wall functions for the near wall treatment.

It is very important for the setup the definition of the inputs at the inlet and the outlet. CFX-Pre offers many choices for the boundary template. For this particular simulation the Total Pressure was selected at the inlet and the Mass Flow at the outlet. The static pressure at the outlet and the velocity at the inlet are part of the solution, whereas total pressure at inlet and mass flow

at outlet are inputs. This selection was made , because according to the CFX manual it gives is a robust simulation model. The inlet that draw flow in from the atmosphere uses a Total Pressure = 0 boundary condition (e.g. as an open window) while the reference pressure at the domain in 101325Pa. This choice can produce more accurate solution, because with this choice a 200Pa increase in the pressure is for example from 300Pa to 500Pa (more than 50% increase), whereas in the case where the reference pressure is 0 and total pressure is 101325, a 200Pa increase would be for example from 101325 to 101525 (less than 1% increase).

The interface of the two domains was defined as "stage". The stage model performs a circumferential averaging of the fluxes through bands on the interface. Stage model allows steady state predictions to be obtained for multi-stage machines. This model allows steady state predictions to be obtained for multi-stage machines. The Stage model usually requires more computational effort than the Frozen Rotor model to converge.

The boundary conditions (inlet, outlet, periodic, wall, symmetry) were added automatically and after checking that this automatic procedure is correct, the total pressure, the reference pressure, the relative pressure, the mass flow and the rotational speed were set respectively to the domains and the subdomains. The simulation domain in CFX-Pre and the boundary condition are shown in figure 5.5

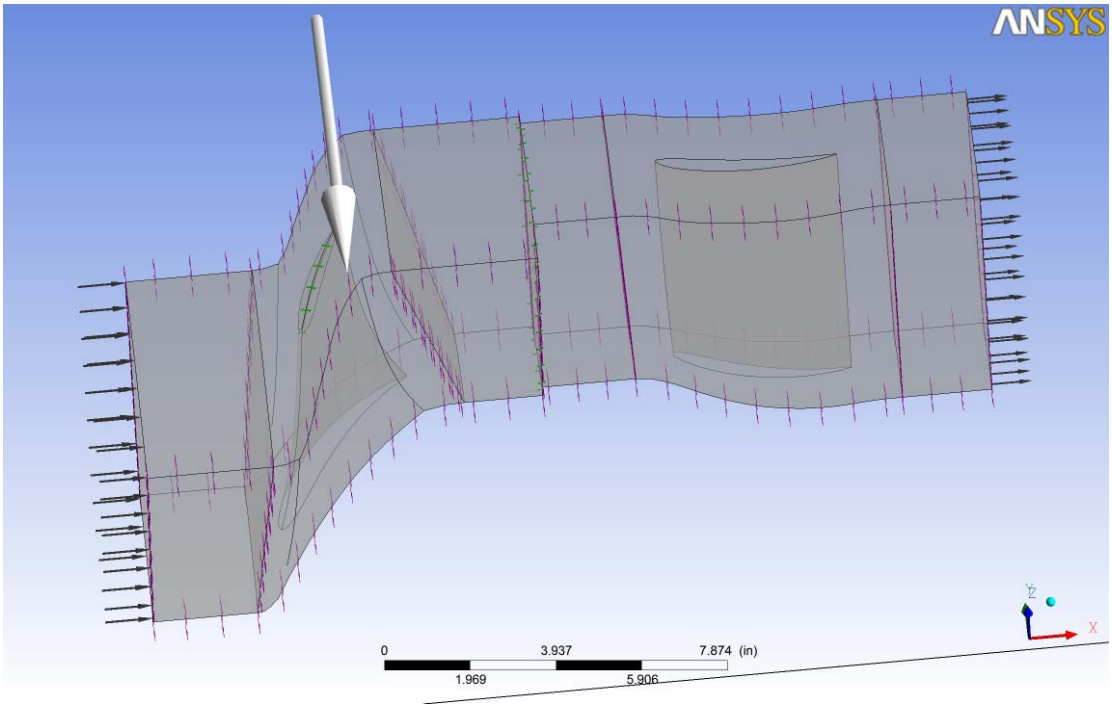

Figure 5.5 Simulation domain (rotor and stator)

5.6 Solver

Another advantage of the "turbo mode" is the auto initialization. The basic settings for the solver control are the convergence control and the convergence criteria. The choice for convergence control was the maximum iterations for this simulation (1000 iterations) and the choice for the convergence criteria was the RMS (residual target 10^{-6}). Other choices for the solver were the high resolution for the advection scheme and the first order for the turbulence numerics.

5.7 Results report

The main result from the high fidelity 3-D simulation is the total pressure rise at the fan. As it was mentioned earlier the mass flow, the rotational speed and the inlet pressure were input data according to the boundary template that was selected, whereas velocity at inlet and the pressure at outlet are results of the simulation.

The simulation converged in less than 300 iterations as it is illustrated in figure 5.6, which means that the model was very well defined and the mesh was appropriate and successful.

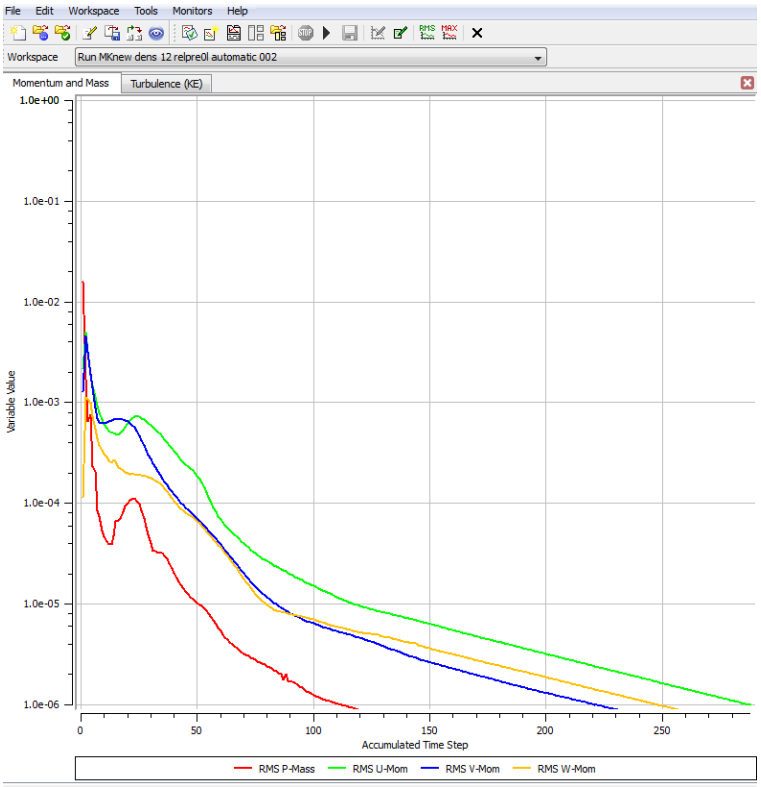

Figure 5.6 Convergence plot

The total pressure at the outlet of the stator domain was found to be 368Pa. The total pressure at the inlet of the inlet of the rotor was set at 0 so the total pressure rise at the fan was **368Pa**.

An interesting part of the results except the pressure magnitude is the fluid flow around the blade and the vane. It is important to check the flow in areas where separation and other disturbance is expected. ANSYS CFX-Post was used to acquire all the above data.

CFX-Post has the turbo option which is very useful for the quicker manipulation of the results. Very representative 3D plots of the flow can be easily generated with the "blade to blade" option. The position that were selected to represent the flow field are the hub (0.1 of the span) the middle (0.5 of the span) and the tip (0.9 of the span)

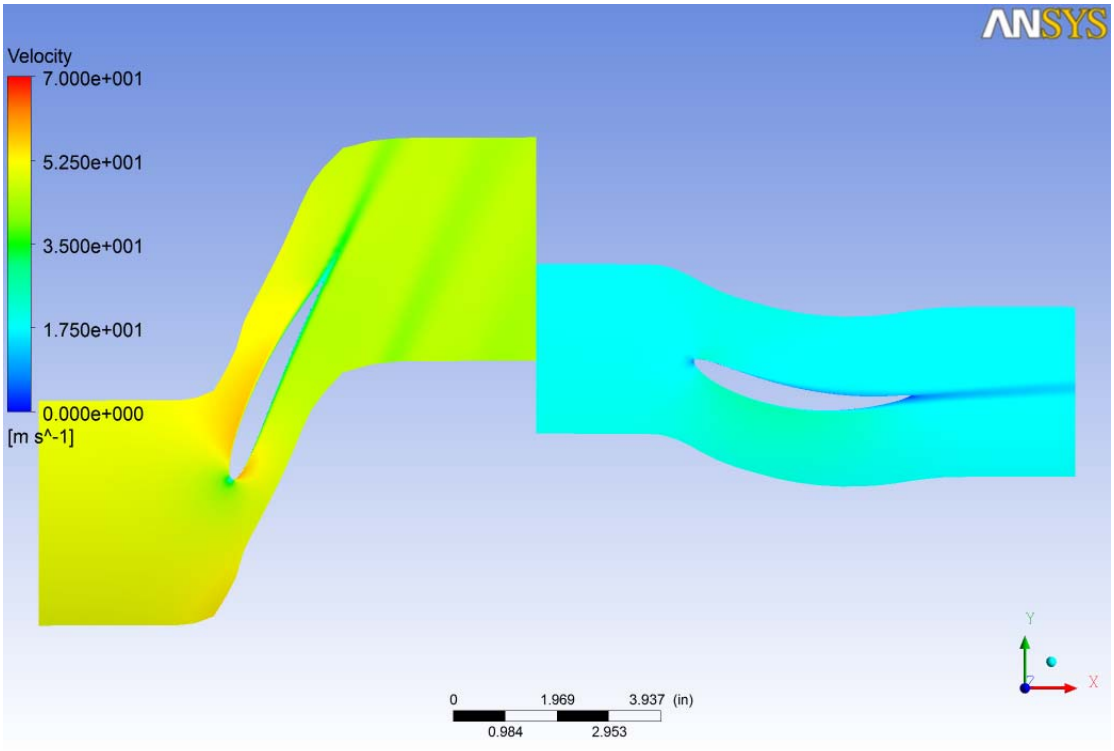

Figure 5.7 Velocity contours at 0.1 of the span

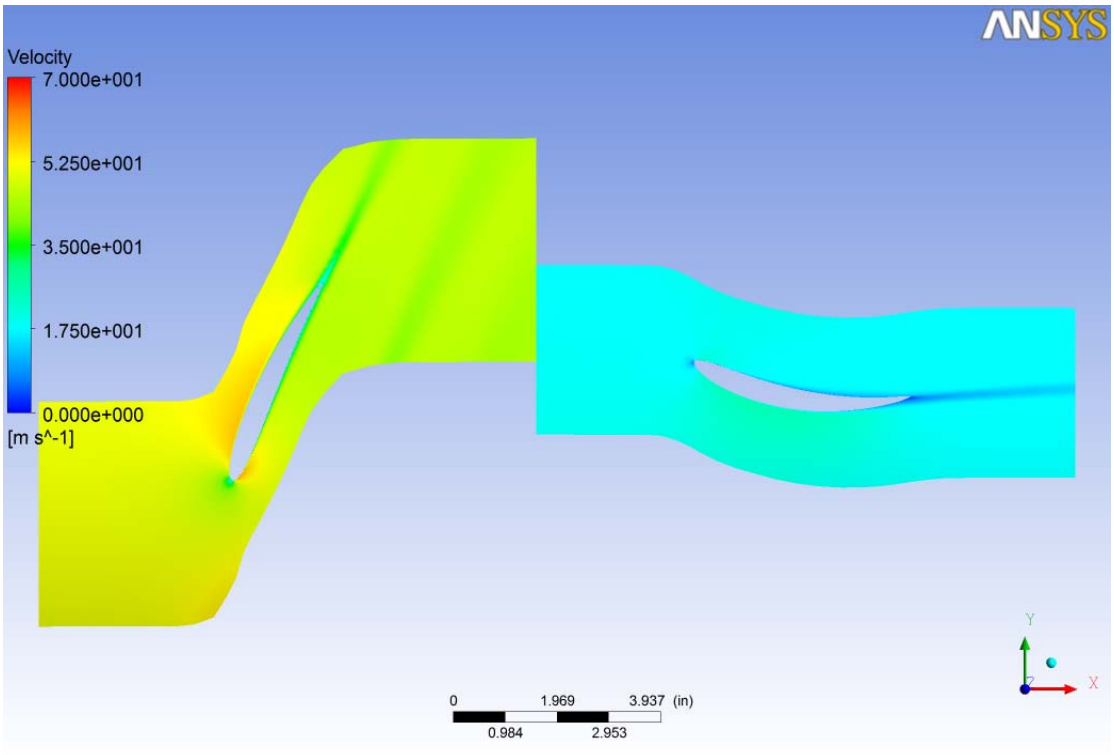

Figure 5.8 Velocity contours at 0.5 of the span

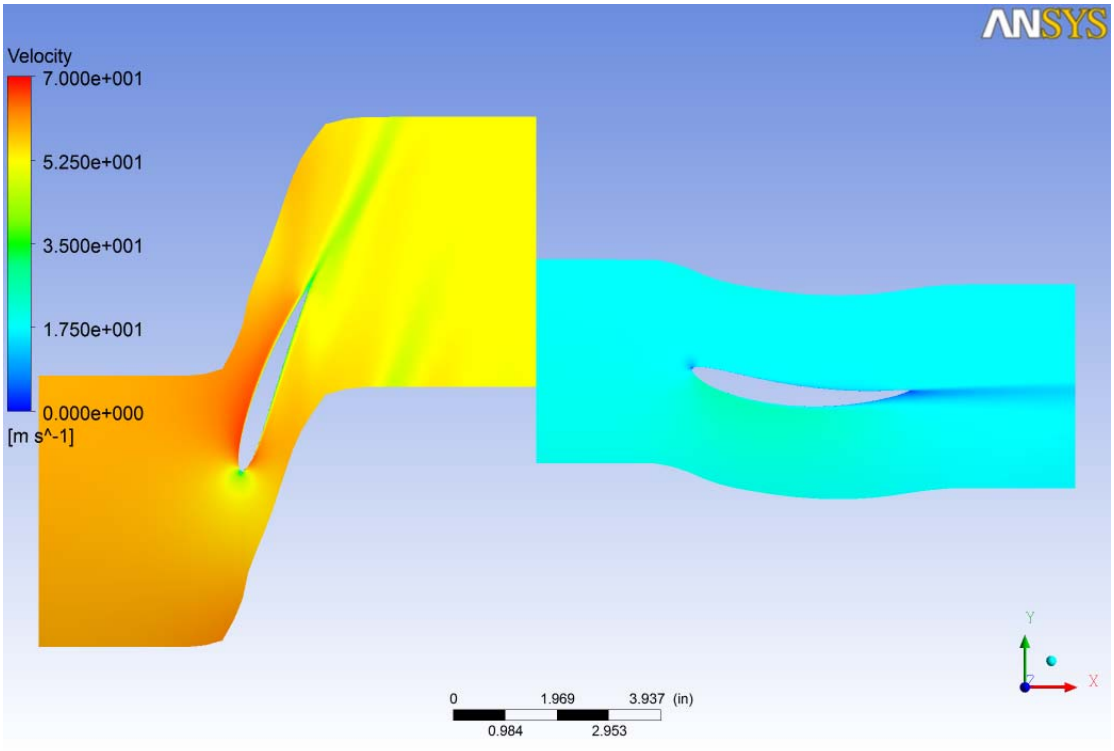

Figure 5.9 Velocity contours at 0.9 of the span

From the above figures it is clear that the design fulfills the requirements of the specification. The flow is smooth around the blade and the vane and there is no sizeable separation. The downstream guide vanes are beneficial in terms of fluid flow at the outlet. They were used in order to remove the high rotational component of the velocity at the exit of the rotor. There is no whirl at the outlet flow so all the rotational component of the velocity was converted to useful pressure rise.

This is even more obvious at the next figure where the velocity vectors are plotted at the 0.1 of the span. The high angle of the velocity at the inlet of the vane can be observed, but after the flow passes the vane, the flow is horizontal.

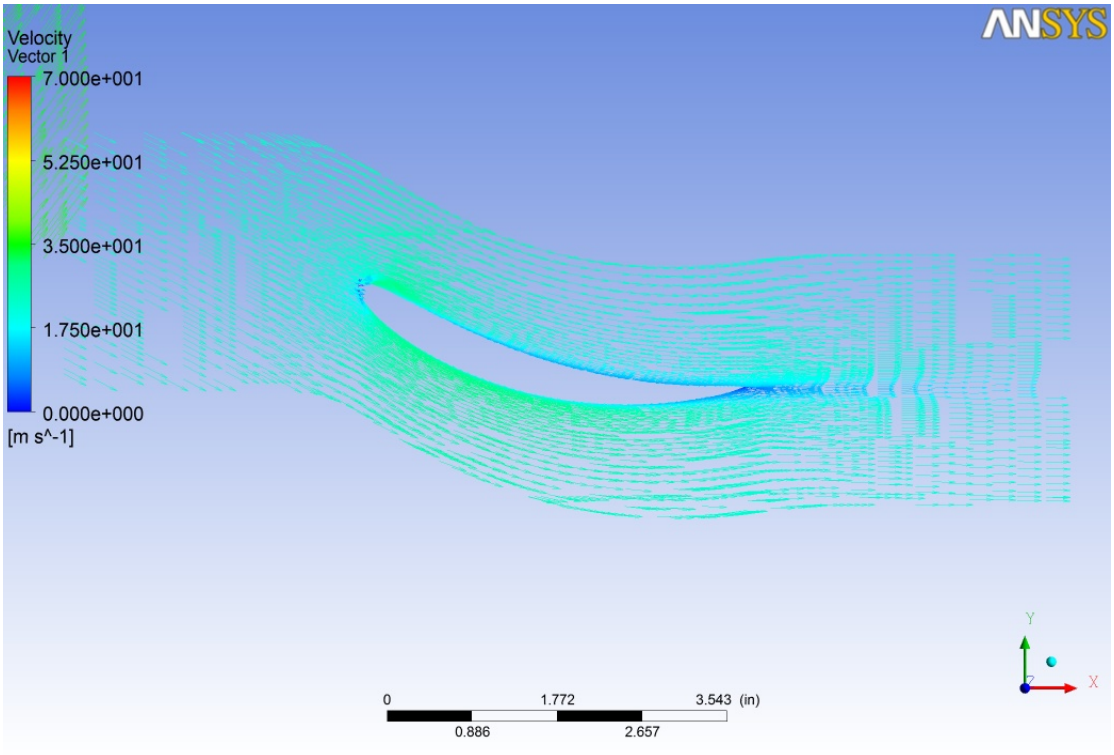

Figure 5.10, Velocity Vector Diagram at 0,1 span

5.8 Validation-Verification of the results

For a CFD solution to be credible, it is important to check the results in many ways. This step can be accomplished through the verification and validation procedure. Verification and validation procedures are the means by which a CFD solution can be properly assessed through distinct procedures.

Verification can be defined as a process for assessing the numerical simulation uncertainty and when conditions permit, estimating the sign and magnitude of the numerical simulation error and the uncertainty in that estimated error [Tu et al, 2008]. A major part of the verification process is to carry out a mesh dependency study. By this means it is investigated the impact of the mesh size (coarse or fine) to the results.

For this particular case the performance of two more models was investigated. In the first model the mesh of its domain had the half size (100k) of the original mess (200k). In the second case the mesh of its domain had the double size (400k) of the original one (200k). The total pressure rise in all three cases is illustrated on the next table

Table 5.1 Mesh Dependency Study

All Domain mesh size (elements)	Total Pressure Rise (Pa)
262,954	**366**
504,364	**368**
995,320	**372**

The above values of total pressure rise for different mesh sizes prove that the results are not mesh dependent.

The validation can be defined as a process for assessing simulation model uncertainty by using benchmark experimental data and when conditions permit, estimating the sign and magnitude of the simulation modeling error itself [Tu et al, 2008].

In this particular case there are no experimental data, so the results cannot be validated this way. The only results that can be compared with the high fidelity 3-D simulation results are the results from the low fidelity 1-D simulation. As it was mentioned earlier in this Chapter the geometry of the fan that was used at the high fidelity 3-D simulation is based on McKenzie fan preliminary design method and the initial requirements of volume flow, total pressure rise, fan size and rotational speed.

The performance of the fan is expected to be similar with the performance that McKenzie's fan has. Since the mass flow, the rotational speed and the size are inputs at the high fidelity 3-D simulation the only variable that can be checked is the total pressure rise.

McKenzie's fan was designed in order to provide a total pressure rise of **500Pa.** The total pressure rise from the CFD simulation is **372Pa** which is **25% less** than the expected performance. This divergence is mainly due to

the fact that the high fidelity 3-D simulation is a more reliable method because it calculates the flow field more precisely than the low fidelity 1-D simulation and it is more thoroughly examined in the next paragraph.

5.9 Results evaluation

The divergence of the high fidelity 3-D simulation results with the results of the he low fidelity 1-D simulation is significant and a few comments can be made about this:

a. The total pressure rise from the high fidelity simulation is less that the low fidelity one and this can be due in the following reasons:

1. The high fidelity 3-D simulation model includes more loss factors than the low fidelity 1-D model.

2. The low fidelity 1-D model takes into consideration less loss factors.

b. Since the flow is smooth in the high fidelity 3-D simulation model that means that there are no extra losses that are due to the flow (separation) and the model fulfills the flow requirements. Therefore the blade angles are proper and manipulate the flow effectively.

c. The high fidelity 3-D simulation model takes into consideration the turbulence of the flow by using the k-e turbulence model. Turbulence causes energy losses especially close to the boundary layer and these losses are not taken into account at the low fidelity process.

d. The 3D effects at hub and tip which have serious impact at the performance of an axial fan, because they increase the losses (Bass, 1987).

e. The interaction of two consecutive blades, because of the small distance between them, which restrict the development of the full lift forces and thus decrease the performance (Bass, 1987).

f. The tip clearance effect cannot be simulated in the low fidelity 1-D simulation. The tip clearance as it was discussed earlier has a major negative impact in the fan performance

5.10 Conclusion

In this chapter an attempt was made to create a high fidelity 3-D simulation model based on a known preliminary fan design, which was calculated according to McKenzie's blade design method, in order to investigate if it is viable to design vaneaxial fans following this method.

There is a significant divergence in the performance between the low fidelity 1-D simulation model and the high fidelity 3-D simulation model. This divergence is due to many reasons that were explained in paragraph 5.9, but the fact is that a vaneaxial fan can be designed according to this method even if the low fidelity 1-D simulation performance does not entirely match the high fidelity 3-D simulation model which is closer to the real performance. The low fidelity 1-D simulation is used to acquire an initial solution that can be later improved using the CFD analysis tools.

The target of this Thesis is to design of a vaneaxial fan with a specific performance and a better efficiency than the performance of an existing model. The above procedure proved that it can be designed, but it should be taken into account that the performance of the high fidelity 3-D simulation model which is going to be closer to the performance of the real model, will be worse than the performance obtained from the low fidelity 1-D solution.

6. New Designs

6.1 Introduction

In this Chapter the process leading to the design of a fan with an improved efficiency compared to the datum vaneaxial fan is described. The dimensions of the fan and the fan characteristics can be obtained from the specifications. The requirements are the volume flow, the size and the pressure rise. The dimensions and the characteristics of an axial fan consist of the following:

1. Outside diameter
2. Hub to tip ratio
3. Number and width of blades/vanes
4. Blades/vanes angles
5. Blade/vanes curvature
6. Fan speed

The design tools that were presented in Chapter 4 and the design procedure that was analysed in Chapter 3 and validated in Chapter 5 were used to accomplish this task. The CFD simulations are the main part of this project. The fan design theory is applied in order to build the simulation model, but only after the post processing of the results from the CFD simulations, can be it concluded if the design theory was correctly applied to design a fan with a fan with a respectable performance.

Three new designs were developed and each design derived from the experience of the previous one.

The analysis procedure for each new design takes place as follows:

1. Geometry definition

2. Domain creation

3. Mesh Generation

4. Domain Assembly

5. Physics set up, boundary definition

6. Case set up

7. Results for the design point

8. Design Optimization

9. Results for the optimized design at design point

10. Off design performance

11. Tip clearance effect

6.2 Fläkt-Woods fan

The datum fan is a vaneaxial machine that derives from a tubeaxial fan. The fan is driven by a motor at 1500rpm and it has a 9 blades impeller. The original tubeaxial fan had a total efficiency of 69%. The efficiency of the tubeaxial fan was relatively low and the requirement for improved efficiency arouse from this. The use of downstream guide vane improves the efficiency, because part of the swirl velocity at the impeller's exit is converted into useful static pressure.

Fläkt-Woods added a vane stage with 11 vanes to this particular tubeaxial fan in order to improve the efficiency of the fan. The improvement in the efficiency is illustrated in Figure 6.1

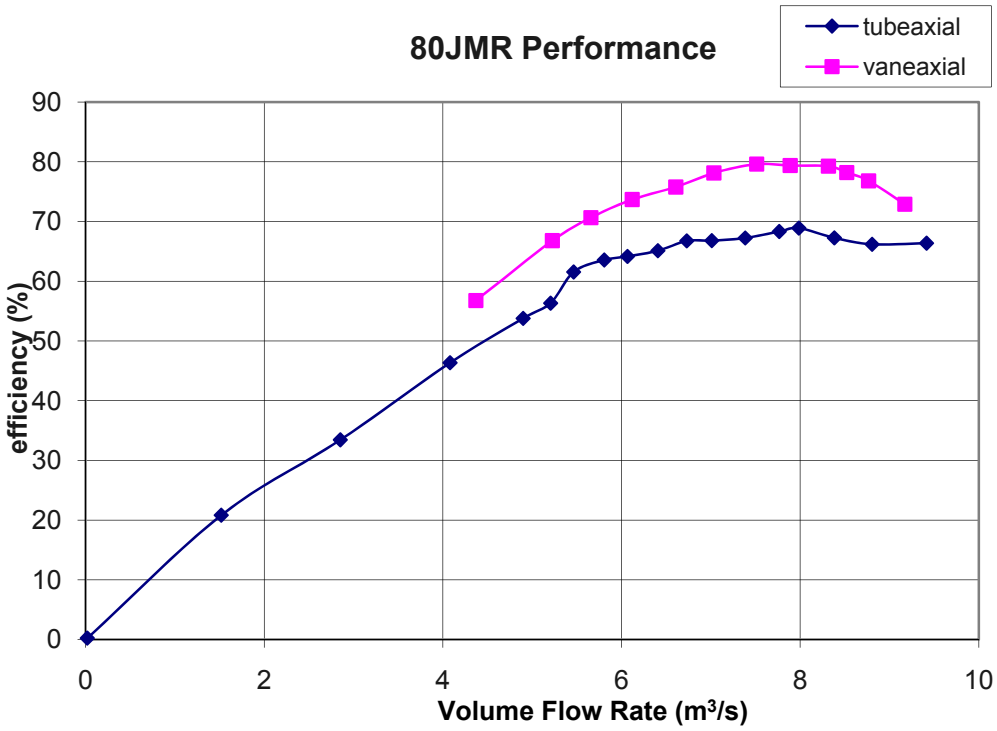

Figure 6.1 Tubeaxial vs vaneaxial efficiency in variation with volume flow (Fläkt-Woods)

The guide vanes that were added in the tubeaxial fan remove the rotational component of the velocity and convert some of the dynamic pressure into useful static pressure. This explains the fact that in the vaneaxial fan the pressure rise is higher for the same volume flow than in a tubeaxial fan. The increased pressure rise result in the higher efficiency as well for the vaneaxial fan.

The maximum efficiency was increased by 16.6% and it reached 79.5% at a volume flow 7.51 m^3/s. The point with the highest efficiency was picked as design point for the new designs. An improvement in efficiency has the following practical meaning:

1. The fan has an improved performance (increased ventilation) in the same environment (increased volume flow under the same pressure rise) without the increased energy consumption penalty.

2. The same fan can operate with higher load a different environment (increased pressure rise) without reducing the volume flow (ventilation level) and without the increased energy consumption penalty.

The increased pressure rise of the vaneaxial fan is illustrated in Figure 6.2

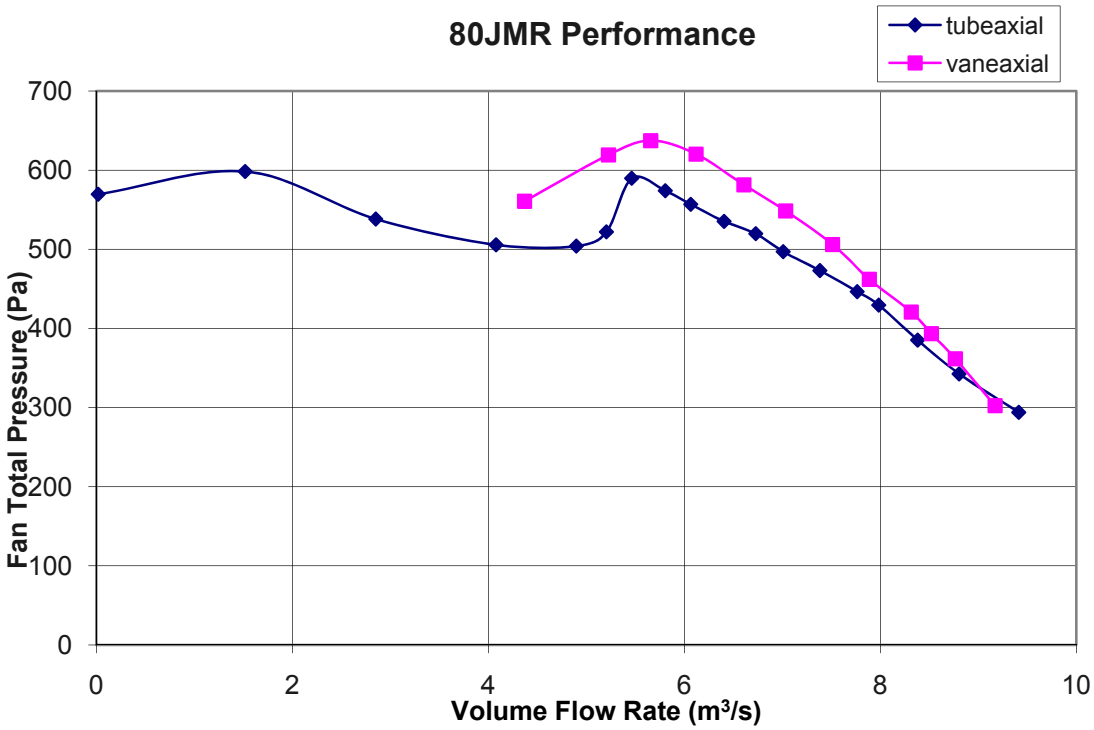

Figure 6.2 Tubeaxial vs vaneaxial total pressure rise in variation with volume flow (Fläkt-Woods)

6.3 New Design

The point with the highest efficiency of the Fläkt-Woods vaneaxial fan was selected as design point. The performance of the given vaneaxial fan at the selected point provides the requirements for the new design as follows:

1. Volume flow : 7.51 m^3/sec
2. Total Pressure rise : 506 Pa
3. Rotational speed : 1500rpm
4. Efficiency > 79,5%
5. Tip Diameter : 0.8m
6. C4 airfoil for the rotor and the stator

Fläkt-Woods stated that the design of the fan can start from a blank paper, however the above inputs are enough in order to design a fan as it was discussed in the Design Procedures Chapter and even more design data can be extracted from the given model in order to start the new design. The given design has 9 blades and 11 vanes, so this configuration can be a starting point for the new design.

The following assumptions were made as well, in order to make the initial calculations for the new design. These assumptions are based on the assumptions that were made from McKenzie and Osbourne in their preliminary designs. Real data for diffusion efficiency and pressure recovery factors cannot be retrieved because they are proprietary information of the fan manufacturers.

1. Diffusion efficiency : 80%
2. Pressure recovery factor : 85%

There are more requirements for the new fan relating to the extreme operating conditions under which the fan should operate. According to http://www.pveuk.com/axial_fans.htm a ventilation fan should be capable to operate under 400^{o}C for 2 hours. This requirement concerns the mechanical integrity of the fan, however a relatively large tip clearance of at least 3mm is necessary, which is about 1.5% of the blade span.

6.4 Design1

6.4.1 Blade Geometry

Design1 is the first attempt to design a brand new fan from customer's requirements. The basic requirements were apposed in the previous paragraph, so the target for Design1 is to have 9 blades and 11 vanes as the given fan has.

The fan geometry has to be determined first. The McKenzie preliminary design method is a trial an error method as was discussed in Chapter 5. The first assumption concerns the hub to tip ratio. The hub to tip ratio consist an essential assumption because it has a direct effect on the axial velocity. McKenzie, 1997 and Bleier, 1998 have similar procedures to check the choice of the hub to tip ratio. McKenzie calculates the ratios of ΔH/Va^2 and Va/U at the hub and plot the values at the diagram of Figure 6.3

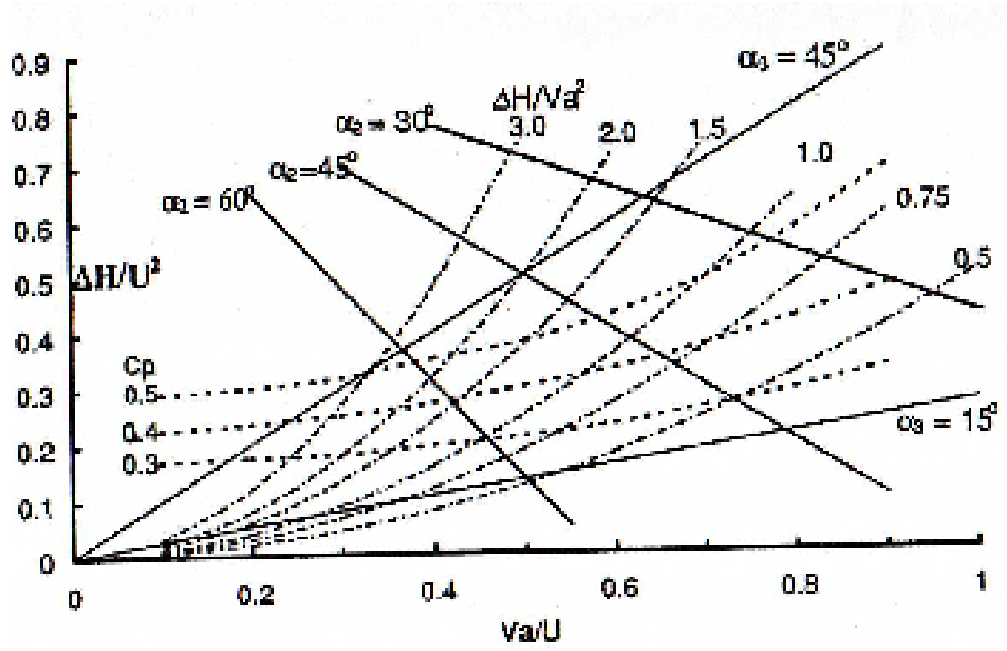

Figure 6.3 Work Coefficient vs flow coefficient diagram (McKenzie,1997)

The point should be as close as possible to the line of C_p=0.5 in order to have a de Haller number of 0.7. A 0.52 hub to tip ratio provides a point close to the line of Cp=0.5.

The annulus is divided to 10 sections and after fixing the hub to tip ratio, the air angles of the relative velocities can be calculated for every section.

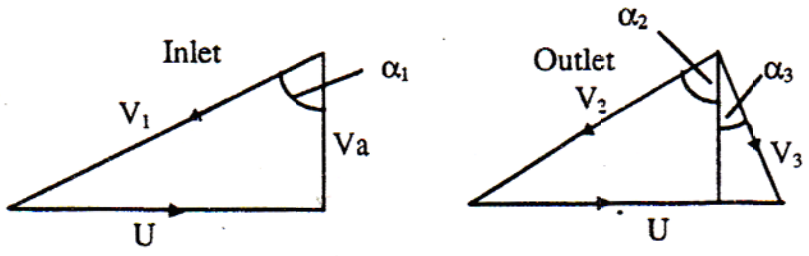

Figure 6.4 Relative Velocities – Angles (McKenzie,1997)

The rotational speed was increased to 1650 rpm in order to maintain the number of blades to 9 without increasing the blade chord more than 15cm. The blade chord is a compromise between the rotational speed and the number of blades. If the rotational speed was 1500rpm the blade chord should have been increased to 21cm at the hub, which is not acceptable.

The next step is to calculate the stagger angle of every section.

$\tan a_m = (\tan a_1 + \tan a_2)/2$ (6.1)

$\tan \zeta = \tan a_m - 0.15$ (6.2)

The blade angle varies with the incidence and the camber is a function of blade angle and stagger angle. The following chain of equations consist an iterative procedure to determine the proper incidence value for the hub. A value for the incidence is assumed and then the S/C ratio is calculated. The value of incidence that gives a reasonable S/C ratio is finally selected for the hub section.

$\beta_1 = \alpha_1 - i$ (6.3)

$\theta = 2(\beta_1 - \zeta)$ (6.4)

$\beta_2 = \beta_1 - \theta$ (6.5)

$\delta = \alpha_2 - \beta_2$ (6.6)

$S/C = \delta/(1.1+0.31\theta)^3$ (6.7)

The peak efficiency can be achieved when the angle of incidence lies between $+5^o$ to -10^o (McKenzie,1997) and the S/C ratio for good efficiency can be checked using the diagrams of Figures 6.5 and 6.6.

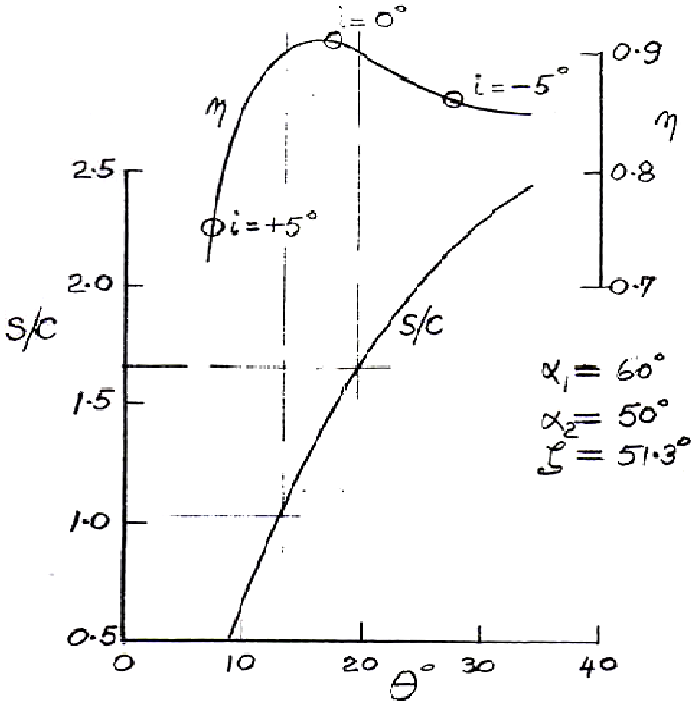

Figure 6.5 Blade geometry for fixed air angles (McKenzie, 1988)

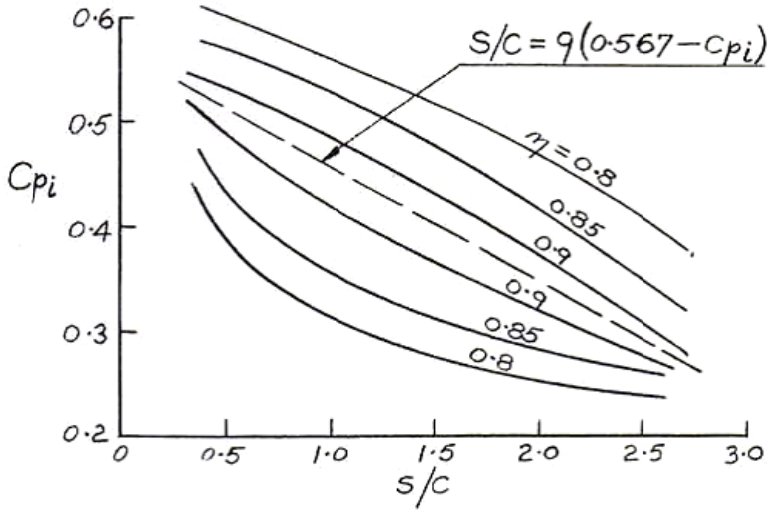

Figure 6.6 Efficiency contours (McKenzie, 1988)

The same procedure can be followed for the tip section in order to check if a reasonable incidence and S/C ratio can be obtained.

Having the S/C ratio fixed at the hub, the S/C ratio at the tip can be calculated assuming that is proportional to the radius and assuming that the blade chord at the tip is ¾ of the blade chord at the hub. As it was discussed in Chapter 3 narrower tip will unfavourably affect the efficiency of a fan, however the centrifugal loading of the blade is less and the mechanical strength will be increased. The blade height can also be calculated and after assuming a reasonable aspect ratio of 1.5, the blade chord can be calculated as well.

All the calculations and the final design of the blade features are summarized in Table 6.1

Table 6.1 Final rotor blade design (Design1)

	HUB									**TIP**
DIAMETER	**0.416**	**0.459**	**0.501**	**0.544**	**0.587**	**0.629**	**0.672**	**0.715**	**0.757**	**0.8**
S/C	0.935	1.098	1.26	1.423	1.585	1.748	1.91	2.073	2.235	2.398
a1	60.36	62.7	64.72	66.48	68.03	69.39	70.6	71.67	72.64	73.52
a2	47.85	53.39	57.61	60.93	63.61	65.82	67.67	69.25	70.61	71.79
tanam= (tana1+tana2)/2	1.431	1.642	1.847	2.049	2.247	2.443	2.637	2.829	3.02	3.21
tanζ=tanam -**0.15**	1.281	1.492	1.697	1.899	2.097	2.293	2.487	2.679	2.87	3.06
ζ (rad)	0.908	0.98	1.038	1.086	1.126	1.16	1.188	1.214	1.236	1.255
STAGGER	**52.03**	**56.16**	**59.49**	**62.22**	**64.51**	**66.44**	**68.09**	**69.53**	**70.79**	**71.9**
CAMBER	**26.67**	**21.71**	**18.59**	**16.7**	**15.69**	**15.33**	**15.49**	**16.1**	**17.12**	**18.59**
(0.5-0.31*(S/C)^(1/3))										
β1=2θ+ζ	65.36	67.02	68.79	70.58	72.35	74.1	75.84	77.58	79.35	81.2
incidence i= (a1-β1)	-5	-4.32	-4.06	-4.09	-4.33	-4.72	-5.25	-5.91	-6.71	-7.68
β2=β1-θ	38.69	45.31	50.2	53.87	56.66	58.77	60.35	61.48	62.23	62.61
deviation δ=α2-β2	9.16	8.077	7.411	7.061	6.956	7.051	7.324	7.765	8.38	9.187
deflection e =a1-a2	12.51	9.316	7.113	5.551	4.413	3.566	2.922	2.425	2.035	1.724
am (rad) =	0.961	1.024	1.075	1.117	1.152	1.182	1.208	1.231	1.251	1.269
am (deg) =	55.06	58.65	61.57	63.98	66.01	67.74	69.23	70.53	71.68	72.7
Cl (from Osbourne) = 2*S/C*(tana1-tana2)*cosam	0.699	0.676	0.65	0.623	0.596	0.571	0.547	0.525	0.504	0.484
CHORD	**0.155**	**0.146**	**0.139**	**0.133**	**0.129**	**0.126**	**0.123**	**0.12**	**0.118**	**0.116**

The same procedure can be followed to acquire the geometry of the vane. A few comments for the vane design as follows:

1. The a_4 angle at the first 3 sections was selected 3^o 2^o 1^o degrees respectively. The a_3 angle is higher at the first sections and the higher the angle the harder is to straighten the flow. So, the penalty of a small swirl is permitted at the 3 first sections of the vane (30% of the total span) in order to avoid the higher penalty of separation is more difficult to straighten the flow.

2. The vane was initially assumed to have the average chord of the blade in order to have a reference point for the design

3. A constant chord was selected for simplicity of the vane design

4. The airfoil of the vane is C4, as the blade airfoil

5. The geometry of the vane was adjusted taking into account that the stator has 11 vanes.

The final design of the stator vane is illustrated in Table 6.2

Table 6.2 Final stator vane design (Design1)

	HUB									TIP
DIAMETER	0.416	0.459	0.501	0.544	0.587	0.629	0.672	0.715	0.757	0.8
a3	33.13	30.62	28.43	26.52	24.83	23.33	22	20.8	19.72	18.74
a3 (rad)	0.578	0.534	0.496	0.463	0.433	0.407	0.384	0.363	0.344	0.327
a4	3	2	1	0	0	0	0	0	0	0
a4 (rad)	0.052	0.035	0.017	0	0	0	0	0	0	0
tanam= (tana3+tana4)/2	0.352	0.313	0.279	0.249	0.231	0.216	0.202	0.19	0.179	0.17
tanζ=tanam -0.15	0.202	0.163	0.129	0.099	0.081	0.066	0.052	0.04	0.029	0.02
ζ (rad)	0.2	0.162	0.129	0.099	0.081	0.066	0.052	0.04	0.029	0.02
STAGGER	11.45	9.278	7.376	5.682	4.651	3.757	2.975	2.286	1.673	1.126
CHORD	0.127	0.127	0.127	0.127	0.127	0.127	0.127	0.127	0.127	0.127
S=	0.119	0.131	0.143	0.155	0.168	0.18	0.192	0.204	0.216	0.228
S/C=	0.936	1.032	1.127	1.223	1.319	1.415	1.511	1.607	1.703	1.799
CAMBER	48.38	42.45	37.86	34.34	29.1	24.55	20.58	17.08	13.97	11.19
β1=ζ+θ/2	35.63	30.5	26.31	22.85	19.2	16.03	13.27	10.83	8.657	6.72
i=a3-β1	-2.51	0.115	2.125	3.669	5.631	7.297	8.73	9.973	11.06	12.02

6.4.2 Blade Design

The definition of the blade and vane geometry is the first step to design a vaneaxial fan. The next step is to examine if a fan with this geometry can perform the

way it was designed for. This can only achieved by simulating the performance of this fan.

First of all the blade and the vane geometry of each section should be converted to 3D coordinates. For this purpose the data of Table 6.3 and Table were imported to the STACK program in order to acquire the 2D coordinates of the 10 sections of the blade and the vane. Similar result is obtained by using the MATLAB code that was developed for this cause.

Table 6.3 Design1 Rotor

SECTION	1	2	3	4	5	6	7	8	9	10
CAMBER	26.7	21.7	18.6	16.7	15.7	15.3	18.6	16.1	17.1	18.6
CHORD	0.155	0.146	0.139	0.133	0.129	0.126	0.123	0.120	0.118	0.116
DIAMETER	0.416	0.459	0.501	0.544	0.587	0.629	0.672	0.715	0.757	0.800
STAGGER	52.0	56.2	59.5	62.2	64.5	66.4	68.1	69.5	70.8	71.9

Table 6.4 Design1 Stator

SECTION	1	2	3	4	5	6	7	8	9	10
CAMBER	-48.4	-42.4	-37.9	-34.3	-29.1	-24.6	-20.6	-17.1	-14.0	-11.2
CHORD	0.127	0.127	0.127	0.127	0.127	0.127	0.127	0.127	0.127	0.127
DIAMETER	0.416	0.459	0.501	0.544	0.587	0.629	0.672	0.715	0.757	0.800
STAGGER	-11.4	-9.3	-7.4	-5.7	-4.7	-3.8	-3.0	-2.3	-1.7	-1.1

The results were manipulated in an excel file and the final output was 2 *profile.curve* file, which contain the 3D coordinates of the blade and the vane.

The coordinates of the hub and the shroud for the rotor and the stator were defined in separate files *hub.curve* and *shroud.curve*. The definition of the hub and the shroud derived from the hub to tip ratio, the tip diameter, the tip clearance and the domain length. The length of the rotor and the stator domain was defined from experience and from the given fan.

6.4.3 Meshing

These 3 *.curve* files were imported to ANSYS Turbogrid to create the domain geometry and visualize the result. A fine size mesh selected with 200000 elements for each domain. Figure 6.7 illustrates the blade and the vane of Design1

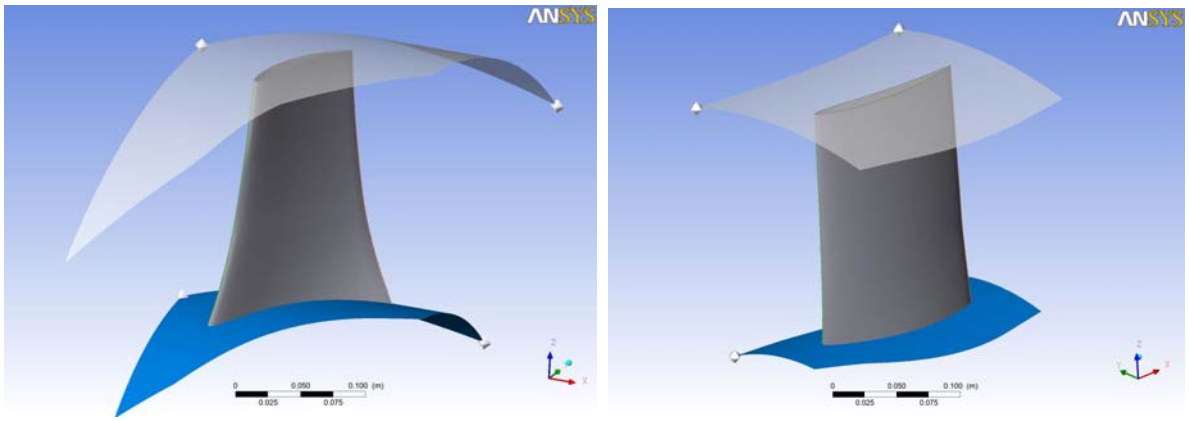

Figure 6.7 Blade and Vane of Design1 in ANSYS Turbogrid

Two more domains were designed to simulate the inlet and the outlet of the fan. The induct domain prepares the free flow to enter the annulus of the rotor domain and the outduct discharges the flow after the stator domain. These two domains were designed in GAMBIT and in ANSYS Design Modeler as well. The length of these domains and their shape were chosen from previous models and experience.

The geometry in GAMBIT has several steps points, edges, faces, volume and each step takes significant amount of time. The meshing has the same steps as well. In Figure 6.8 the mesh of the induct domain is illustrated.

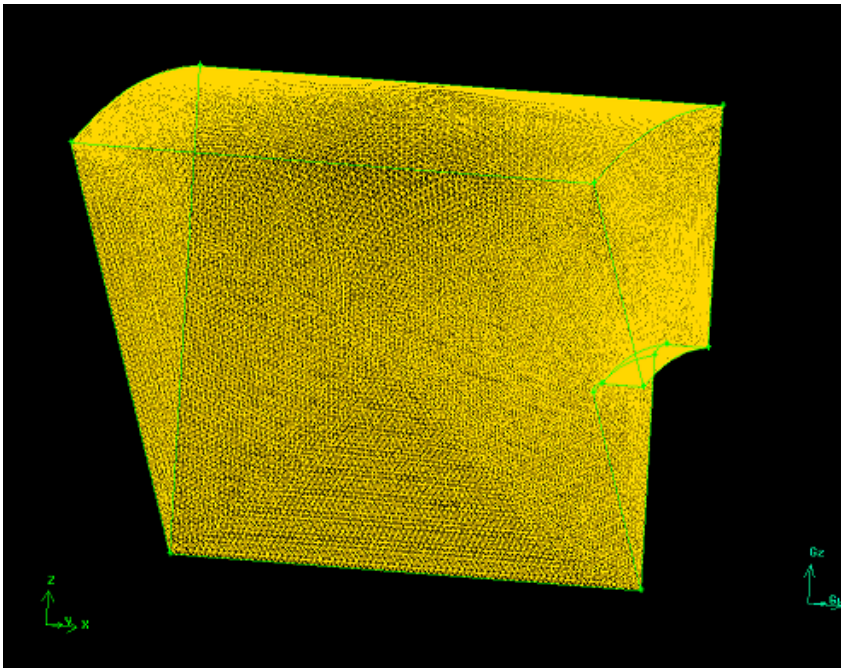

Figure 6.8 Induct domain from GAMBIT

The ANSYS platform is easier to use; the geometry is designed in ANSYS Design Modeler which is a CAD like software and the mesh is generated automatically using the ANSYS Meshing software. The mesh of the ouduct domain is illustrated in Figure 6.9.

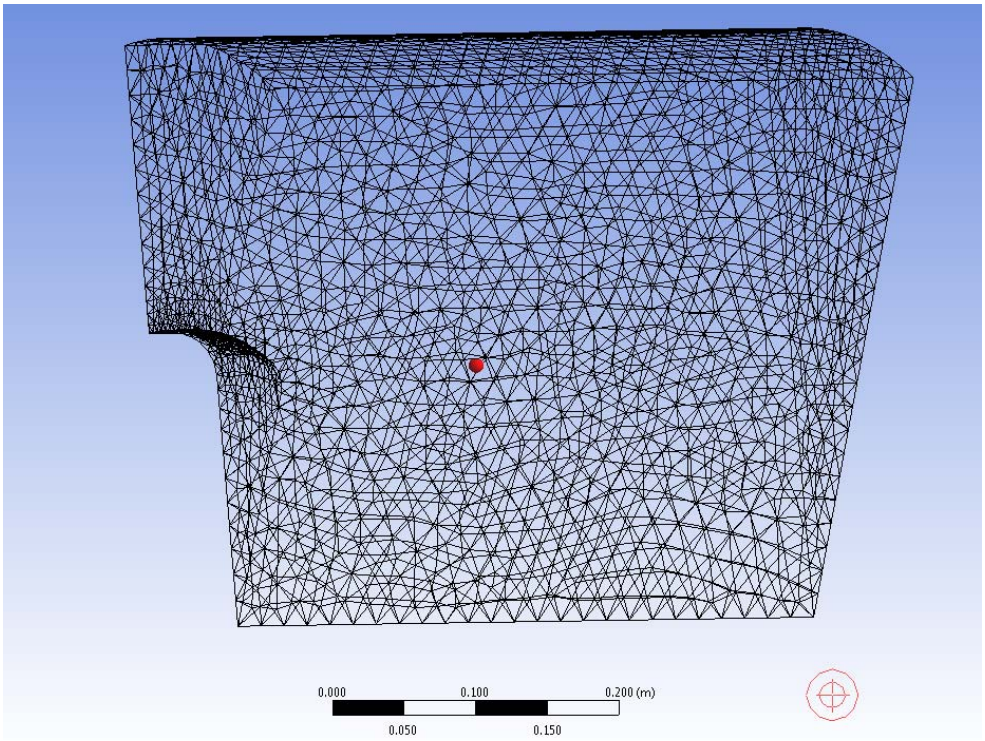

Figure 6.9 Outduct domain from ANSYS Meshing

6.4.4 CFX-Pre

The next step is to assembly the domains in ANSYS CFX Pre. ANSYS CFX-Pre is the physics-definition pre-processor for ANSYS CFX-Solver. The 4 separate domains (induct, rotor, stator, outduct) are imported into CFX-Pre and the physical models are selected for the CFD simulation. ANSYS CFX-Pre is used to assembly the domains, set the physics and the boundary conditions and finally set the case before the solver. The simulation model with all the domains assembled is illustrated in Figure 6.10.

The Turbo mode was selected for the assembly of the meshes and the boundary settings. The boundary template that was selected for this simulation was Total Pressure at the inlet and Mass Flow at the outlet. The Total Pressure was set to 0 Pa,

because the reference pressure of the flow field was already selected to 101325Pa and the volume flow of the design point was converted to Mass Flow.

Other settings for the CFX-Pre are as follows:

1. Turbulence model: k-ε model
2. Interface model: General connection, stage
3. Pitch change: Automatic
4. Mesh Interface: GGI
5. Convergence criterion: rms residual 10^{-4}

The case was written to a "*.def*" file to be ready for the solver.

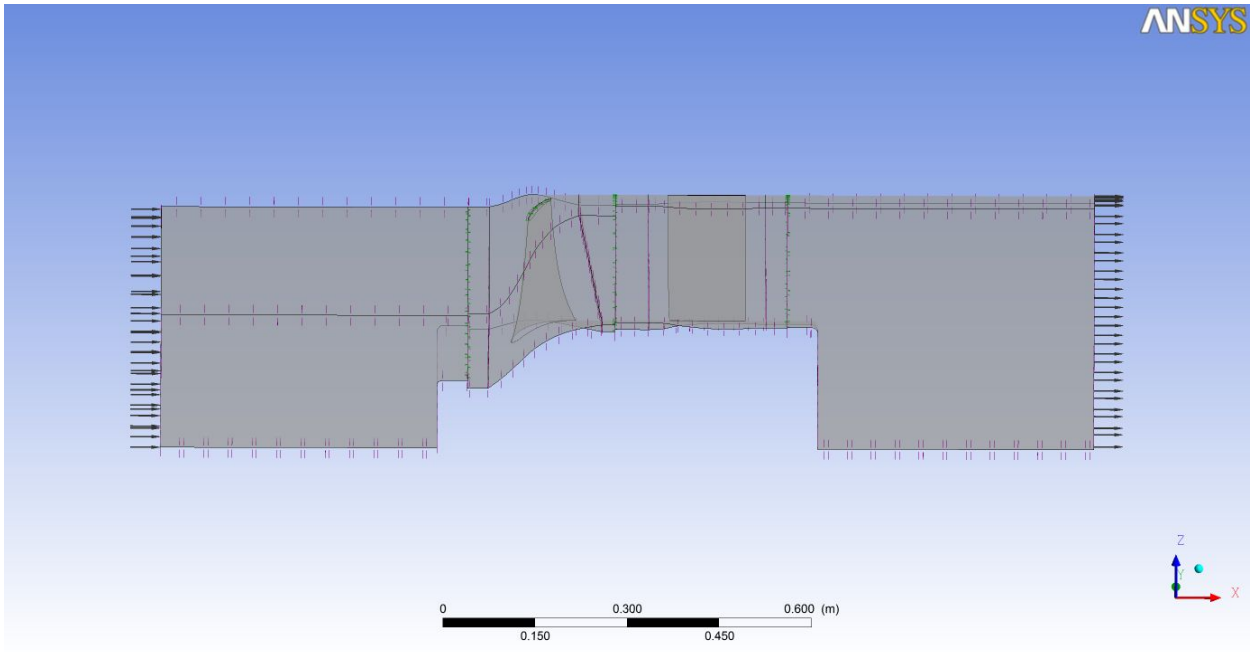

Figure 6.10 Simulation Model in CFX-Pre

6.4.5 Results

The Total Pressure rise was found 487Pa and the Static Pressure rise 479Pa.

The efficiency was calculated 78.5% using the following formula:

$$\eta = \frac{volume\ flow * \Delta P}{(rotational\ speed\ *\ number\ of\ blades\ *\ torque)} \quad (6.8)$$

Total Pressure rise (ΔP), Static Pressure rise (Δp) were the result from the subtract of the pressure in Outduct's outlet minus the pressure at the Induct's inlet. The torque was the sum of the torque at the rotor blade and the rotor's hub. All the values were calculated using the "function calculator" of CFX-Post.

The next step is to check the flow at the rotor and the stator. The "blade to blade" view was selected at CFX-Post, in order to visualize the flow. The flow is examined at the hub (0.1 of the span), the middle (0.5 of the span) and the tip (0.9 of the span). The best way to visualize the flow is the velocity variation. The velocity range is set to a range from 0 m/s to 80 m/s. The results are plotted in Figures 6.11, 6.12 and 6.13 respectively.

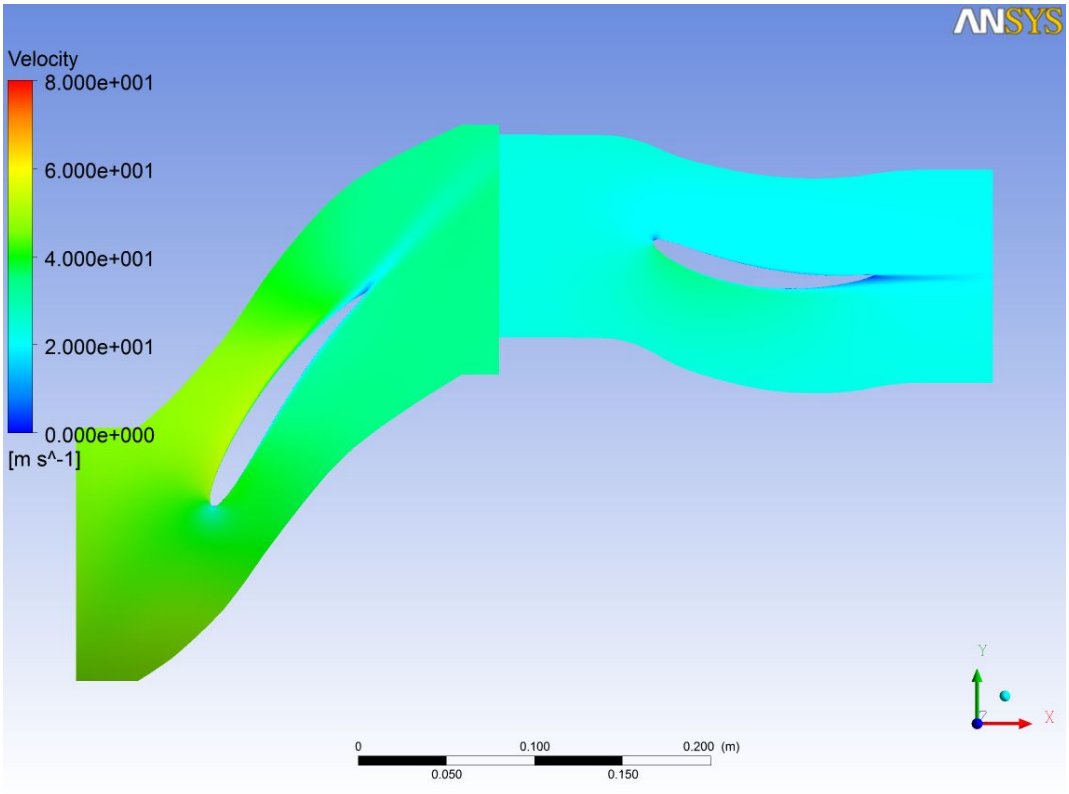

Figure 6.11 Rotor-Stator Velocity Contour Plot at 0.1 span

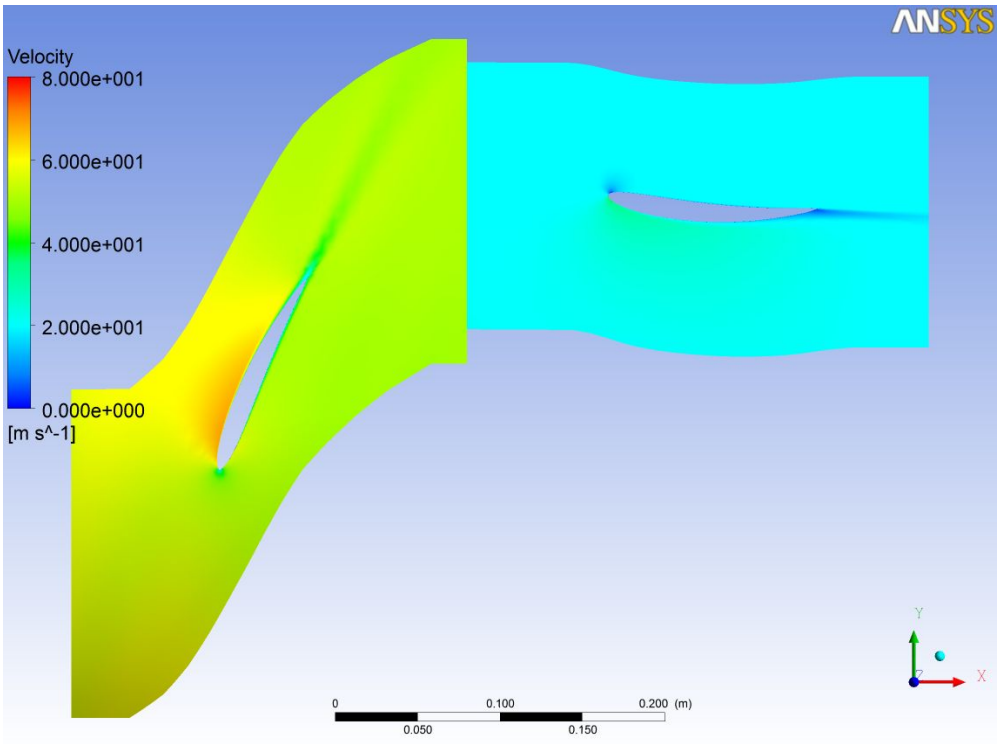

Figure 6.12 Rotor-Stator Velocity Contour Plot at 0.5 span

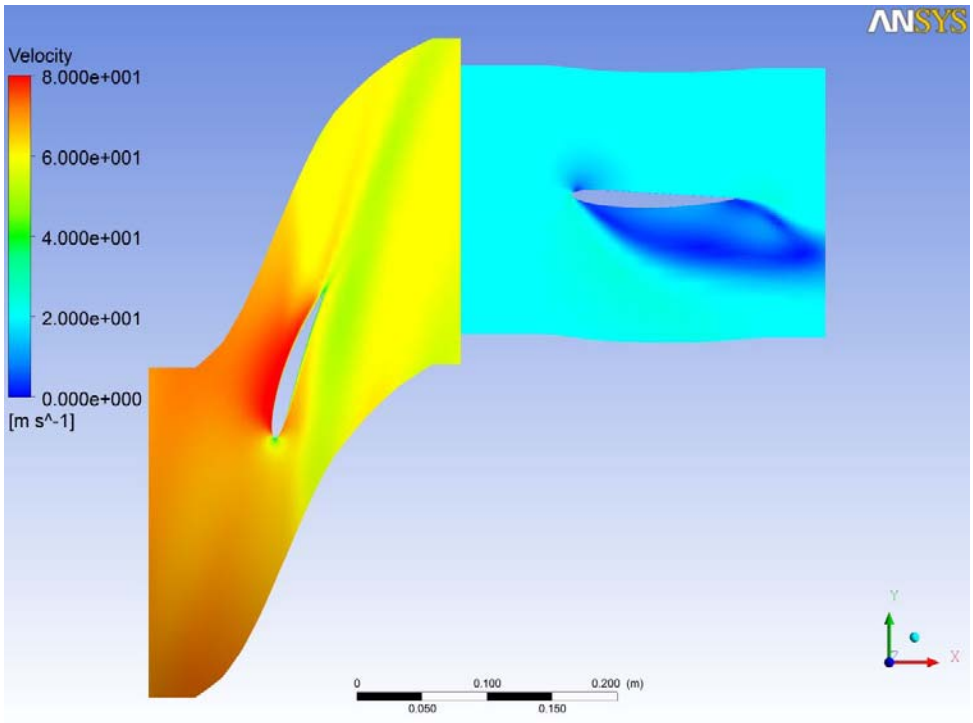

Figure 6.13 Rotor-Stator Velocity Contour Plot at 0.9 span

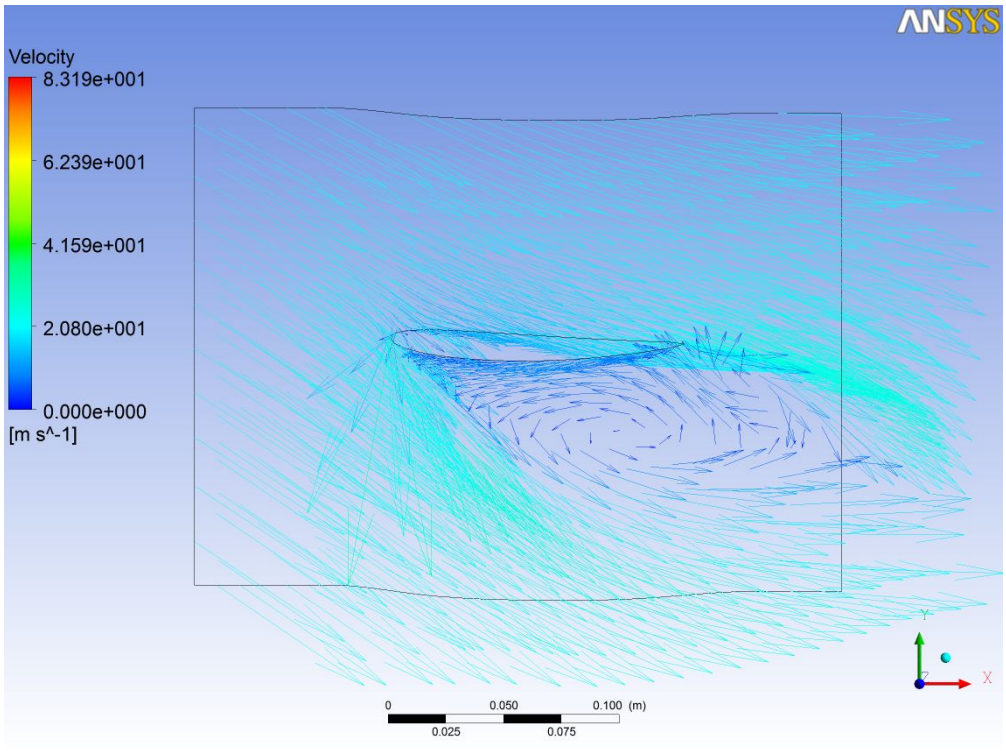

Figure 6.14 Rotor-Stator Velocity Vector Plot at 0.9 span

High separation is noticed at the tip area which has to be examined more thoroughly. The velocity vector diagram of Figure 6.14 depicts the separation better. It is obvious that the vane geometry cannot handle the flow which is not able to follow the curvature of the suction area and separates very quickly causing losses.

The next step is to examine the total area that the separation problem exists. In Figures 6.15, 6.16, 6.17 the velocity contour is plotted at 0.8, 0.7, 0.6 of the span respectively. The range of the velocity is fixed to a range 0-80 m/s, therefore the velocity contours for each span can be immediately compared.

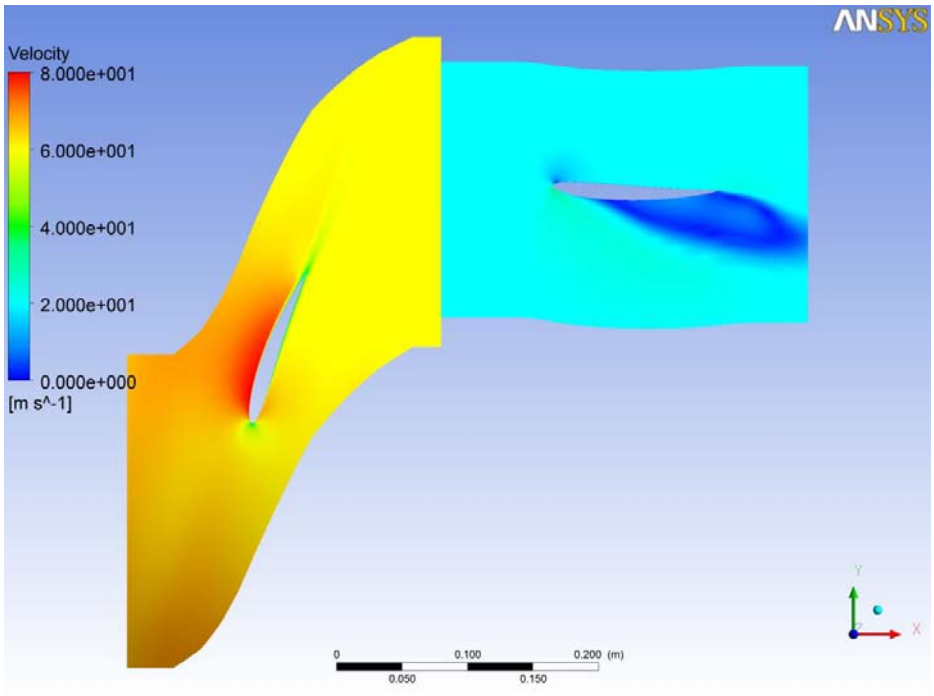

Figure 6.15 Rotor-Stator Velocity Contour Plot at 0.8 span

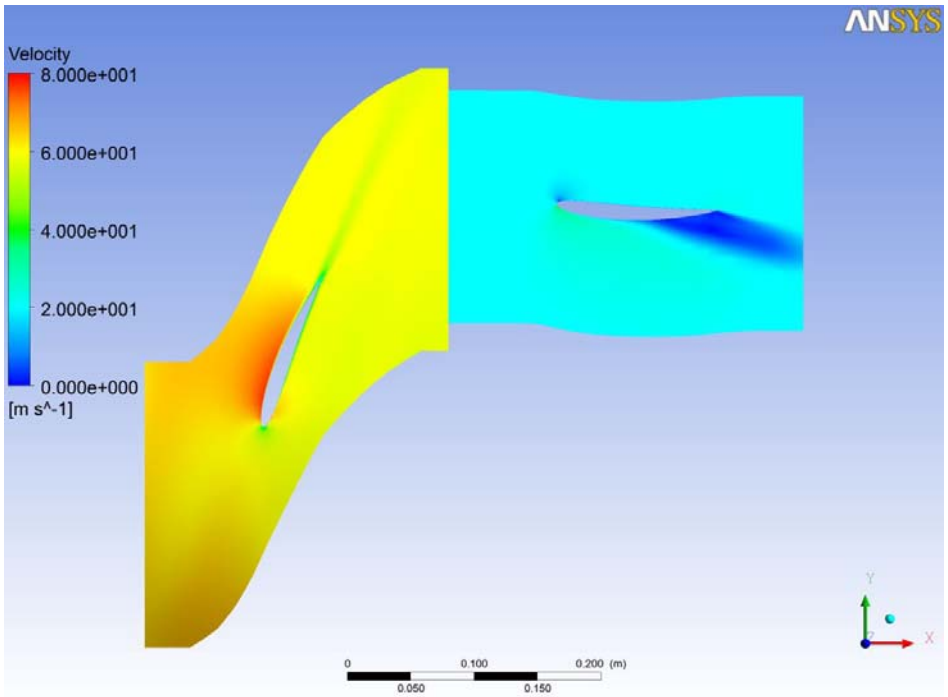

Figure 6.16 Rotor-Stator Velocity Contour Plot at 0.7 span

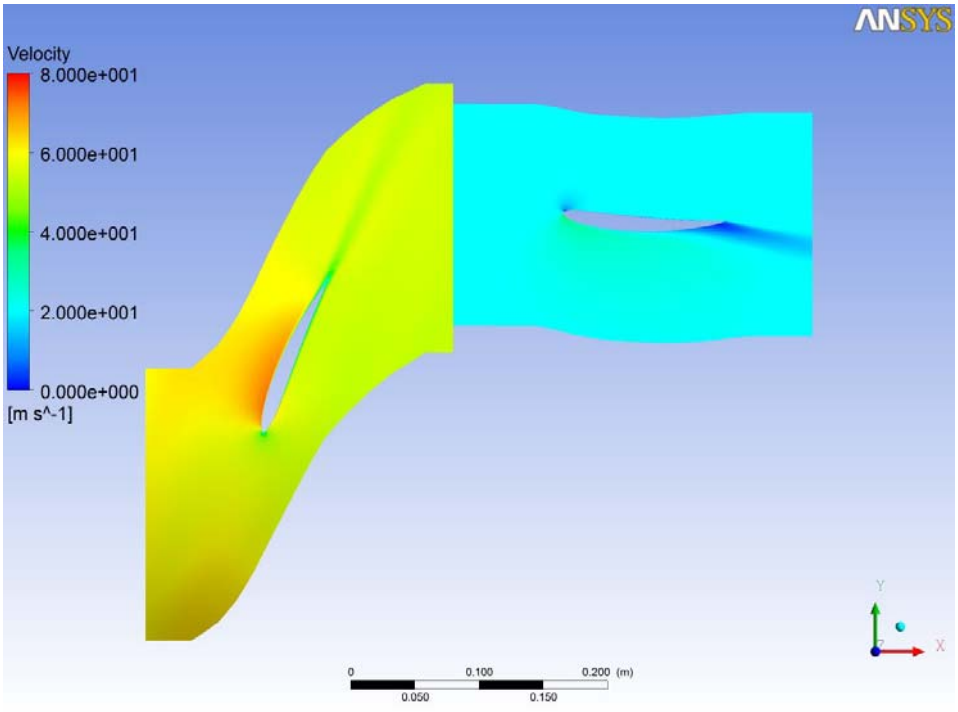

Figure 6.17 Rotor-Stator Velocity Contour Plot at 0.6 span

The separation starts from 0.6 of the span and worsens as the span is getting greater. This situation should be investigated and the best way to start is the vane geometry that is depicted in Table 6.2 (incidence line)

i=a3-β1	-2.51	0.115	2.125	3.669	5.631	7.297	8.73	9.973	11.06	12.02

The examination of Table 6.2 shows that the incidence after the 0.6 of span is greater than 7. Figure 6.5 shows that there is a vertical decrease in the efficiency for incidence angles greater than 5, so the high separation after 0.6 of the span is not a surprise.

6.4.6 Design1 optimisation

The high separation at the vane and the resulting losses affect the efficiency of the fan and an attempt to improve the design of the vane is necessary in order to achieve better performance.

The root cause of the high separation is the high angle of incidence at the sections above the 0.6 of span. The angle of incidence depends on the stagger and the camber angle.

$i = a_3 - \beta_1$ (6.9)

$\beta_1 = \zeta + \theta/2$ (6.10)

The fact that the camber and the stagger can improve the flow over the vane can be extracted from Figure 6.14. It is obvious that an increase in the stagger and in the camber of the vane airfoil will provide a less aggressive environment to the flow and the separation can be reduced.

After many trial and error attempts the stagger angle was increased properly from section 3 and above (in order to have smoother transition to higher stagger angles) and the camber angle was adjusted automatically in order to provide the zero swirl at the fan outlet (a_4=0). The new vane geometry is illustrated in Table 6.6

Table 6.5 Optimized Stator

SECTION	1	2	3	4	5	6	7	8	9	10
CAMBER	-50.7	-44.8	-41.0	-39.2	-36.4	-33.7	-31.7	-30.1	-28.4	-26.6
CHORD	0.164	0.164	0.164	0.164	0.164	0.164	0.164	0.164	0.164	0.164
DIAMETER	0.416	0.4587	0.5013	0.544	0.5867	0.6293	0.672	0.7147	0.7573	0.8
STAGGER	-13.2	-10.9	-9.1	-7.7	-7.1	-6.5	-6.0	-5.7	-5.3	-4.9
i=a3-β1	-2.9	-0.2	1.2	1.5	1.7	2.0	2.1	2.0	2.0	2.3

The new geometry of the vane requires the redesign of the vane from the beginning. The vane was redesigned using the procedure that was presented in chapters 6.4.2, 6.4.3, 6.4.4 and 6.4.5. The improvement in design is depicted in Figures 6.18, 6.19

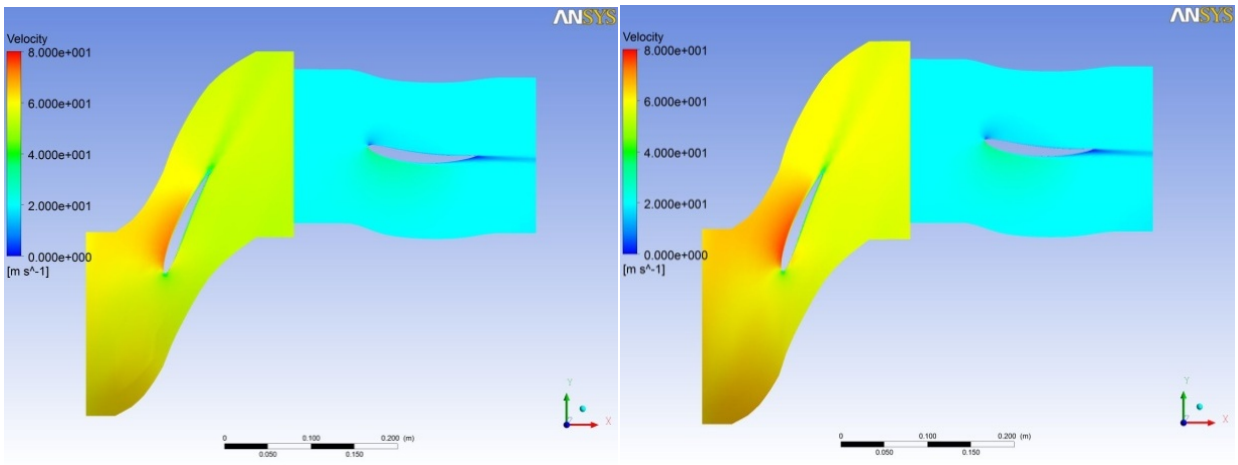

Figure 6.18 Rotor-Stator Velocity Contour Plot at 0.6 and 0.7 span (optimized)

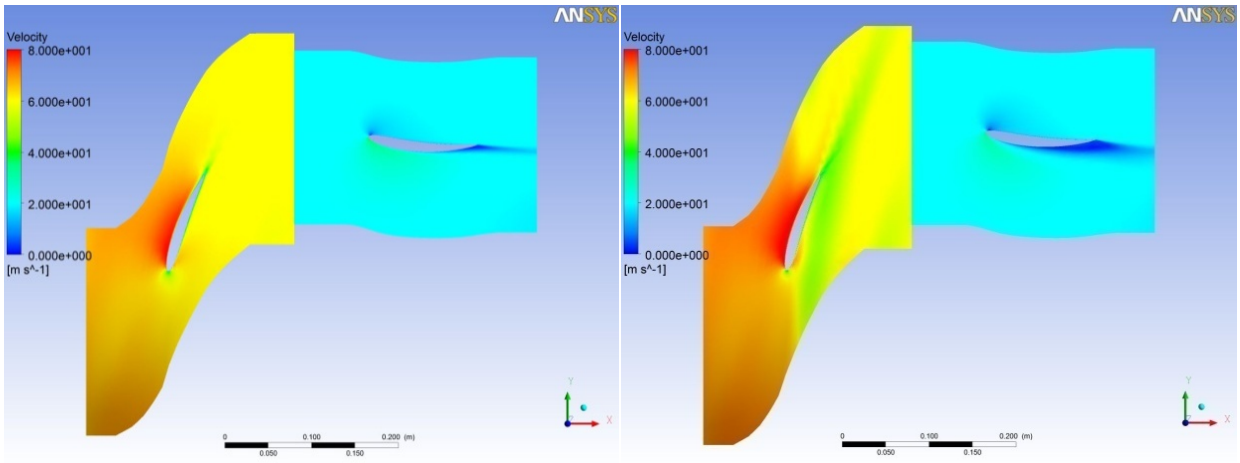

Figure 6.19 Rotor-Stator Velocity Contour Plot at 0.8 and 0.9 span (optimized)

The separation decreased significantly in the improved design and the performance was affected positively. The improvement of stagger angle and camber increased the performance; the Total Pressure rise was found 529Pa, the Static Pressure rise 529Pa and the efficiency was calculated 79.3%

Table 6.6 Improved Design Performance

	Design1	Optimized Design1	% Improvement
Total Pressure Rise (Pa)	487	529	8.6%
Static Pressure Rise (Pa)	479	525	10.4%
Efficiency	78.1%	79.3%	1.5%

6.4.7 Validation-Verification of the results

For a CFD solution to be credible, it is important to assess the results through verification and validation procedures.

A major part of the verification process is the mesh dependency study. By this means it is investigated the impact of the mesh size (coarse or fine) to the results.

For this particular case the performance of three more models was investigated. The original mesh of the rotor and the stator has 200k elements. The cases that were selected for the mesh dependency study have 50k, 100k and 400k elements. The induct and the outduct meshes remained the same. The total pressure rise in all four cases is illustrated in table 6.7

Table 6.7 Results Verification

Rotor mesh (thousands elements)	Stator mesh size (thousands elements)	Total Pressure Rise (Pa)
55.6	59.7	**530**
114.9	119.5	**524**
235.7	237.8	**529**
462.8	462.8	**534**

The above mentioned mesh dependency study that was carried out verify that the results of the CFD simulation are not grid dependant, as the divergence in the values of Total Pressure Rise is about 1%.

6.4.8 Off-design performance of Improved Design1

The off designed performance off the fan should be examined as well. The fan is supposed to be installed in a certain environment (e.g. tunnel) where the operating conditions are well established. However the different operating altitude or the specific weather conditions affect the ambient conditions and a flat performance curve is desirable.

The off design performance of the fan was examined at the same range of volume flow that was used for the off design performance off the given fan. The volume flow of the off design cases is illustrated in Table 6.8.

Table 6.8 Off design cases

	1	2	3	4	5	6	7	8	9	10	11	12
volume flow (m^3/s)	9.17	8.77	8.52	8.32	7.89	7.51	7.03	6.61	6.12	5.66	5.23	4.37

The off design performance of Design1 in variation with the off design performance of the given fan is depicted in Figures 6.20 and 6.21. Figure 6.20 depicts the variation of volume flow with total pressure rise and Figure 6.21 depicts the variation of volume flow with the efficiency.

It is interesting to notice that there is no characteristic stall area at Design1. As the volume flow decreases Design1 there is no stall at the fan, but an area where the total pressure does not increase but remains the same. After that area and as the volume flow decreases, the total pressure increases again as it was described in Chapter 2.

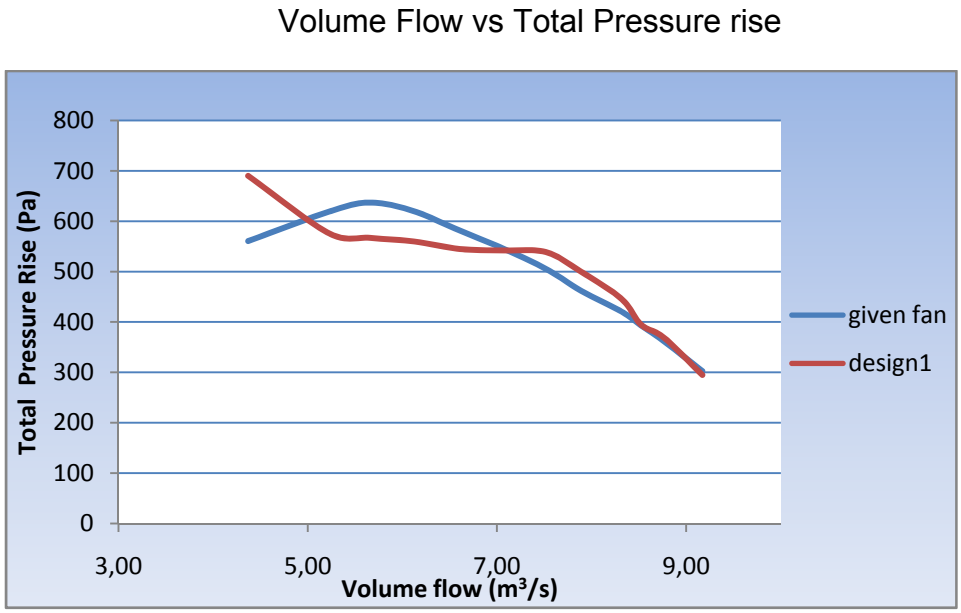

Figure 6.20 Volume flow in variation with total pressure rise

The efficiency curve has similar shape with the efficiency curve of the given fan, however the efficiency given fan is higher at lower volume flow.

The maximum efficiency of the final model was about the same with the efficiency of the given fan and a new fan with an increased efficiency should be designed.

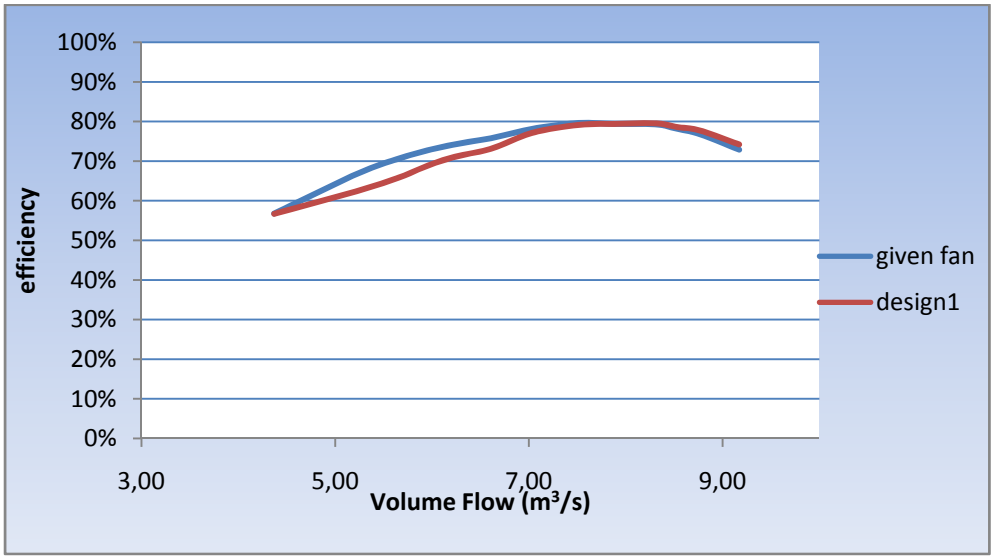

Figure 6.21 Volume flow in variation with efficiency

6.5 Design2

6.5.1 Design2 concept

Design2 is the second attempt to achieve a fan design with better efficiency and performance. The basis for design2 was design1 and some new ideas incorporated in the new design.

The velocity contour plots showed that the flow in the rotor was smooth and uniform across the pressure surface and the suction surface. This fact means that maybe the blade loading is not as high as the geometry of the blade can stand and an increase in the blade loading would increase the efficiency of the fan.

The blade loading parameter is the $\Delta H/U^2$ ratio which depends on the fan work per unit of mass flow $\Delta H=\Delta P/eff*\rho$. If the efficiency of the fan increases, more energy will be converted to useful fan work and the blade loading will increase. Therefore the idea is to keep the main design features the same and increase the design efficiency in order to increase the blade loading. The CFD simulation will prove if the increase in efficiency of the analytical solution can be incorporated in the simulation model

The main design features remain the same as follows

1. Hub to tip ratio : 0.52

2. Rotational speed : 1650rpm

The design efficiency was increased to 90% and the blade loading was significantly increased. The problem that arises from the increased blade loading is the required increase in the blade chord in order to increase the fan work. The chord length that was calculated is not acceptable and the only solution is to increase the number of blades to 11.

The main new features of design2 are the following:

1. Increased design efficiency

2. Increased number of blades and vanes (11 blades and 13 vanes)

6.5.2 Blade Geometry-Design-Meshing- Optimisation

The same procedure that was used in Design1 simulation was followed for Design2 as well.

The McKenzie method that was described in the Chapter 6.4.1 was followed to obtain the blade geometry. The geometry of the blade and the vane are illustrated in Table 1 and Table 2 of Appendix “A” respectively.

The new design data, that are illustrated in Table 3 and Table 4 of Appendix “A”, were imported to STACK software in order to generate the 2D coordinates for the blade and the vane and the third dimension was added in an excel file. Three new ".curve" file were generated for the rotor and for the stator as well (*profile.curve, hub.curve, shroud.curve*)

Design2 has 11 blades and 13 vanes, so the domains have different pitch angles. The different pitch angles for the blade and the vane domain are incorporated automatically by choosing the new number of blades and vanes at the machine data. The domains of the rotor and the stator were created in Turbogrid with the same procedure as Design1. The induct and the outduct domains have different pitch angles and they were designed from the start.

The assembly of the domains in CFX-Pre has the same settings for the physics, the turbulence model, the boundary conditions and the interfaces.

The efficiency of the new design was 80.5% which is higher than the maximum efficiency of the given fan. The experience acquired from Design1 was used for the examination of Design2. The vane performance was checked first and it was shown that the shape of the vane produced the same separation problems as the vane of design1.

The same optimisation method was followed to decrease the separation and increase the efficiency of design2. The stagger angle of the vane increased as it was increased during the optimisation of Design1. The optimized vane geometry is illustrated in Table 5 of Appendix “A”.

The vane was redesigned and re-meshed. The new stator domain was assembled with the induct domain, the outduct domain and the rotor domain and a new simulation took place.

6.5.3 Results

The Total Pressure rise for the design point was found **550Pa** and the Static Pressure rise **544Pa**.

The efficiency was calculated **82.1%** using the following formula (6.8):

$$\eta = \frac{volume\ flow * \Delta P}{(rotational\ speed\ *\ number\ of\ blades\ *\ torque)}$$

The 82% efficiency is a satisfactory result, because it is 3% higher than the efficiency of the given fan.

The visualization of the flow is depicted in the following velocity contours of Figures 6.22, 6.23 and 6.24 for the hub the middle span and the tip. The flow follows the curvature of the blade and the vane across the span without serious separation at any point. The modification of the stagger angle worked well and the result is depicted from the flow of the following Figures. The range of the velocity is fixed to a range 0-80 m/s, therefore the velocity contours for each span can be immediately compared.

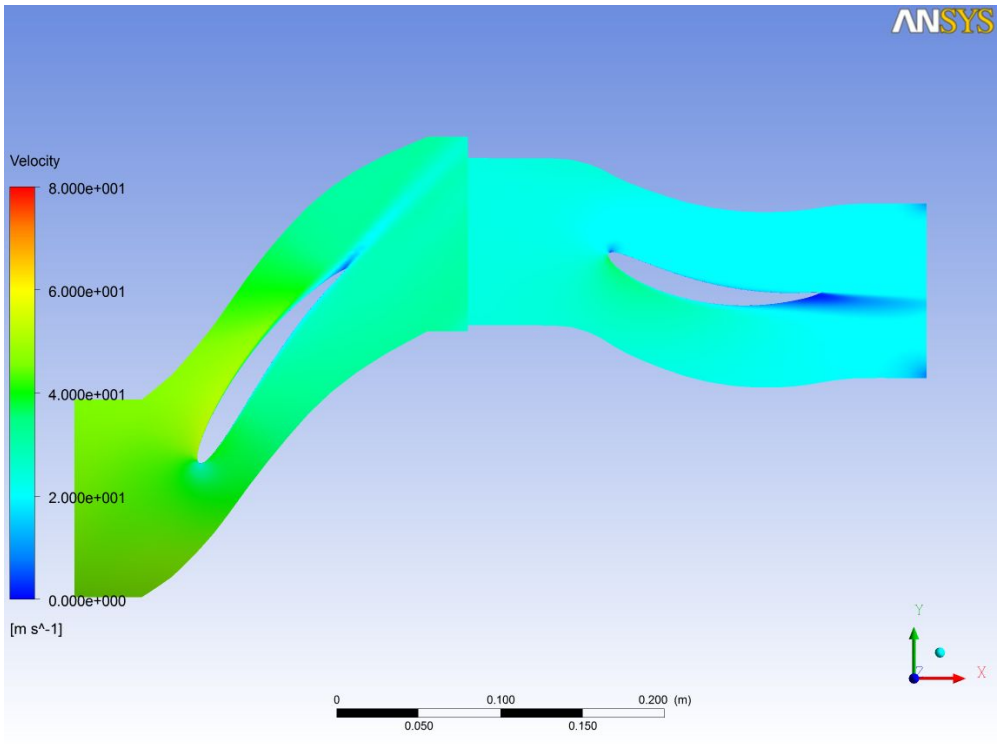

Figure 6.22 Rotor-Stator Velocity Contour Plot at 0.1 span

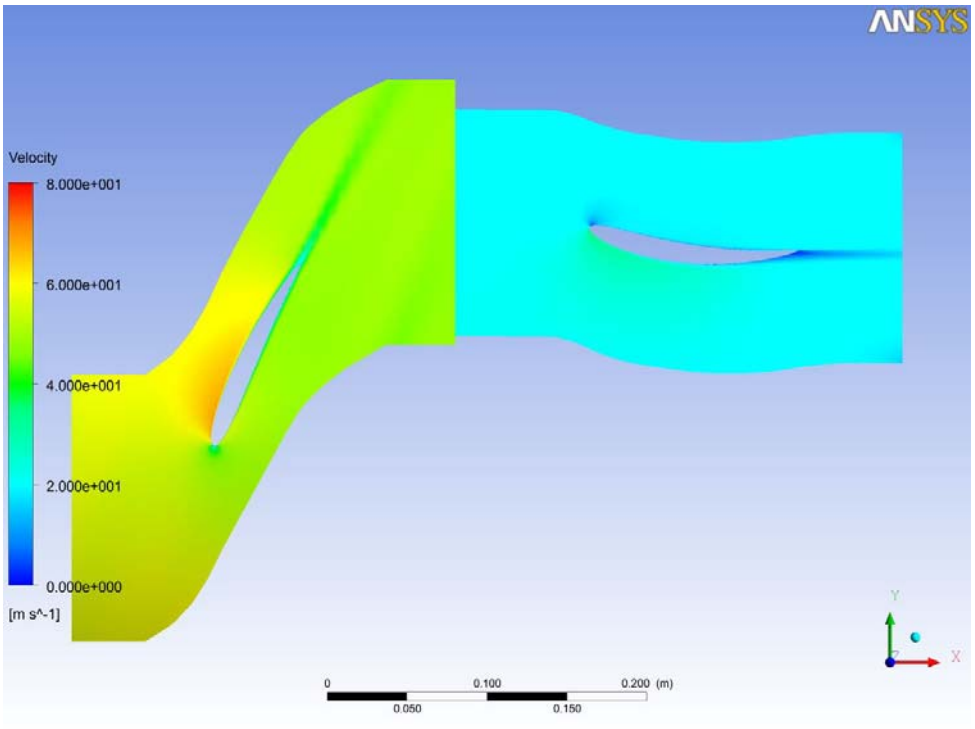

Figure 6.23 Rotor-Stator Velocity Contour Plot at 0.5 span

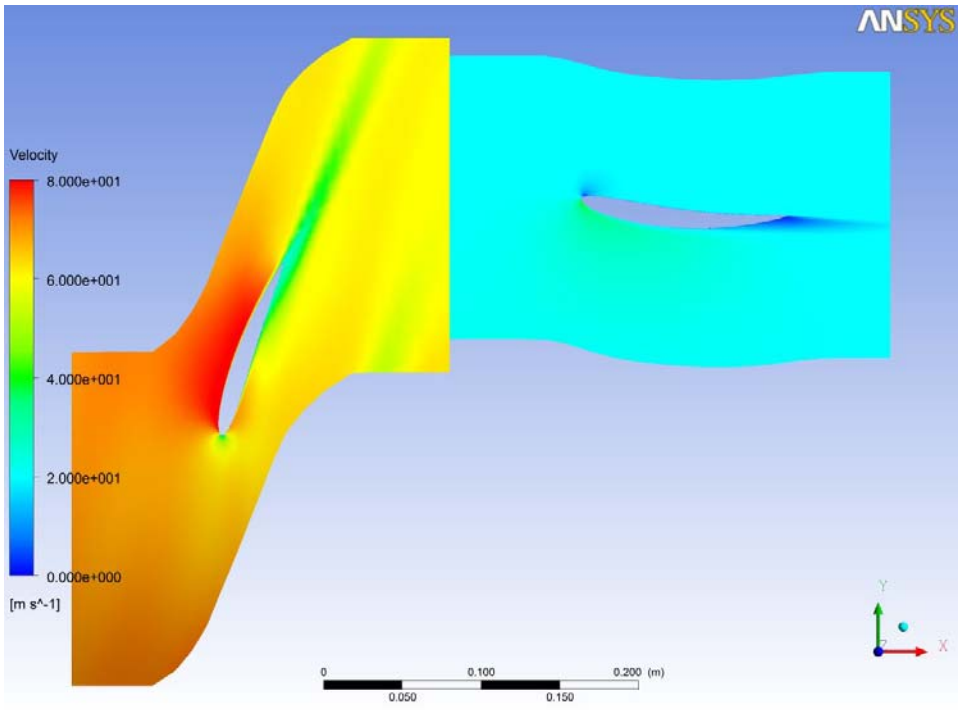

Figure 6.24 Rotor-Stator Velocity Contour Plot at 0.9 span

The velocity vector plot shows that the stator performs as designed. According to the design data the velocity exit angle is very small at the hub as it is shown in Figure 6.25 and zero at the middle of the vane as shown in Figure 6.26. At the tip area the velocity exit angle is zero according to the design data, however a small angle is noticed in Figure 6.27 due to the 3D effects that the tip clearance generates.

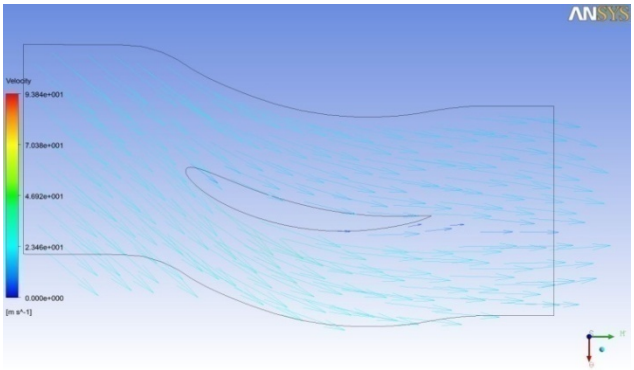

Figure 6.25 Stator Velocity Vector Plot at 0.1 span

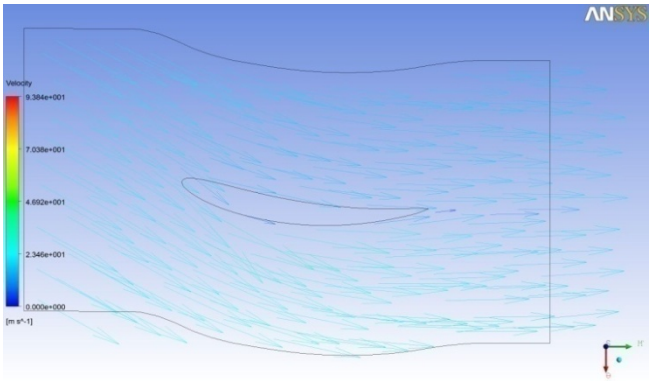

Figure 6.26 Stator Velocity Vector Plot at 0.5 span

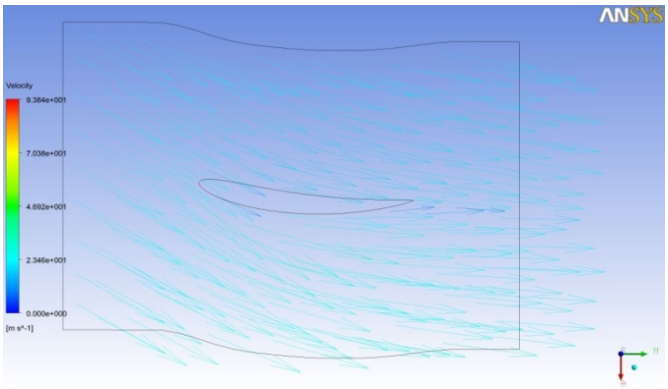

Figure 6.27 Stator Velocity Vector Plot at 0.9 span

6.5.4 Turbulence model comparison

Design2 has better performance comparing with the performance of the given fan and Design1 fan. The simulation was carried out using the k-ε turbulence model. The same simulation carried out with different turbulence model. The turbulent model that was used was the k-ω model which does not overestimates the turbulence as the k-ε model does (Tu et al, 2007). The losses due to turbulence are less and the performance of the fan is better as shown in the computational result of Table 6.7. The same conclusion for the turbulence models k-ε and k-ω was drawn from Strohmeyer, 2009 as well.

Table 6.7 Design point performance for k-ε and k-ω turbulence models

Turbulence model	P_s rise (Pa)	P_t rise (Pa)	Total Efficiency
k-ε	526	532	82%
k-ω	557	560	83.2%

6.5.5 Verification

For this particular case the performance of three more models was investigated. The original mesh of the rotor and the stator has 200k elements. The cases that were selected for the mesh dependency study have 50k, 100k and 400k elements. The induct and the outduct meshes remained the same. The turbulence model was the k-ε.

The differences in the computational results for different size meshes are below 1%. The results can be found in Table 6 of Appendix “A”.

6.5.6 Off-design performance

The off design performance of Design2 is examined for the different volume flows of Table 6.8 as well. The off design performance of Design2 in variation with the off design performance of the given fan is depicted in Figures 6.28 and 6.29. Figure 6.28 depicts the variation of volume flow with total pressure rise and Figure 6.29 depicts the variation of volume flow with the efficiency.

The total pressure curve has the same shape with the total pressure curve of Design1. There is no significant stall region, which means less noisy operation in lower volume flows.

Volume Flow vs Total Pressure rise

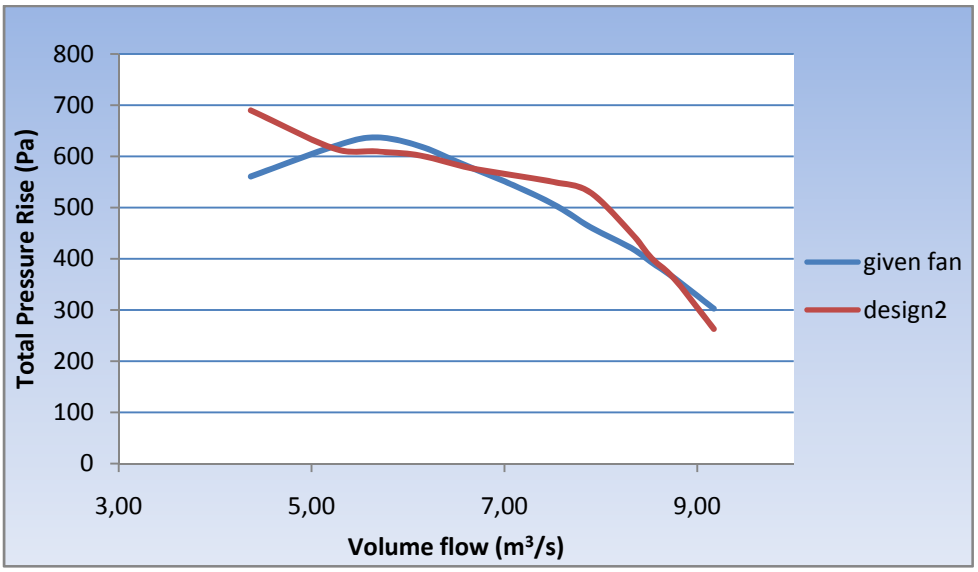

Figure 6.28 Volume flow in variation with total pressure rise

The efficiency of Design2 is better than the efficiency of the given fan in the design point area, however it has the same efficiency for high volume flows and lower efficiency for low volume flows. Although the fan has quieter operation in lower volume flows, the efficiency of the fan low volume flow is lower than the corresponding efficiency of the given fan.

Volume Flow vs Efficiency

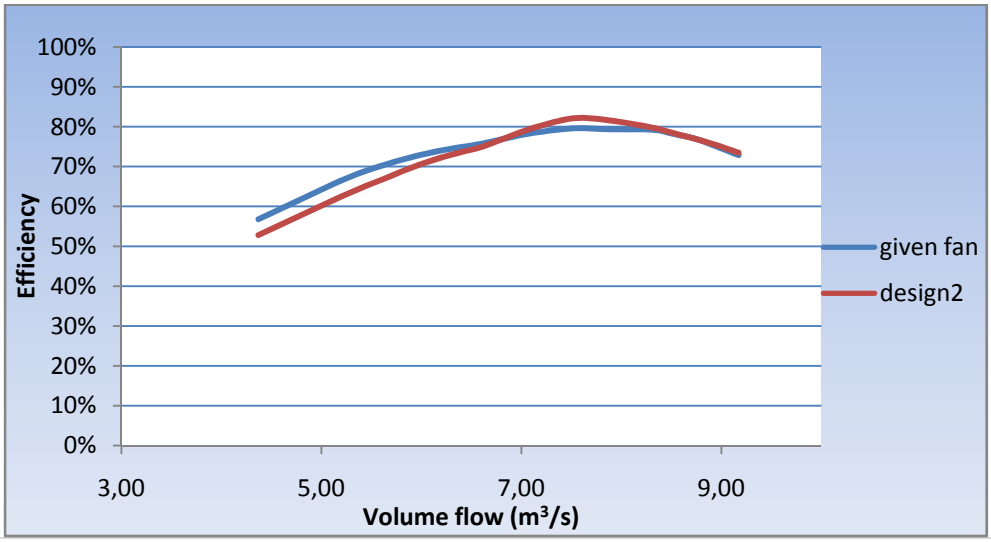

Figure 6.29 Volume flow in variation with total efficiency

6.6 Design3

6.6.1 Design3 concept

Design3 is the final attempt to achieve a fan design that has better efficiency and performance than the given fan has. The lessons learned from design1 and design2 were a good guide for the new design. A better performance has already been achieved with Design2.

The following conclusions were drawn from the design analysis of a free vortex vaneaxial fan:

1. Increasing the design efficiency has the following effects:
   a. Lower angle a_3 of the relative velocity V_3 at the rotor exit
   b. Higher angle of incidence
   c. Smaller blade chord
2. Decreasing the rotational velocity has the following effects:
   a. Higher angle a_3 of the relative velocity V_3 at the rotor exit
   b. Smaller angle of incidence
   c. Higher blade chord
3. Decreasing the hub to tip ratio has the following effects:
   a. Lower angle a_3 of the relative velocity V_3 at the rotor exit
   b. Higher angle of incidence
   c. Higher blade chord

The hub to tip ratio of Design1 and Design2 has the same value 0.52. In Chapter 3.10 the influence of hub to tip ratio was discussed. The rotational speed of Design1 and Design2 was the same as well 1650rpm.

Design3 was the field to experiment with the rotational speed and the hub to tip ratio. The number of blades and vanes is the same with Design2 11 and 13

respectively. The final design is a compromise between the rotational speed, the design efficiency, the hub to tip ratio and the blade chord.

The above design features (angle a_3, angle of incidence i, blade chord) were selected because they have immediate impact to the final design.

A relative high blade chord is not desirable because it will add material to the blade, increase the rotor domain length, increase the blade mass

The higher the angle a_3 is, the higher is the difficulty to design a stator that can straighten the flow (a_4=0)

The high angle of incidence leads to low efficiency; therefore it must be kept into a certain range of values.

Design3 target is to investigate the performance of a fan with lower hub to tip ratio and lower rotational speed. The rotational speed was reduced to 1600rpm and the hub to tip ratio reduced as well to 0.48, which is closer to the hub to tip ratio of the given fan. The design efficiency was increased in order to reduce the length of the blade chord

6.6.2 Blade Geometry-Design-Meshing- Optimisation

The same procedure that was used in Design1 and Design2 simulation was followed for Design3 as well.

The McKenzie method that was described in the Chapter 6.4.1 was followed to obtain the blade geometry. The geometry of the blade is illustrated in Table 1 of Appendix “B”.

Design3 has 11 blades and 13 vanes as Design2 has, however the hub to tip ratio is smaller, so the domains have different size. The domains of the rotor and the stator were created in Turbogrid with the same procedure as Design1. The induct and the outduct domains have different size and they were designed from the start as well.

The assembly of the domains in CFX-Pre had the same settings for the physics, the turbulence model, the boundary conditions and the interfaces.

The original Design3 was optimized according to the experience from the optimization of Design1 and Design2. The stagger angle of the vane was increased as it

was increased during the optimisation of the previous designs. The optimized vane geometry is illustrated in Table 2 of Appendix “B”.

The new design data, that are illustrated in Table 3 and Table 4 of Appendix ”B”, were imported to STACK software in order to generate the 2D coordinates for the blade and the vane and the third dimension was added in an excel file. Three new ".curve" file were generated for the rotor and the stator as well (profile.curve, hub.curve, shroud.curve). The hub.curve file has different data comparing with the hub.curve file of Design1 and Design2 because of the different hub to tip ratio.

6.6.3 Results

The Total Pressure rise for the design point was found **483Pa** and the Static Pressure rise **478Pa**.

The efficiency was calculated **79.5%** using the formula (6.8):

$$\eta = \frac{volume\ flow * \Delta P}{(rotational\ speed\ *\ number\ of\ blades\ *\ torque)}$$

The 79,5% efficiency is not a satisfactory result, because it is the same efficiency with the given fan.

The visualization of the flow is depicted in the following velocity contours of Figures 6.30, 6.31 and 6.32 for the hub the middle span and the tip. A severe separation can be noticed at 0.9 of the span. The modification of the stagger was proven insufficient and further optimization of the design can take place.

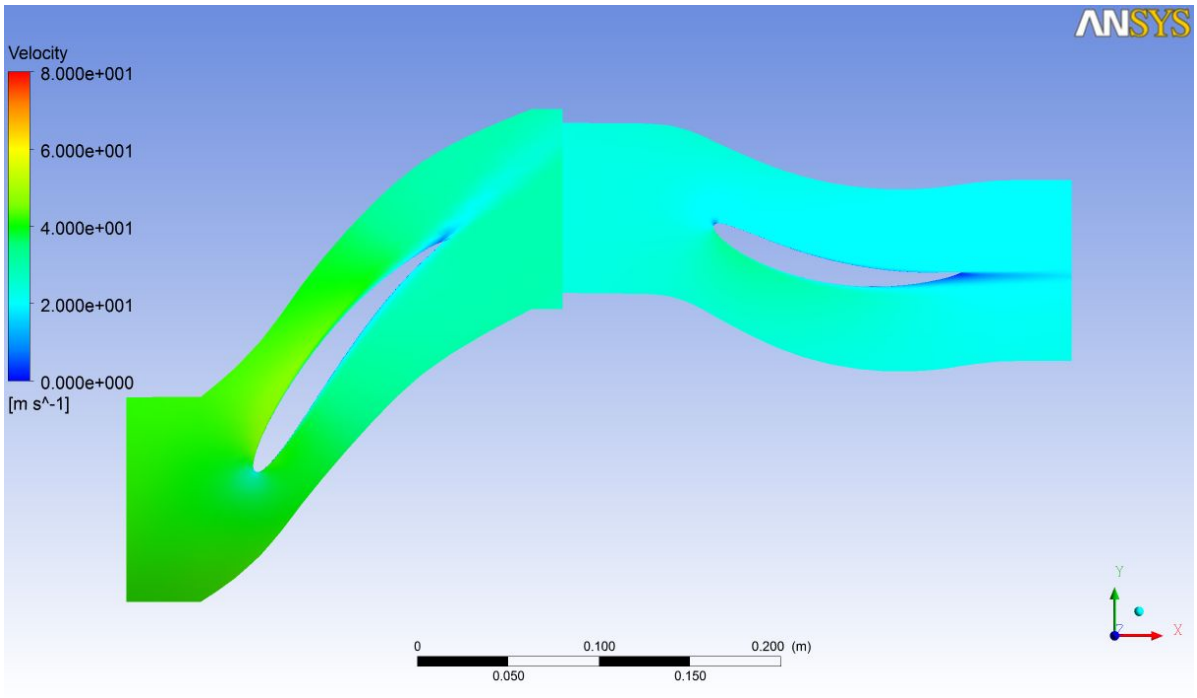

Figure 6.30 Rotor-Stator Velocity Contour Plot at 0.1 span

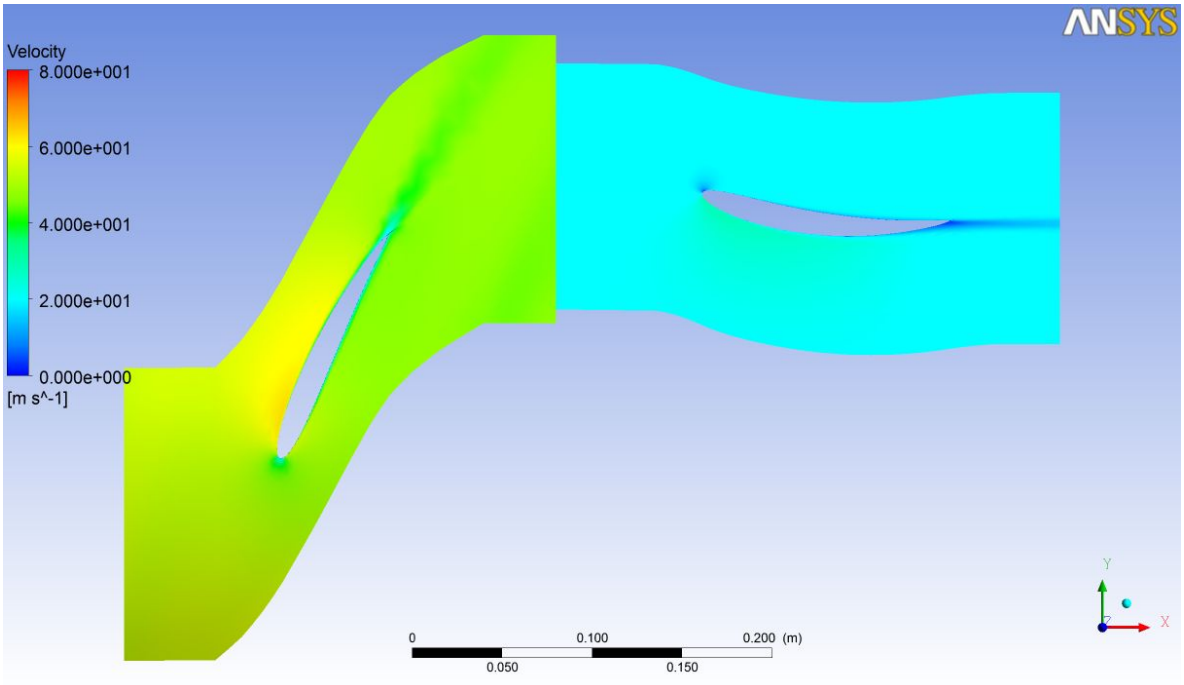

Figure 6.31 Rotor-Stator Velocity Contour Plot at 0.5 span

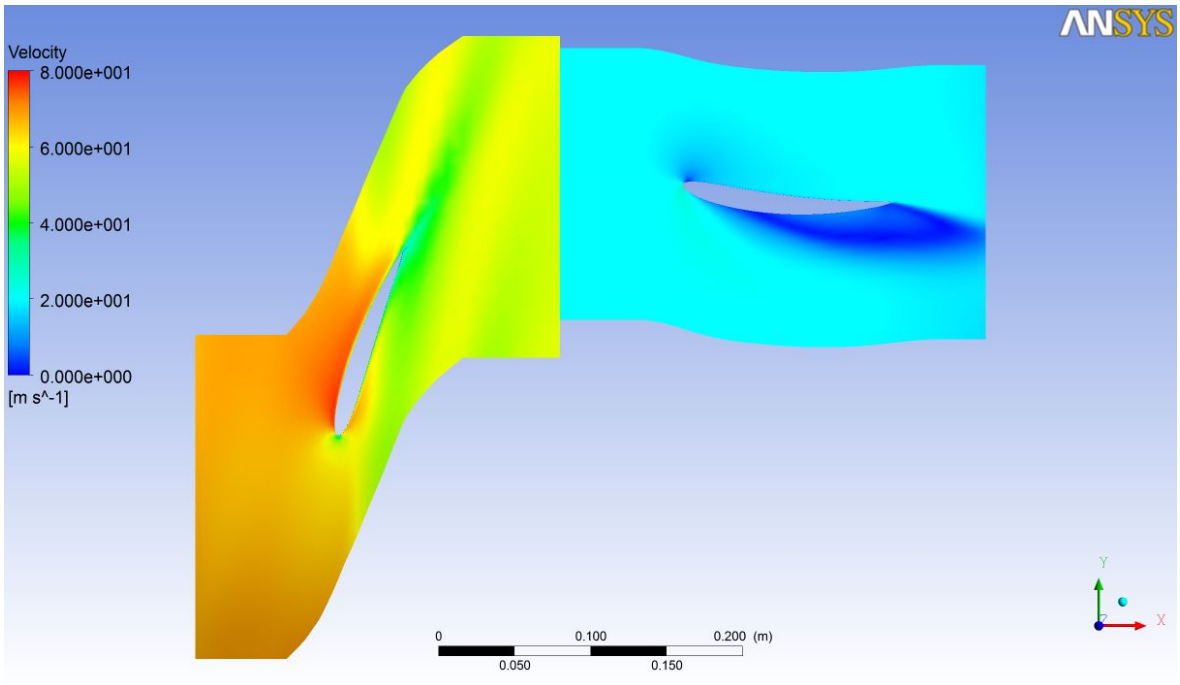

Figure 6.32 Rotor-Stator Velocity Contour Plot at 0.9 span

6.6.4 Verification

Design1 and Design2 results were verified with the mesh dependant study that was carried out. Design3 was the product of the same procedure; therefore it is believed that no extra verification is needed for Design3.

6.6.5 Off-design performance

The off design performance of Design3 is examined for the different volume flows of Table 6.8 as well. The off design performance of design3 in variation with the off design performance of the given fan is depicted in Figures 6.33 and 6.34. As it was noticed in Design1 and Design2 there is no visible stall area according to the plot of Figure 6.33. There is only an area where the total pressure remains constant or increases in a lower rate

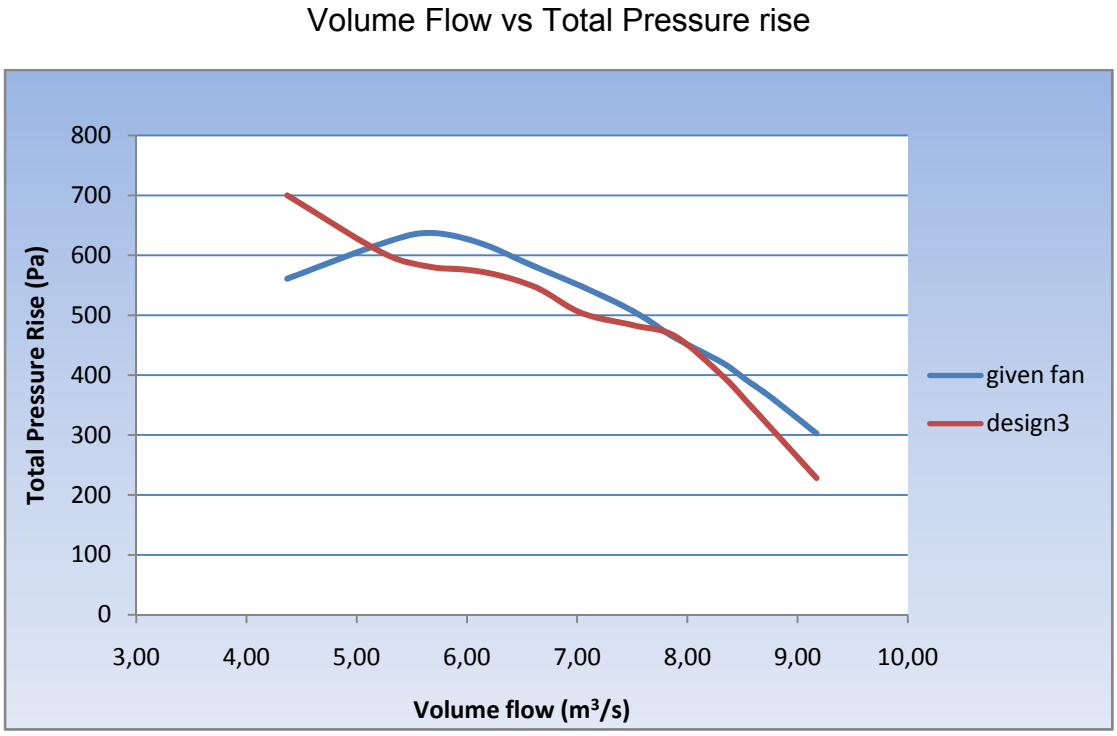

Figure 6.33 Volume flow in variation with total pressure rise

The efficiency curve has the same shape with the efficiency curve of the given design. Generally is slightly lower comparing with the efficiency of the given fan, except the design point area where the efficiency of Design3 is the same with the efficiency of the given model.

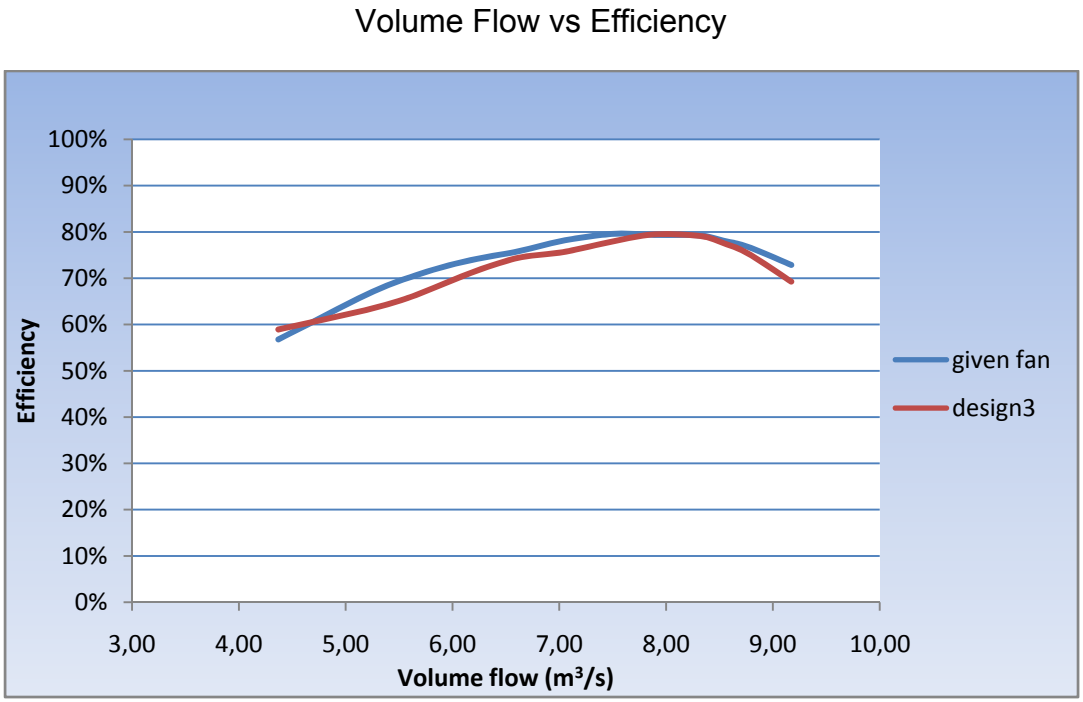

Figure 6.34 Volume flow in variation with total efficiency

6.7 Tip clearance effect

The tip clearance was set to 1.5% which is about 3mm for a 200mm blade. It is interesting to investigate the performance of the fan with higher tip clearance. Bass 1987 states that the behavior of a fan with higher tip clearance can be completely different.

The main advantage of an increased tip clearance is the safety margin that it offers in a hostile working environment (high temperature). The main disadvantage is the deterioration of the fan performance. The performance of Design1, Design2 and Design3 with higher tip clearance was simulated to prove the deterioration of the performance. The new tip clearance was set to 3% which is about 6mm for a 200mm blade.

The new tip clearance was incorporated to the rotor domains of each new design, while the rest of the domains remained the same. The new cases have the same settings and the new simulation carried out for the design point and the off design points. The results for the design point are illustrated in Table 6.8.

Table 6.8 Design point performance with tip clearance 1.5% and 3.0%

Design	TP (1.5%)	TP (3%)	%	η (1.5%)	η (3%)	%
Design1	529	422	-20.2%	79.1%	72.6%	-8.2%
Design2	550	438	-20.3%	82.1%	74.3%	-9.5%
Design3	493	408	-17%	78.0%	73%	-6.4%

The comparison of the off design performance data of new Designs with nominal tip clearance (1.5%) and high tip clearance (3%) are illustrated in Appendix "C".

The off design total pressure rise comparison for the two different tip clearances is illustrated in Figure 6.35 for the 3 new designs.

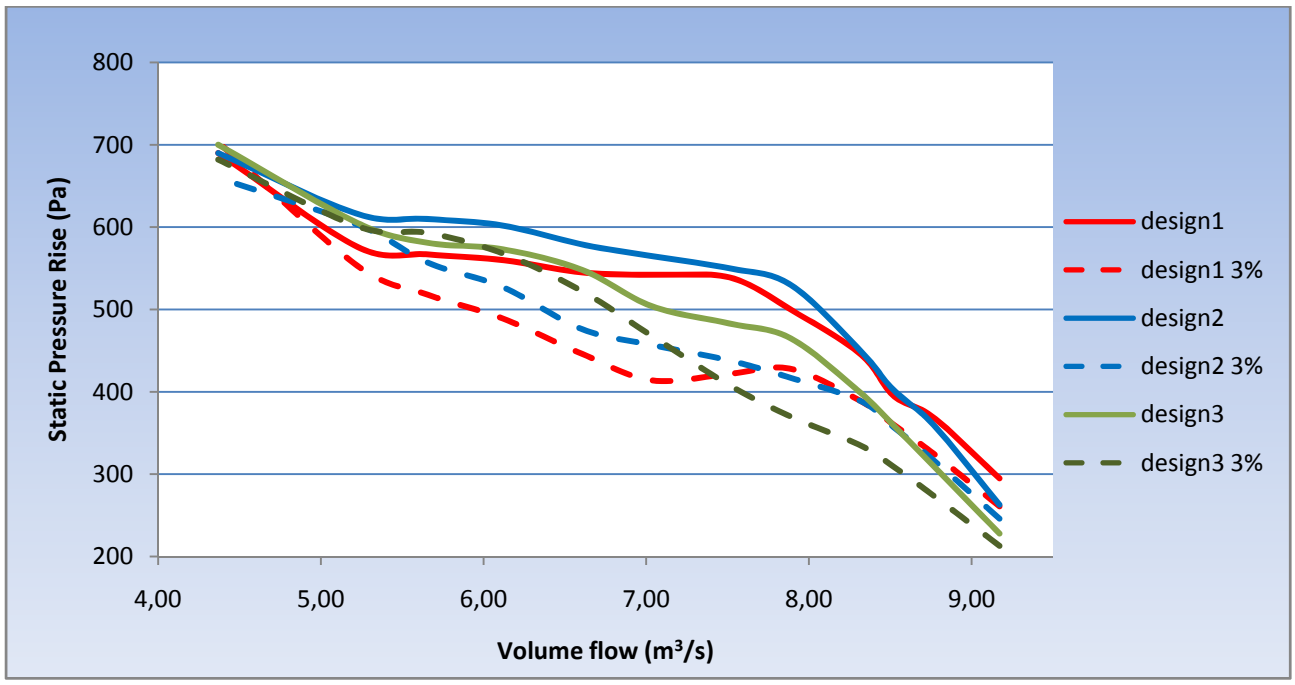

Figure 6.35 Volume flow in variation with static pressure rise

The comparison of the behavior of the case with the nominal and the high tip clearance shows that the difference in behavior is similar with the difference in behavior that Bleier, 1997 noticed in his experiments and are depicted in Figure 6.36.

From Figure 6.36 it can be noticed that for low and high volume flows the effect of tip clearance to the pressure rise is lower comparing with the effect of tip clearance at

volume flows close to the design point area. The same pattern can be noticed in the simulation results in Figure 6.35

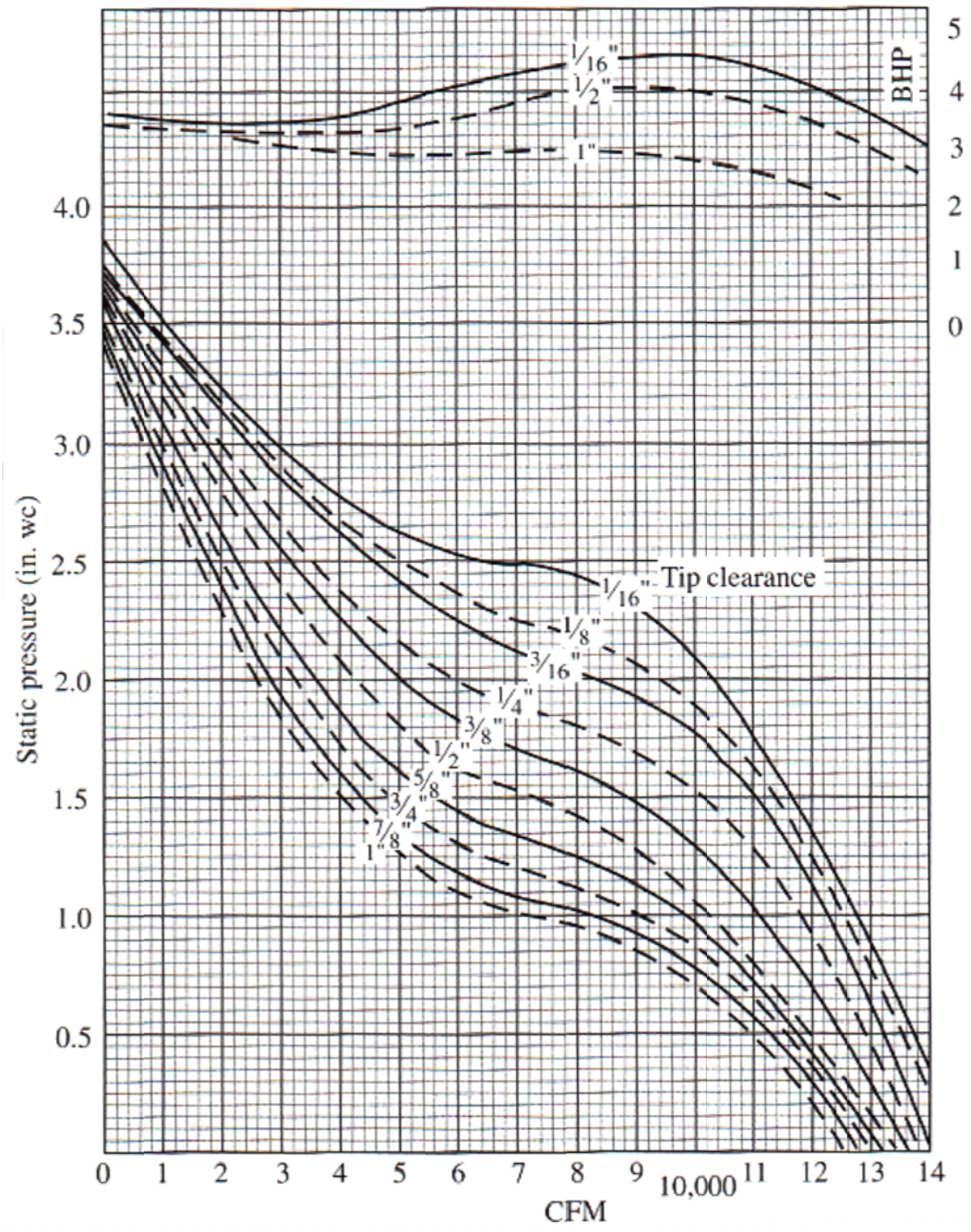

Figure 6.36 Effect of tip clearance at static pressure rise and brake horse power (Bleier, 1997)

The off design efficiency comparison for the two different tip clearances is illustrated in Figure 6.37 for the 3 new designs.

The efficiency with higher tip clearance is lower in all the range of volume flow. However in low volume flows the comparison is more difficult, due to the fact that the effect of tip clearance to efficiency is lower. The lower effect of tip clearance to efficiency is depicted in Figure 6.38. The value of efficiency at for both high tip clearance and nominal tip clearance converge to zero for zero volume flow. Therefore as the volume flow decreases the effect of tip clearance to efficiency is less that in higher volume flow efficiency

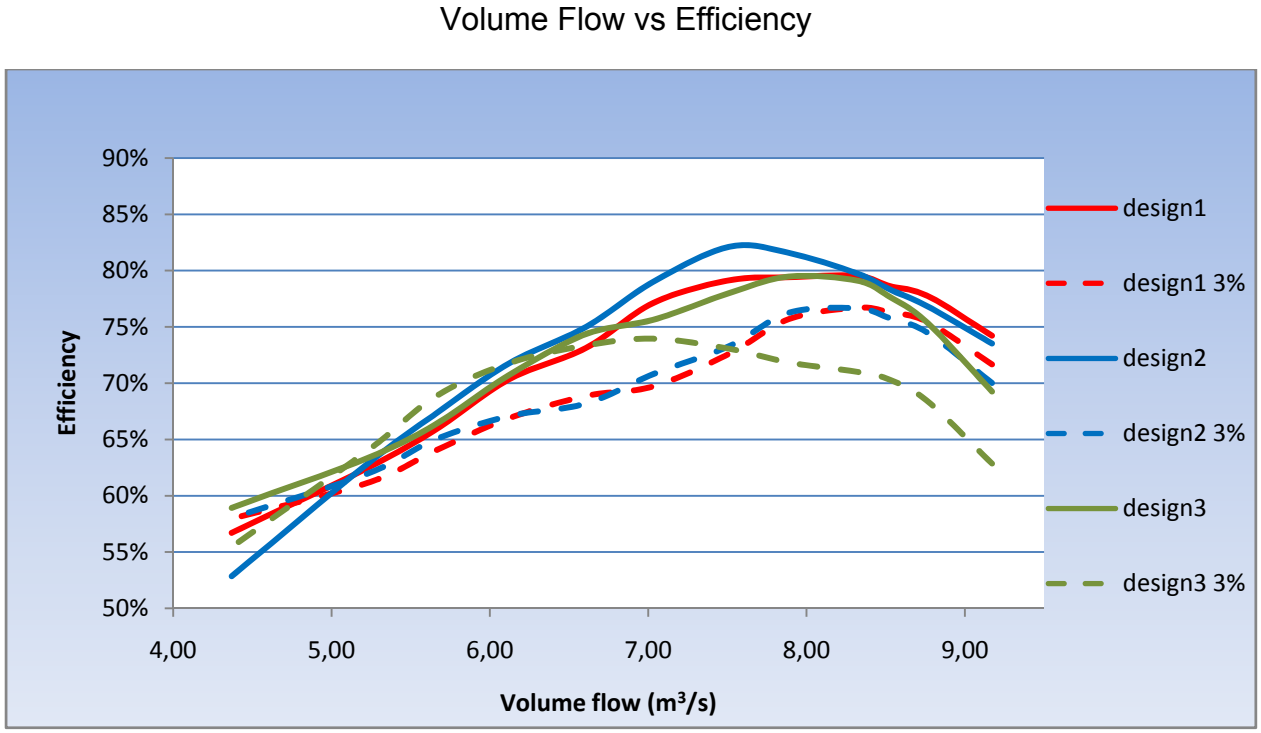

Figure 6.37 Volume flow in variation with total efficiency

The tip clearance effect can be summarized as follows:

a. Volume flow decreases slightly, because a backflow is expected which is proportional to the tip clearance

b. Maximum Static Pressure decreases considerably, because the flow resists to the pressure increase and escape backwards.

c. Power consumption decreases, but not as much as the pressure, because less volume flow is pressurized in a lower static pressure.

d. Mechanical efficiency decreases considerably, because the pressure loss is considerably higher than the power consumption decrease.

e. Small increase in the noise level at the free delivery, because of the flow that moves through the tip.

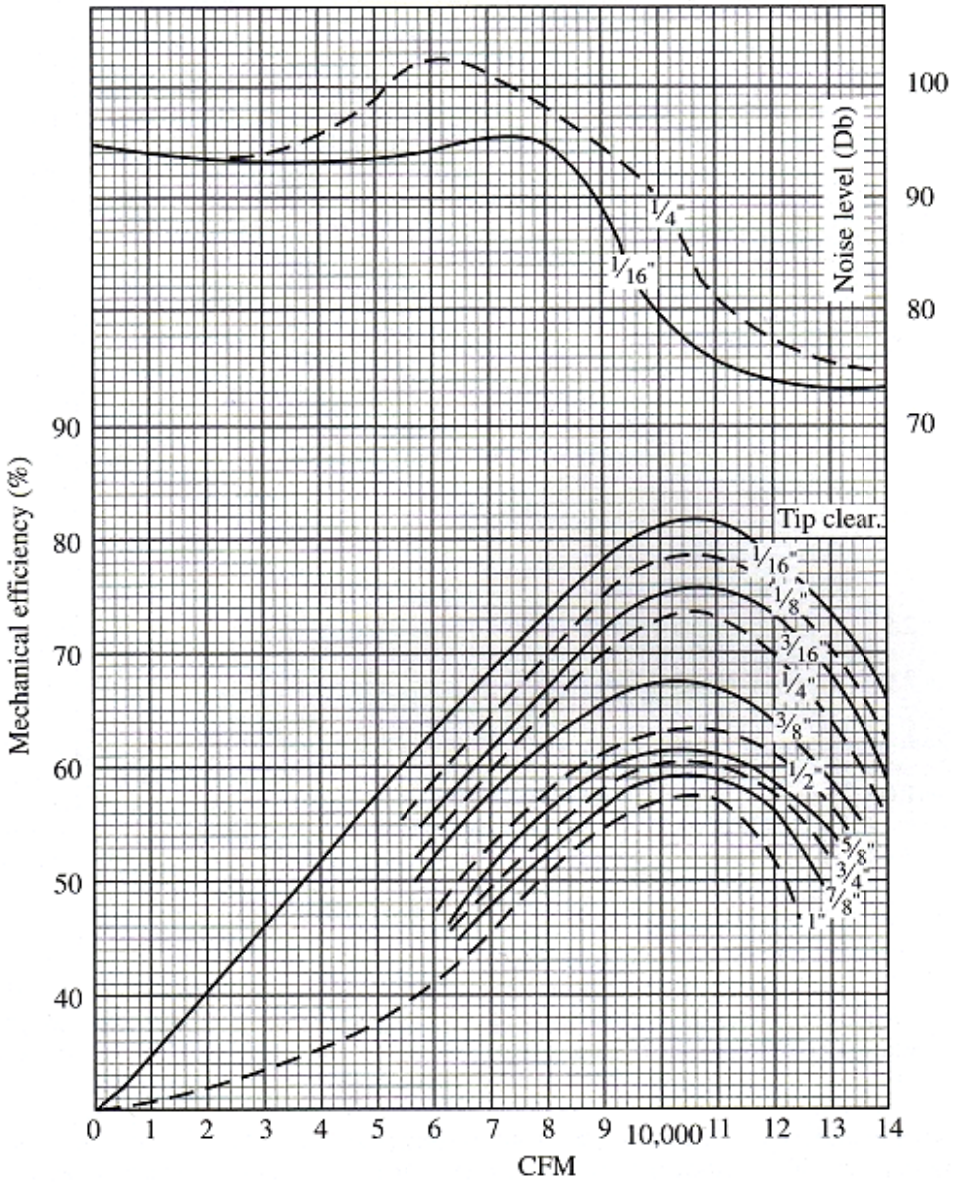

Figure 6.38 Effect of tip clearance in efficiency and noise level (Bleier, 1997)

7. Mechanical Integrity

7.1 Introduction

The mechanical integrity of axial fans depends on the loading of the fan and the available manufacturing materials. The loading of industrial and ventilation axial fans is relatively low, because the rotational velocity that generates the centrifugal loading is relatively low. The variety of the available materials for fan manufacturing is large and the designer has many options for the selection of the material.

However, in a few cases the loading of the fan is quite high because there are requirements for operation in hostile environment. A hostile environment can be a tunnel where a ventilation fan is required to operate continuously in case of a fire or a corrosive environment where the strength and the durability of the material of the fan deteriorate. In cases like this a more careful study should be take place in order to validate the safe operation of the fan under the adverse conditions.

In this chapter an attempt will be made to investigate the mechanical integrity of Design2, which was selected as the design with the better efficiency and performance. The part of the fan that will be examined is the blade, which has the higher loading. The blade is the only part of the fan that rotates and the centrifugal force has significant magnitude. The stress distribution at the blade and the blade deformation will be estimated for normal operation and for operation in high temperature condition.

The tip clearance was set at 2.9mm which is 1.5% of the 192mm blade height. The target is to estimate the deformation of the blade in order to examine if the tip clearance is large enough to ensure the safe operation.

7.2 Blade stressing

The steady stresses in a rotating blade are negligible comparing to the no steady stresses. The sources of no steady stresses in fan blades arise from the fan operation and the working environment. The major sources are as follows according to Haslam, (2007):

1. Centrifugal loading that acts at all sections of the blade, produced by the action of inertia.

2. Gas bending moment that is produced when the fluid passes across the blade and change in momentum and pressure take place.

3. Bending moment: when the centrifugal loading acts at a point which does not lie above the centre of the root datum section.

4. Shear load which arises from the centrifugal untwisting of the blade or the gas pressure.

5. Thermal stress that arise in a hostile environment.

The blade stressing in a fan depends on the volume flow rate. Cory (2005) carried out tests on a fan with Gottingen airfoil blades. The results of the experiments are illustrated in figure 7.1.

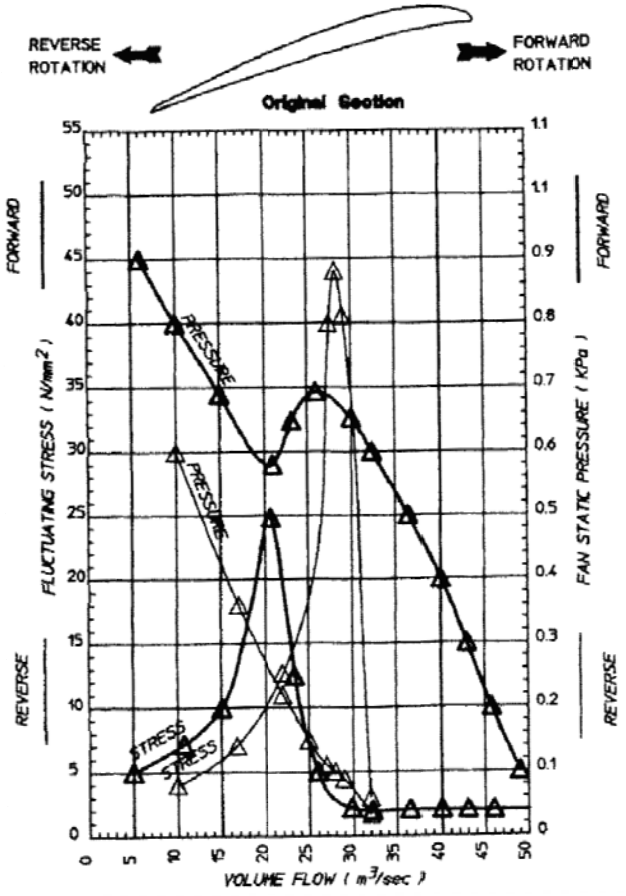

Figure 7.1 Pressure and stress distribution against volume flow (Cory, 2005)

The regular line illustrates the reverse rotation and the bold line the forward rotation line. As the volume flow decreases, the pressure increases and the stress increases as well. However, an interesting point is that the maximum stress is not coincident with the stall point.

7.3 Centrifugal stresses

The centrifugal load at the blades is due to the rotation of the cascade and the mass that the blades have. The inertial field in aero engines, where the blade operates, commits more than 50% and often 80% of the material strength to overcome the stress (Haslam, 2007). However in low speed fans the centrifugal loading has lower order of magnitude comparing with aero engines. A simple model of centrifugal loading is shown in figure 7.2.

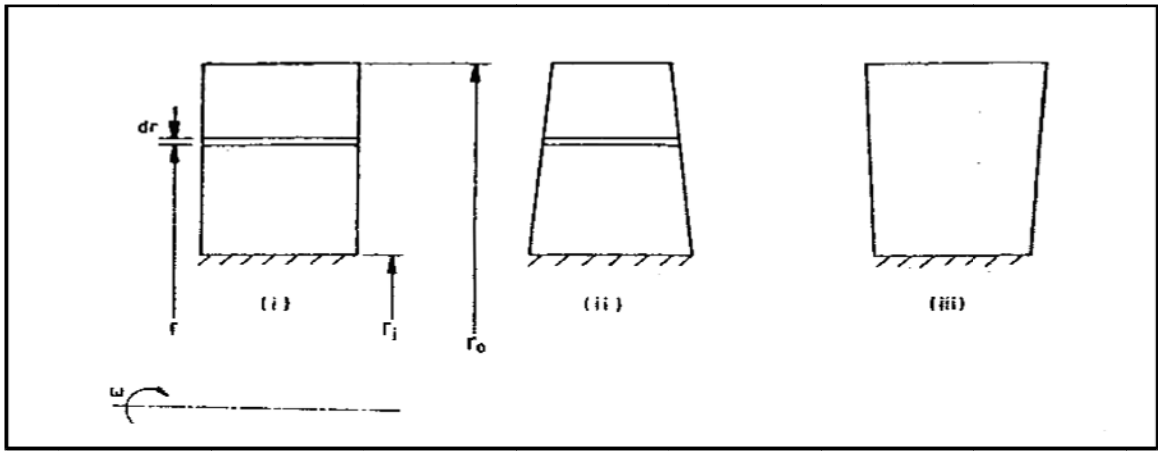

Figure 7.2 Centrifugal loading (Haslam, 2007)

$CF = mass * r_{cg} * \omega^2$ (7.1)

The mass of this blade can be written as:

Mass = Density * Cross-sectional area * height

Thus,

$CF = p * A * h * r_{cg} * \omega^2$ (7.2)

For a component with cross-sectional area of A the stress is:

$\sigma_{cf} = \rho * h * r_{cg} * \omega^2$ (7.3)

It is obvious that the stress is proportional to the square of the rotational speed, which is proven to be a crucial factor for the mechanical integrity of the blade. In low speed fans the importance of the rotational speed is downgraded.

The tapering of the blade is an important factor for the centrifugal loading. A tapered blade has less mass at the tip, which decreases the total inertia of the blade. Haslam (2007) mentioned that for a 25cm blade the centrifugal loading can be reduced about 40% if the area of the tip is half the area of the hub, comparing with a blade with constant blade area for a given rotational speed.

The centrifugal loading can be calculated by dividing the blade into sections, and calculate the centrifugal force for each section where the rotational speed is assumed constant. The individual loading of each section is divided with the cross sectional area and the result is the individual centrifugal stress. The sum of the individual forces gives the centrifugal loading and the sum of the individual stresses gives the centrifugal stress.

7.4 Fluid Forces

The change in velocity from the blade leading edge to the blade trailing edge and the pressure difference across the blade generate stresses and moments. The fluid forces act in both axial and tangential direction. The gas loads are considered individually as follows:

1. Axial Bending moment due to Pressure change.

The pressure distribution around a blade can be found by dividing the total pressure change by the number of the blades. The bending moment can be found by multiplying the total pressure force around a blade by the distance from the section under consideration to the centre of gravity of the pressure element.

$$Force = \frac{2 * \pi * r * dr * dp}{N} \qquad (7.4)$$

The bending moment can be found by multiplying the total pressure force around a blade by the distance from the section under consideration to the centre of gravity of the pressure element.

$$Moment = \frac{2 * \pi * r * (r_{av} - r) * dr}{N} \qquad (7.5)$$

2. Axial Bending and Tangential Bending moment due to Momentum change.

The force that is produced by the change of momentum is the product of the mass multiplied by the rate of velocity change. The bending moment due to momentum change is usually so small that it is ignored.

Specific mass flow = mass flow/unit annular area = m,

$$m_i = \frac{M}{\pi * (r_{TDS}^2 - r_{RDS}^2)} \qquad (7.6)$$

$$Force\ on\ the\ element(axial) = \frac{dV_A * m_i * 2 * \pi * r_{av} * dr}{N} \qquad (7.7)$$

$$Force\ on\ the\ element\ (tangential) = \frac{dV_T * m_i * 2 * \pi * r_{av} * dr}{N} \qquad (7.8)$$

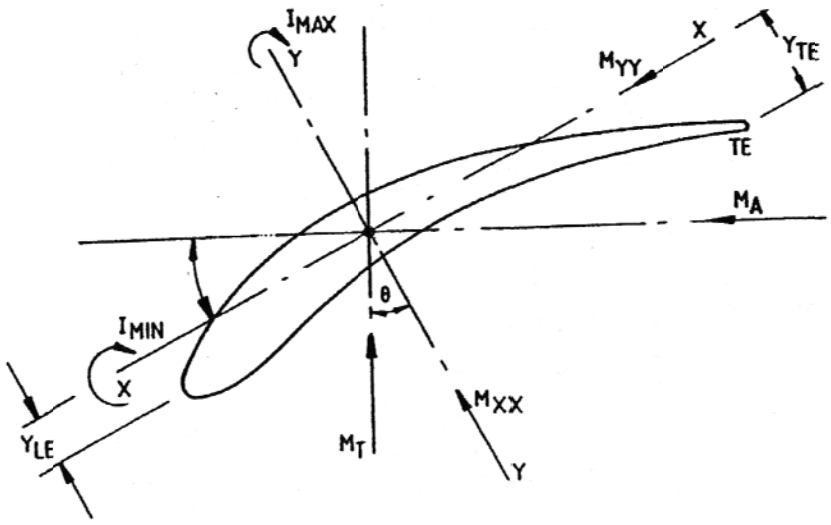

Figure 7.3 Bending Moments from gas forces (Haslam, 2007)

The bending moments in an airfoil are illustrated in figure 7.3

3. Bending Stress due to Centrifugal loading.

The bending moment is the product of inertia load of the section and the displacement from the section centre of gravity to the line through the centre of the root

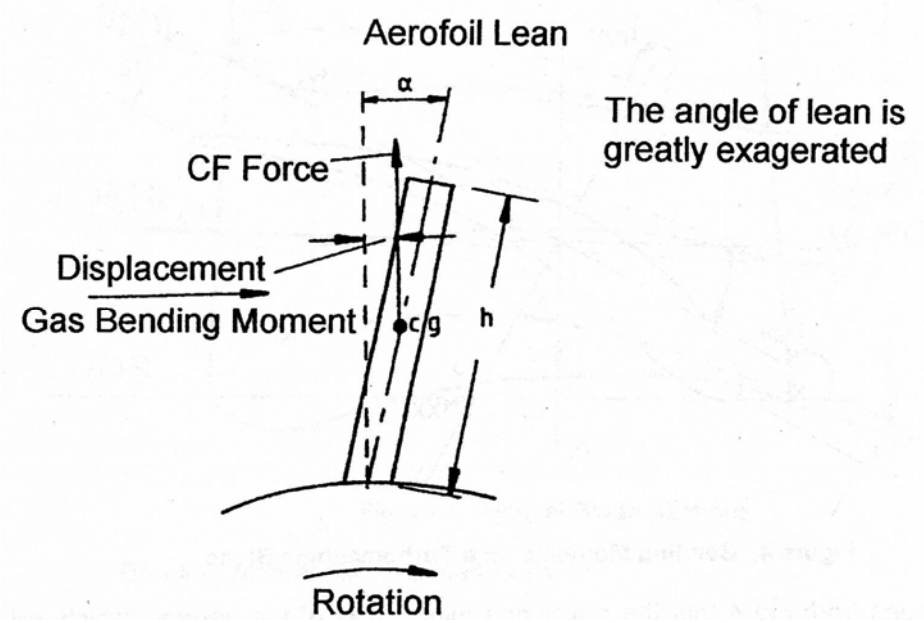

Figure 7.4 Bending Moments from centrifugal loading (Haslam, 2007)

7.5 Stresses due to Thermal Gradients

The stresses produced by the increase ambient temperature within a blade can be very destructive and are often much greater than any of the other forms of stress. An industrial fan is required to operate in case of fire for a certain period for safety reasons. In cases like this the loading is very complex because there is a combination of centrifugal loading, gas loading and thermal loading.

The maximum operation temperature for a ventilation fan is about 400^{o}C (Cory, 2005) and it is required to operate in this temperature for 2 hours as it is stated in the specifications of a emergency smoke extract fan that is already in the market (http://www.pveuk.com/axial_fans.htm).

The materials that are used for industrial fans have often poor properties comparing with the advances alloys that are used in aero engines in order to reduce the manufacturing cost. Therefore the industrial fan material properties are affected significantly in high temperatures as it is illustrated in figure 7.5.

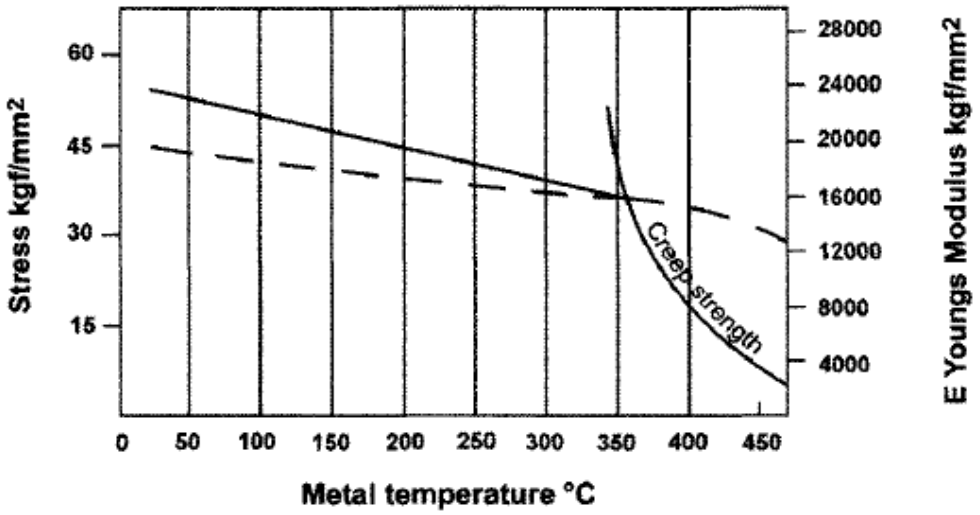

Figure 7.5 Strength and Young modulus variation with temperature for typical carbon steel (Cory, 2005)

The important material properties for ventilation fan blades are the ultimate tensile strength (100-500MPa), the elongation at break (15-20%), the ductility (4%), creep resistance (400^{o}C), the corrosion resistance, the impact strength, the fatigue strength.

7.6 Blade loading simulation software

An attempt is made to simulate the blade loading for various combinations of mechanical loading and thermal loading. The blade that was used for the simulation is the blade from Design2.

The software that is used for the simulation is the Static Structural component of ANSYS Workbench. The procedure to carry out the simulation was as follows:

1. Geometry: The geometry of the blade that was used for the simulation was exported from Turbogrid.

2. Meshing: the meshing of the blade is a straight forward procedure especially for a simple geometry like a single blade. For mechanical applications

and there are three options for the mesh quality: coarse, medium, fine. A fine mesh was selected for the simulation with 6226 elements.

3. Inertia loading: These loads act on the entire system. The setting of the rotational velocity and the axis of rotation are set. The rotational speed was set to 172.8 rad/sec which is 1650rpm. The centre of rotation was set to 208mm which is the radius of the hub of Design2.

4. Structural loads: The aerodynamic forces and moments are imported from the CFX simulation of the fluid flow.

5. Structural supports: The constraints that prevent movement on certain regions. In this case the constraint is the blade hub. The blade hub constraint represents the connection of the blade with the hub.

6. Thermal loads: The thermal loads which result in a temperature field causing thermal expansion/contraction in the model. The Thermal loading that were simulate were 0^{o} C, 50^{o} C, 100^{o} C, 300^{o} C and 400^{o} C.

7.7 Blade loading simulations

Simulations were carried out for steady mechanical loading under different thermal loading. As it was mentioned before the mechanical loading depends on the rotational speed and the volume flow. The rotational speed is steady in an industrial fan and the volume flow that was selected is the volume flow of the design point. The temperature ranges from 50^{o} C to 400^{o} C.

The stress depends only on the loading from the centrifugal force and gas forces. The temperature contributes only to the total deformation of the blade and not to the stress. The target is to calculate the deformation of the blade in the above mentioned conditions and estimate if the tip clearance is high enough to ensure the safe operation under high temperature.

The material choice is a challenge for the designer. For this particular study Aluminum 6061-T6 was used. The first simulation carried out for without thermal loading in order to calculate the stress distribution and the deformation for normal operation. Figure 7.6 illustrates the deformation distribution of a fan blade from aluminum alloy 6061-T6. The maximum deformation is 0.077mm at the thinnest area of the tip.

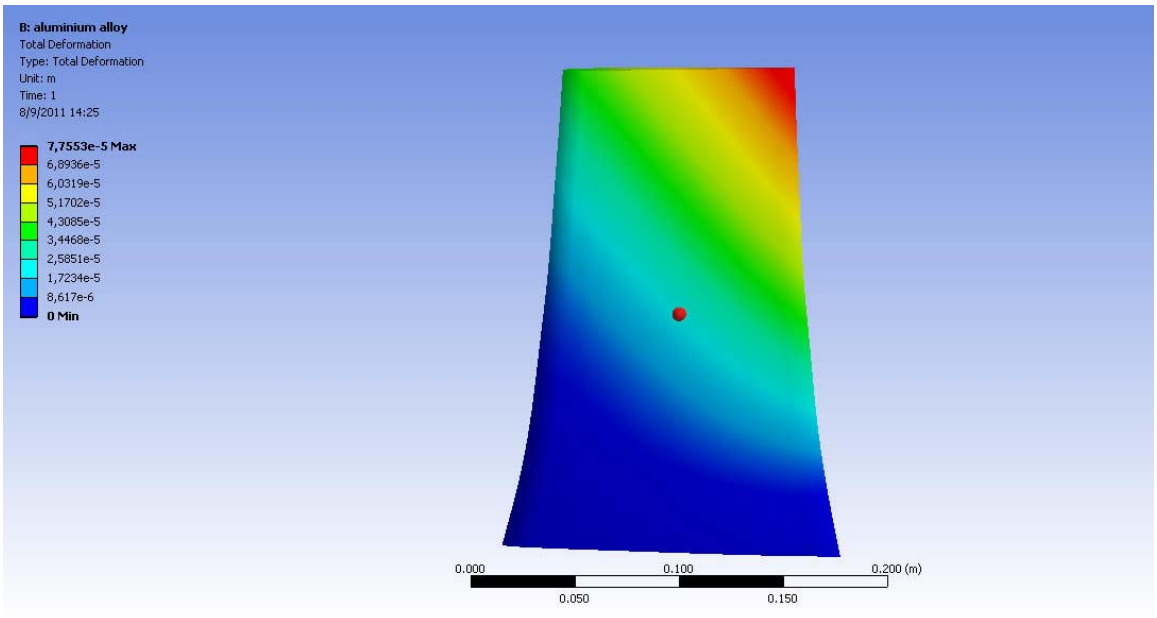

Figure 7.6 Blade deformation for normal operating conditions for aluminum 6061-T6

The deformation is higher at the tip because the centrifugal force highest value is at the tip according to Haslam (2007) and the thinnest area is more susceptible to deformation. The deformation pattern is the expected one according to Naeem et al.

The stress distribution at the blade is shown in figure 7.7 and figure 7.8.

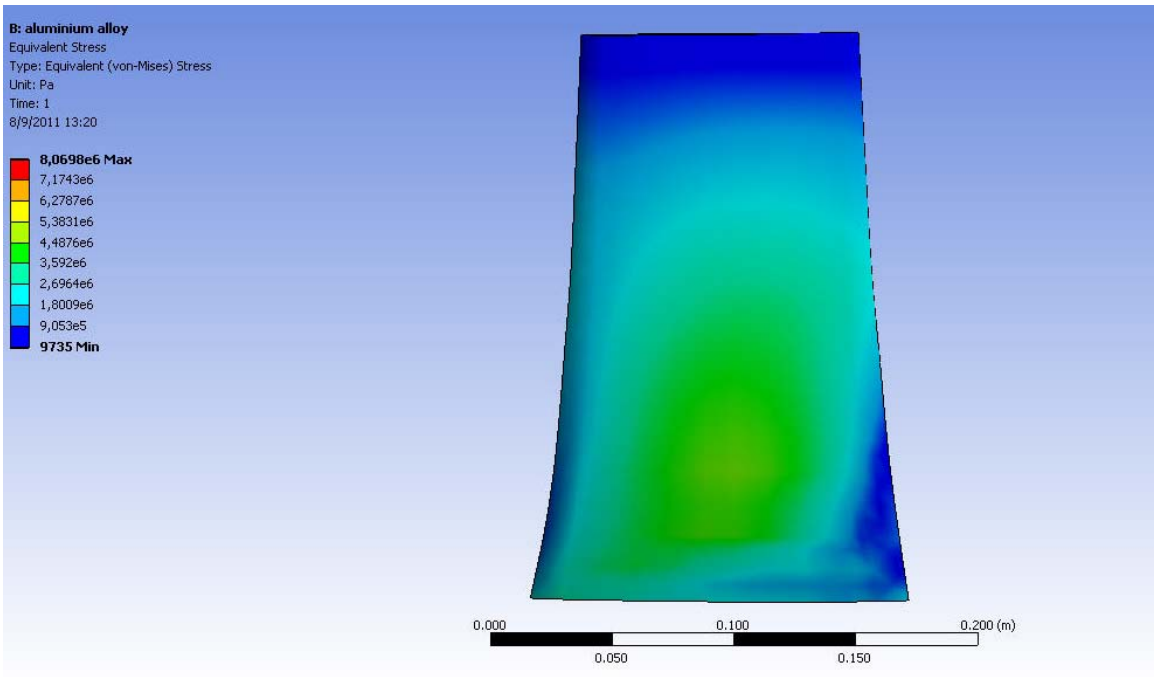

Figure 7.7 Stress distribution for normal operating conditions for aluminum 6061-T6

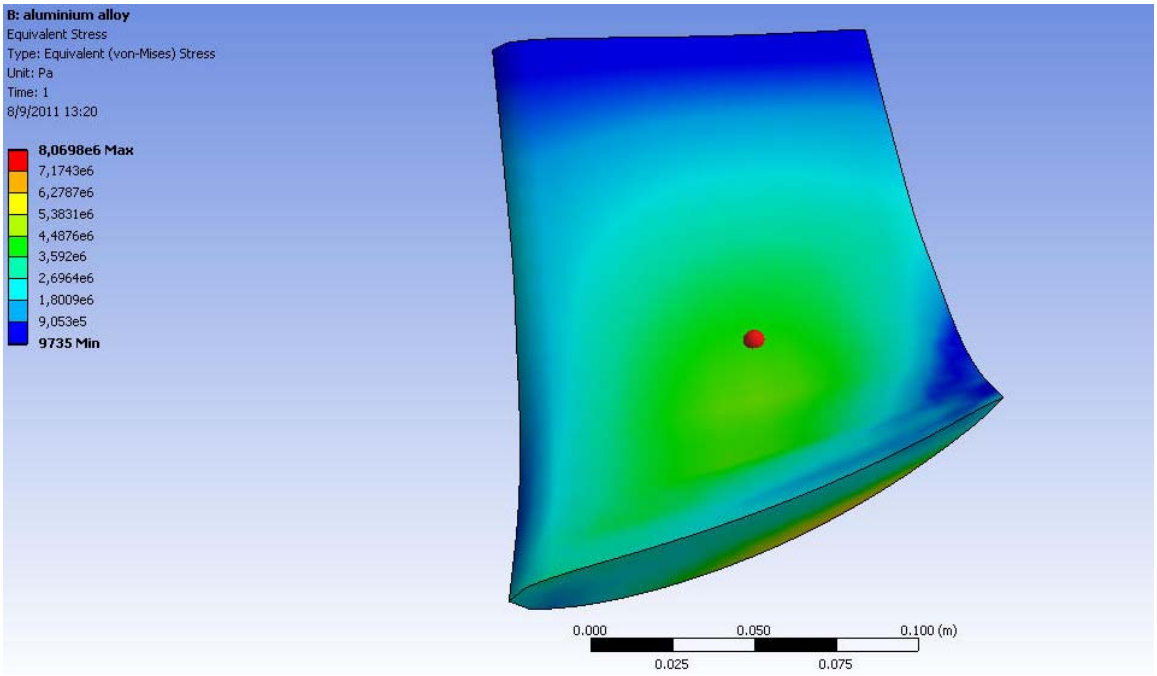

Figure 7.8 Stress distribution for normal operating conditions for aluminum 6061-T6

The maximum equivalent stress (von Mises stress) at the blade is approximately 8 MPa or 1.16 ksi which was expected for an industrial fan with 1650rpm. Osbourne (1979) estimated the equivalent stress for a smaller fan (60% outside diameter) and with lower rotational speed (960rpm) at 0.7 MPa, therefore 8MPa for a 0.8m fan with 1650rpm is a logical value.

The next step is to simulate the blade operation in an environment with higher temperature. The first simulation was carried out for a temperature of 50^{o} C and the deformation is depicted at figure 7.9.

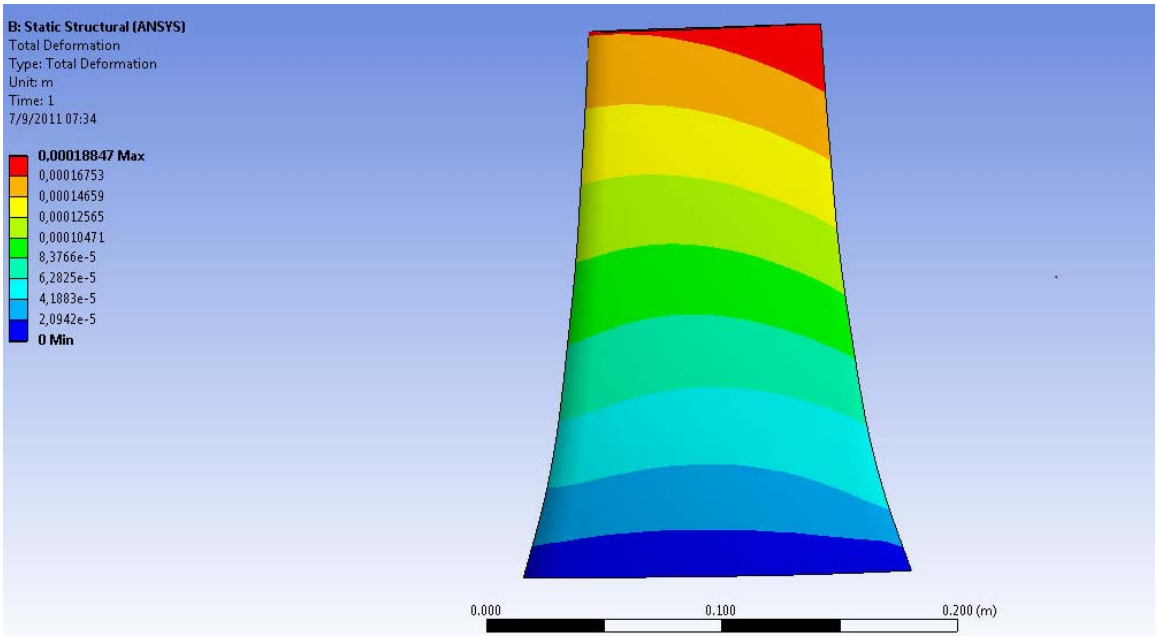

Figure 7.9 Blade deformation for operation in 50^{o} C for aluminum 6061-T6

The deformation is 0,18mm and the distribution is different comparing with the deformation distribution at normal conditions of figure 7.6. This is due to the fact that the thermal gradient generates uniform deformation at every section of the blade. The combination of the uniform deformation from the thermal gradient and the deformation from mechanical loading creates this deformation pattern. The tip clearance is 2,9 mm so the operation in 50^{o} Celsius is safe as it was expected.

Figures 7.10, 7.11, 7.12, 7.13 illustrate the deformation of the blade for temperatures of 100^{o}C, 200^{o}C, 300^{o}C and 400^{o}C respectively. The deformation pattern in figures 7.10, 7.11, 7.12, 7.13 shows that the deformation due to the thermal gradient dominates over the deformation due to mechanical loading, from the temperature of 100^{o}C.

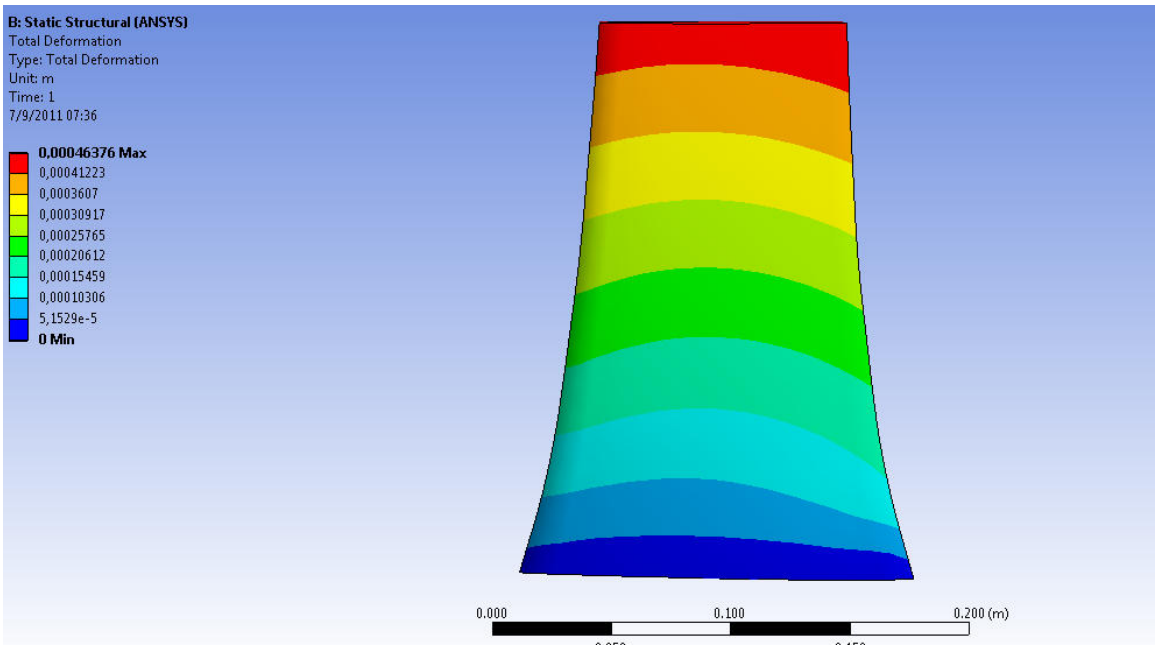

Figure 7.10 Blade deformation for operation in 100^{o} C for aluminum 6061-T6

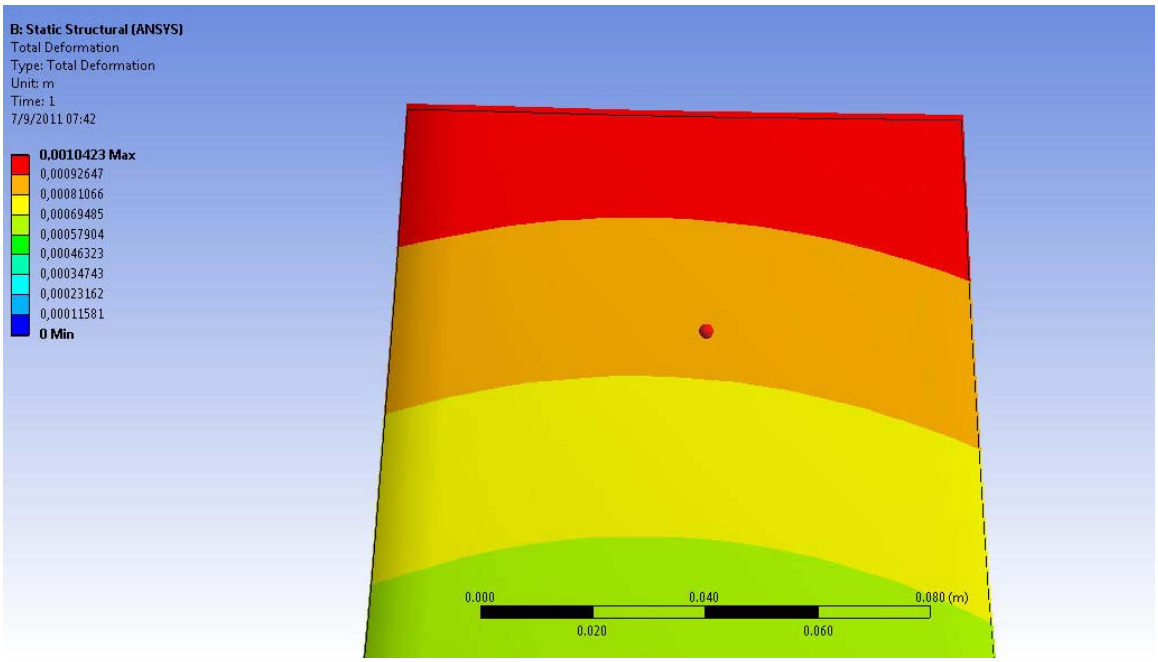

Figure 7.11 Blade deformation for operation in 200^{o} C for aluminum 6061-T6

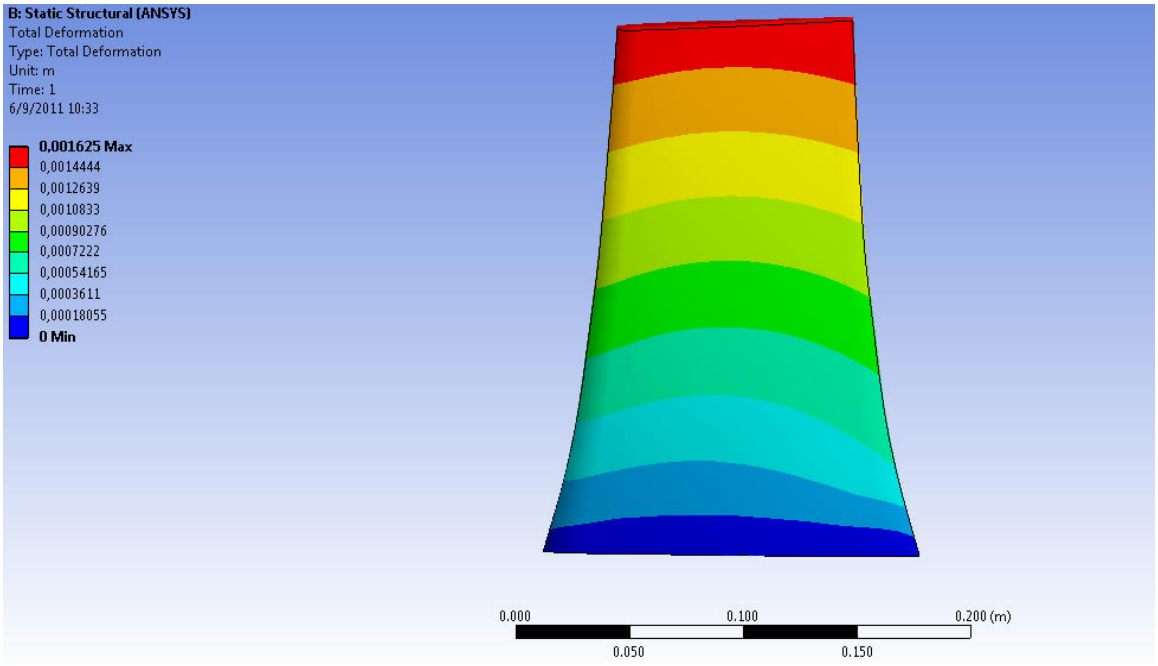

Figure 7.12 Blade deformation for operation in 300^{o} C for aluminum 6061-T6

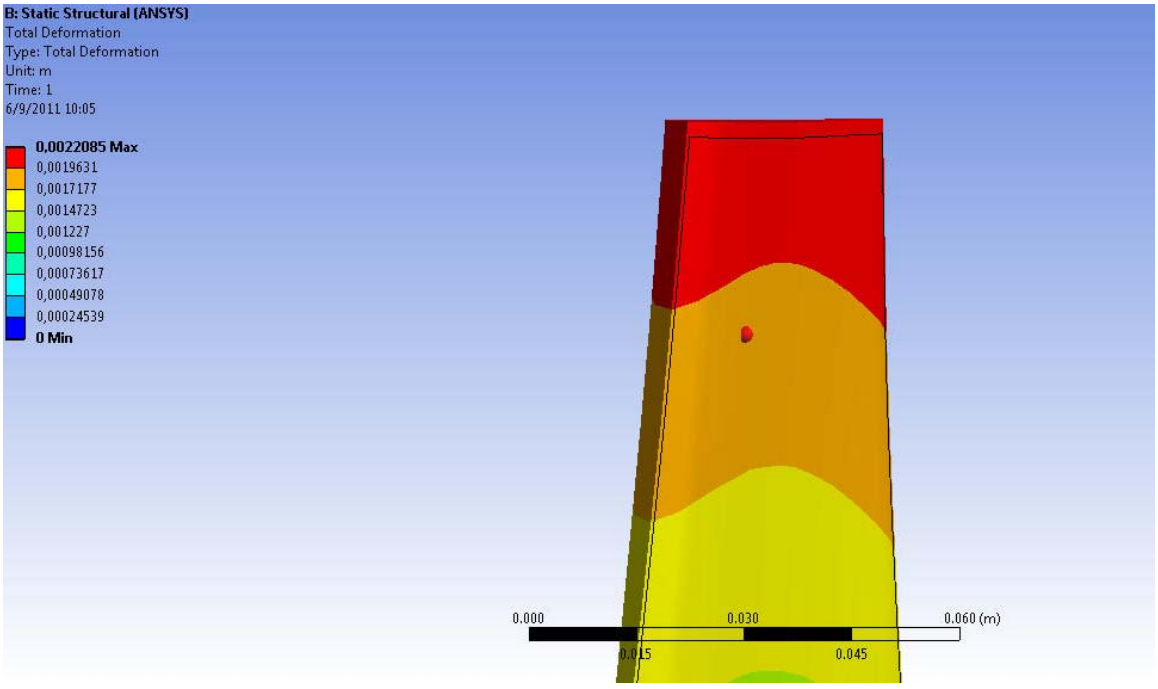

Figure 7.13 Blade deformation for operation in 400^{o} C for aluminum 6061-T6

In figure 7.11 the deformation in actual scale can be observed. The black line shows the blade before the deformation, therefore the value actual deformation of the blade can be estimated. Figure 7.12 depicts the deformation

pattern at 300°C. It is obvious that the deformation due to thermal gradient dominates over the deformation due to mechanical loading. In figure 7.13 the actual deformation for 400°C can be better observed because it is two times higher than the deformation in 200°C. The blade deformation for various temperatures is shown in table 7.1

Table 7.1 Deformation variation with temperature

	rotational speed (rad/sec)	Temperature(C)	Total Deformation max (mm)
1	172	22	0.077
2	172	50	0.188
3	172	100	0.463
4	172	200	1.042
5	172	300	1.625
6	172	400	2.208

The diagram in figure 7.14 depicts the deformation variation with temperature and gives a better reflection of the variation.

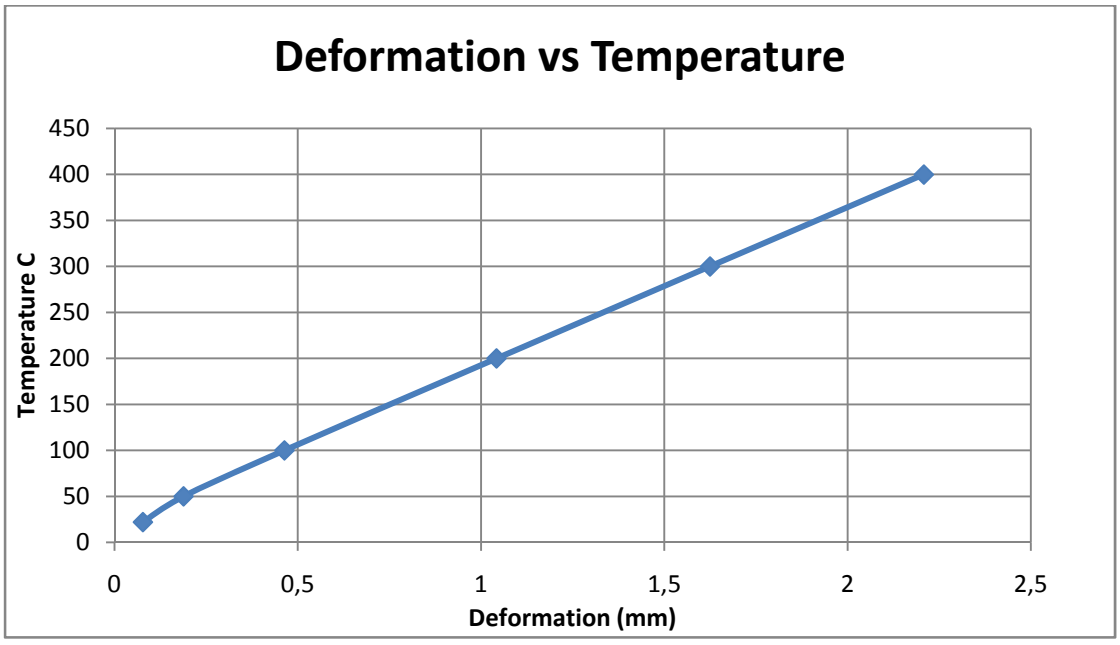

Figure 7.14 Blade deformation variation with temperature under constant mechanical loading for aluminum 6061-T6

Another way to calculate the deformation of the blade in various temperatures is to use the material properties. The material properties of aluminum 6061 T6 were found on the internet at http://asm.matweb.com/search/SpecificMaterial.asp?bassnum=MA6061t6.

The deformation of a material can be calculated using the coefficient of thermal coefficient. The thermal expansion coefficient describes by how much a material will expand for each degree of temperature increase. It was assumed that the total deformation is the sum of the deformation due to thermal gradient dominates plus the deformation due to mechanical loading. The results are summarized in Table 7.2

Table 7.2 Deformation variation with temperature

Temperature (C)	Coefficient of thermal expansion	Deformation due to thermal gradient (mm)	Deformation due to mechanical loading (mm)	Total deformation (mm) calculated	Deformation max (mm) from simulation	Difference (%)
22	0	0.000	0.115	0.115	0.078	48.77
50	0.0000236	0.236	0.115	0.351	0.188	86.44
100	0.0000252	0.504	0.115	0.619	0.464	33.56
200	0.0000252	1.008	0.115	1.123	1.042	7.78
300	0.0000252	1.512	0.115	1.627	1.625	0.15
400	0.0000252	2.016	0.115	2.131	2.209	-3.49

The maximum deformation for 400^{o}C operating temperature was calculated 2.2mm, while the tip clearance is 2.9mm. This means there is a 31% safety margin which is not necessary enough to ensure the safe operation for long period. The maximum deformation was 1.62mm at 300^{o}C and this means there is a 50% safety margin which gives a safety factor of 1.5.

7.8 Creep life calculation

The next step is the attempt to examine the influence of the time to deformation. The influence of time can be calculated using the Larson Miller parameter for the estimation of the creep life.

Creep is the progressive deformation of a material under a constant load at elevated temperature. The strength of materials reduces with increasing

temperatures. This happens, mainly, because high temperatures result in greater mobility of dislocations by the mechanism of climb and in an increase in the equilibrium concentration of vacancies. Prolonged exposure at elevated temperatures can also produce deformations at grain boundaries (re crystallization and grain growth). The same combination of load and temperature can lead to possible destructive oxidation with possible intergranular penetration of oxide.

The phenomenon of creep is dependant to load, temperature and time of exposure at the high temperature. Materials have resistance to creep loading, which is described by homologous temperature. Homologous temperature of a material is the absolute temperature to absolute melting temperature ratio. Usually aero-engines alloys will creep at $0.5*T_{melting}$ to $0.7*T_{melting}$ temperature. There are three stages of creep, as it is illustrated in figure 7.15

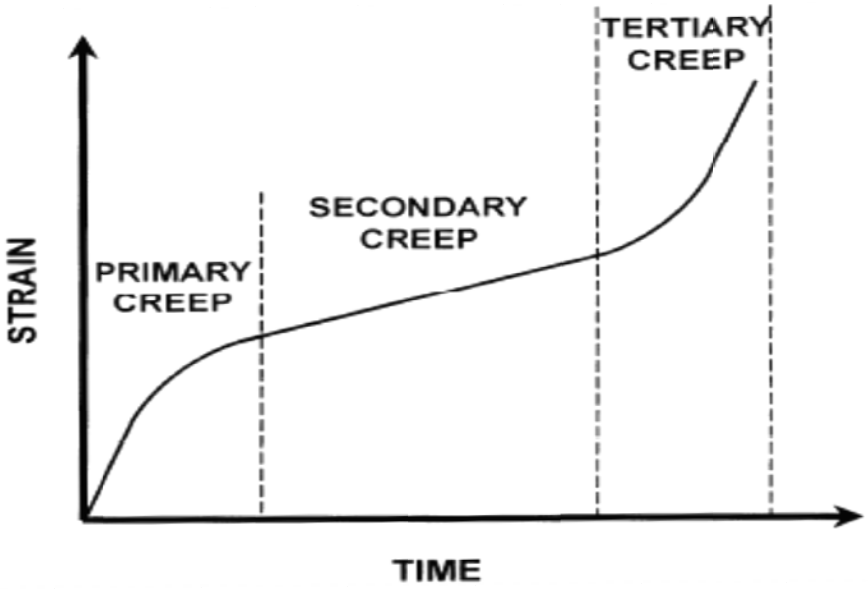

Figure 7.15 Three phases of creep (Andreadis, 2009)

The most popular of the time-temperature parameters is the Larson-Miller parameter. If the Larson-Miller parameter is known as well as the load and the working temperature of a material, a reliable predicted creep life can be calculated.

The equation for Larson Miller parameter is:

$$LMP = \frac{T}{1000} * (logt + C) \qquad (7.9)$$

Where:

T : operating temperature,

t : the time to failure

C : constant, usually about 20 for most of the applications, but it can vary according to the conditions.

The Larson Miller parameter can be found at the material properties. From Kaufman's (2008) database for high temperature aluminum alloys it was observed that the magnitude of stress, which in the case that is examined is 8 MPa or 1.16 ksi, is relatively very low for an aluminum 6061-T6. The minimum value for the stress that was used to create the database was 2 ksi and the maximum temperature 750^{o} F which is approximately 400^{o} C.

The Larson Miller Parameter that was used to calculate the creep life of the fan derived from the plot of figure 7.16.

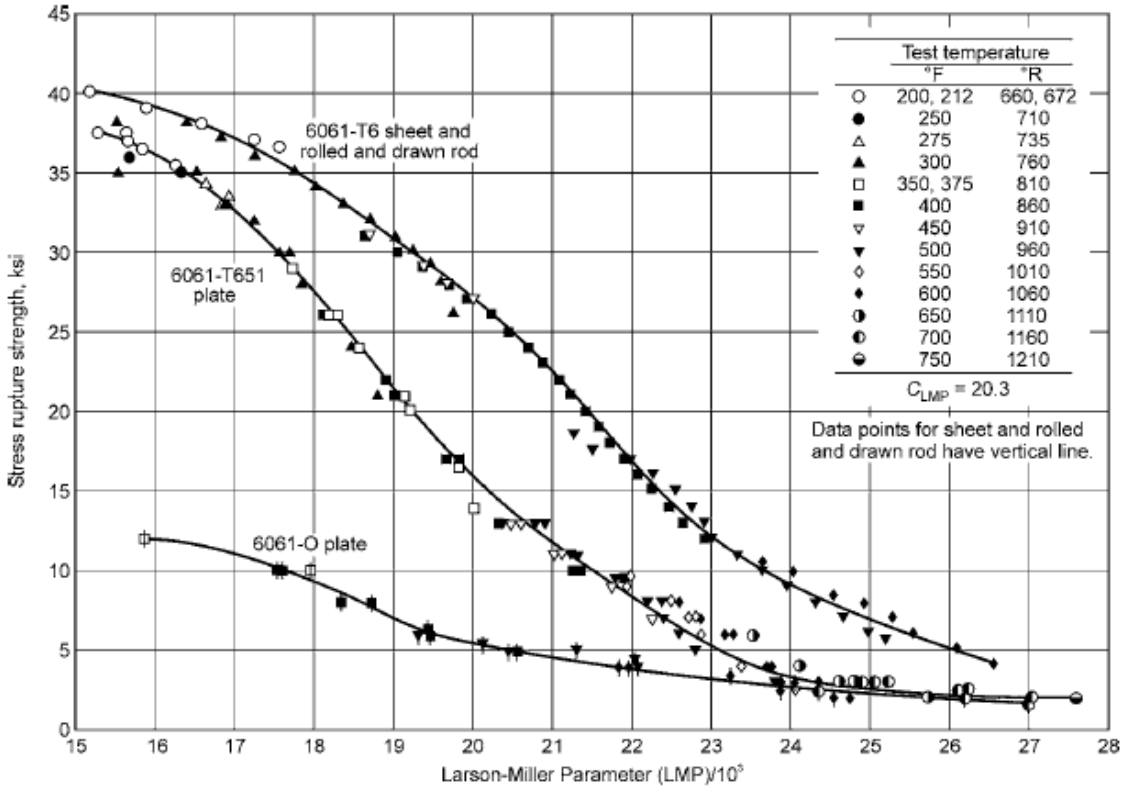

Figure 7.16 Larson Miller parameter for aluminum 6061-T651 for C-=20.3 (Kaufman, 2008)

The lower the value of the Larson Miller Parameter is, the higher the expected creep life. A conservative choice for the Larson Miller Parameter is 26. The choice is conservative because for 1.16 ksi of stress there is no LMP at the diagram which means that the amount of stress can not cause creep whatever the temperature.

For LMP=26 and for 400^{o}C which are converted to 673^{o}K, the time to rupture t is 2.15 * 10^{18} hours which is practically infinite.

The time that was calculated was time to fracture. From the material properties it is known that the elongation at break is approximately 17% of the length. For a 192 mm blade, the elongation at break will be 32,6 mm, while the tip clearance is 2.9 mm. This means that the deformation will be critical at the first phase of the creep period. However, and taking into account the infinite time to failure, creep does not consist a critical factor for the fan safety.

7.9 Conclusions

The preliminary examination of the mechanical integrity of the new designed fan can be summarized as follows:

1. There is no concern about mechanical integrity when the fan operates at normal conditions.

2. The safety factor for 300^{o}C was calculated 1.5 and for 400^{o}C it was calculated 1.25. The 25% safety margin at 400^{o}C is not acceptable and alternative solution should be introduced.

a. Selection of a material with better resistance in thermal loading. This will increase the manufacturing cost of the fan

b. Revaluation of the worst case scenario (400^{o}C). If the upper limit is 300^{o}C there is no need to improve the thermal strength of the fan.

3. Under the worst loading (400^{o}C), there is no risk of blade rupture (break) due to creep. The total deformation (elongation) when the material fails (break) was calculated 32.6mm, while the tip clearance is 2.9mm. This means that a lot before the break, the deformed blade will reach the shroud and the operation of fan will stop. The time needed for the blade operating at 400^{o}C to reach the shroud cannot be calculated.

The mechanical design of arduous duty fans can be extremely complex because the thermal gradient effect can only be estimated. Modern materials are not always fully documented and their limitations may be found only through experience. Nevertheless, the application of principles from strength of materials and theory of machines can produce acceptable designs.

8. Conclusions and recommendations

8.1 Project Summary

The main objective of this project was the review of low speed design methodologies and the application of one such approach to the redesign of a datum geometry. A suitable fan design procedure has been established based on the existing literature employing the free vortex design concept. The applicability of the design procedure, and to a certain extent its degree of accuracy, have been established by using appropriate CFD software for the simulation of the fan performance. Three new fans have been designed by using the validated design procedure, the existing design tools and MATLAB codes that have been developed as part of this study. The efficiency of the second design was higher than the efficiency of the datum fan and the off design performance has been demonstrated to be satisfactory. The mechanical integrity of the new fan is acceptable, but the thermal strength has to be improved in order to give an higher safety factor when operating in a high temperature scenario such as a in the vicinity of a fire.

8.2 Conclusions

The fan design process is a compromise between the customer requirements and the aerodynamic and mechanical constraints. As Bass, 1987 states, it is difficult to design a very bad fan and it is difficult to design a very good one. Between a very bad fan and a very good one lie a large number of fans with acceptable performance and satisfactory efficiency. In this Thesis a design procedure has been established which was used to design vaneaxial fans with higher efficiency than similar size existing designs have. Three new fans were designed and optimized and the experience from the older design was used for the newer design. Finally the best efficiency achieved was 82.1% which is about 3% higher than the efficiency of the given fan.

The maximum efficiency and the total pressure rise for the design point of the 3 new designs and the given fan are summarized in Table 8.1

Table 8.1 Summary of the 3 new designs

	Total Pressure Rise (Pa)	Efficiency
Given Fan	506	79.5%
Design1	529	79.3%
Design2	550	82.1%
Design3	483	79.5%

The power consumption is not an important factor for small fans, but it becomes a significant factor for large fans that operate continuously. In cases like this, small efficiency improvement can represent substantial cost reduction. In this work has been proven that the efficiency of a vaneaxial fan can be improved with the careful design of the downstream guide vanes in order to reduce the losses from separation and convert the energy of the swirl velocity to useful static pressure rise.

The tip clearance is a critical factor for the performance and the mechanical integrity of a vaneaxial fan. The increase of tip clearance from 1.5% of the blade span to 3% of the blade span reduces the efficiency by 6.5-9.5%. The mechanical integrity of the fan is better with higher tip clearance because the fan can operate in higher temperature for longer period of time.

All the above mentioned results were outputs from CFD simulations. The performance of the new designs has been examined only with CFD and there are no experimental data. A divergence was noticed between the performance of the model that was the output of the design procedure and the performance according to the CFD results. The main reason for this divergence is the three dimensional effects that are not taken into account in the design procedure. Another important observation is that the selection of the turbulence model during the set up of the physics in the CFD has an immediate impact in the performance of the fan. The k-ω turbulence model does not overestimate the turbulence as the k-ε model does and the performance acquired using the k-ω model is better than with the k-ε model. The disadvantage of the k-ω model is the difficulty in convergence.

8.3 Recommendations for further work

During the design process many compromises and arbitrary choices have been made. A small change in these choices can influence the performance of the fan. All these factors can be separately examined in order to estimate their impact to the performance of the fan.

1. Wide tip blade

Wide tip blades generally give better efficiency than the narrow tip blades. All the new designs have narrow tip in order to have better mechanical integrity. The examination of the mechanical integrity proved that the centrifugal loading is relatively low, so there is enough safety margin to design a wide tip blade for further efficiency improvement. A wide tip blade can be easily incorporated to the established design procedure.

2. Free Vortex Design

The free vortex design concept was selected because it is more convenient to standardize a design procedure based on this design concept. The three new designs are then free vortex designs Sorensen, 2000 developed an aerodynamic model for arbitrary vortex flow and Lewis, 1996 as well. These design concepts can be used alternatively to give a fan design.

3. Rotational Speed

The rotational speed of the new designs is from 1600-1650 rpm. It's difficult to achieve this rotational speed with the existing motors. The motors that are in the market for this range of rotational speeds usually give 1500rpm or 1750rpm and the given fan has a motor that gives 1500rpm. New models can be further developed with these rotational speeds.

4. Alternative airfoil

The base airfoil that has been used for the new designs is the C4 airfoil. The MATLAB code that has been developed can use any airfoil. The NACA 65 airfoil is an established alternative choice for the airfoil. New design can be developed using the NACA65 airfoil and incorporated it to the design procedure.

5. Correlation of blade angles with air angles

The design procedure that has been established correlates the blade angles with the air angle with a formula which was the result of experiments in a C4 cascade. The use of different airfoil requires the re-establishment of the correlation between the blade angle and the air angle. Since it is quite difficult and expensive to set a series of new experiments, a good alternative could be the trial and error method using CFD simulations.

6. Vane design

The vanes of the new designs have airfoil shape. Airfoil shaped vanes increase the total cost of the fan. The performance of the new designs can be examined with single thickness vanes.

7. Coding of the design procedure

The design procedure has been developed in an excel file. The use of data from Tables and Figures has made the coding of the procedure quite difficult. An attempt to code the design procedure can make the procedure more convenient for the user.

8. Material properties

The material that was selected for the fan blades is the Aluminum 6061-T6. The safety factor for the extreme use under 400^{o} C is 1.25 and it can be further improved with the use of a material with better thermal strength. The mechanical integrity of a model with wide tip blades and better material can be additionally examined.

1 Strohmeyer, H. (2009), *Improving the Efficiency of an Industrial Low Speed Fan*, MSc Thesis, School of Engineering, Cranfield University

2 Bleier, Frank P. (1998), *Fan Handbook: Selection, Application, and Design*, McGraw-Hill Companies. Inc., New York

3 McKenzie A.B. (1997), *Axial Flow Fans and Compressors*, Aerodynamic design and Performance, Ashgate

4 Osborne William C. (1977), *Fans 2nd Edition (in SI/Metric Units)*, Pergamon Press

5 Eck, Bruno (1973), *FANS Design and Operation of Centrifugal, Axial Flow and Cross Flow Fans*, Pergamon Press

6 Tu J., Yeoh G.H., Liu C. (2008), *Computational Fluid Dynamics a Practical Approach*, Butterworth-Heinemann

7 Ramsden, K. W. (2008), *Course Notes for Axial Compressor Design and Performance*, Lecture Notes, Cranfield University

8 Lewis, R. I. (1996), *Turbomachinery Performance Analysis*, Butterworth-Heinemann

9 Cumpsty, N. A. (1989), Compressor Aerodynamics, Longman Singapore Publishers Ltd

10 Terzis A., Kalfas A. I., Zachos P., Ramsden K. W. (2009), *Experimental, Performance Evaluation of Axial Ventilators,* The 9th International Conference on Industrial Ventilation

11 Bass, R.M. (1987), *Factors influencing the aerodynamic design of low pressure axial fans*. In: Industrial Fans-aerodynamic design, London, April 09, 1987

12 Palmer J.R., Pilidis P. (2008), *Gas Turbine Theory and Performance, Lecture Notes*, Cranfield University

13 Rubini P.A, *Turbine Blade Cooling, Lecture Notes*, Cranfield University, 2008

14 Walsh Philip P., Fletcher Paul (2004), *Gas Turbine Performance Second Edition*, Blackwell

15 Cookson R.A., Haslam A.S. (2008), *Mechanical Design of Turbomachinery, Lecture Notes*, Cranfield University

16 Angoy C.H. (1984), *Fan Design : a novel flat blade design,* Thesis, School of Engineering, Cranfield University

17 Turner R. C. (1966), *Notes on Ducted Fan Design,* Ministry of Aviation Aeronautical Research Council Current Papers

18 Terzis A, Stylianou I, Kalfas A, Ott P. (2011), *Effect of Stators on the Performance and the Thermal Capabilities of Small Axial Cooling Fans,* The 10th International Symposium on Experimental Computational Aerothermodynamics of Internal Flows

19 Hay N, Mather J. S. B., Metcalfe R (1989), *Fan blade selection for low noise,* Proceedings of the Institution of Mechanical Engineers, Part A: Journal of Power and Energy *August 1989 vol. 203 no. 3 149-154*

20 Smith T. W., *A practical approach to the design of axial and mixed flow fans*

21 McKenzie A. B. (1988), *The selection of fan blade geometry for optimum efficiency,* Proceedings of the Institution of Mechanical Engineers, Part A: Journal of Power and Energy *February 1988 vol. 202 no. 1 39-44*

22 Cory W. T. W. (2005), *Fan and Ventilation,* Elsevier, ISBN 0-080-44626-4

23 Kaufman G. J. (2008), *Parametric analyses of high temperature data for aluminum alloys,* ASM International

24 Naeem M. T., Jazayeri S. A., Rezamahdi N., Failure Analysis of Gas *Turbine Blades, Paper 120, ENG 108, Proceedings of The 2008 IAJC-IJME International Conference ISBN 978-1-60643-379-9*

25 Wallis, A. R. (1983). *Axial Flow Fans and Ducts*. John Willey & Sons.

26 Sorensen D.N. (2000), *Towards Improved Rotor-Only Axial Fans-Part I: A Numerically Efficient Aerodynamic Model for Arbitrary Vortex Flow,* Transactions of the ASME Vol. 122, June 2000

27 Dixon S. L. (1998), *Fluid Mechanics and Thermodynamics of Turbomachinery (4th Edition),Elsevier*

APPENDIX “A”. Design2 Data

Table 1 Final Rotor Blade Design (Design2)

	HUB									TIP
DIAMETER	0.416	0.459	0.501	0.544	0.587	0.629	0.672	0.715	0.757	0.800
S/C	0.77	0.90	1.04	1.17	1.30	1.44	1.57	1.70	1.84	1.97
a1	60.36	62.70	64.72	66.48	68.03	69.39	70.60	71.67	72.64	73.52
a2	46.43	52.37	56.86	60.37	63.18	65.48	67.39	69.02	70.42	71.64
tanam= (tana1+tana2)/2	1.40	1.62	1.82	2.03	2.23	2.43	2.62	2.81	3.01	3.20
tanζ=tanam -0.15	1.25	1.47	1.67	1.88	2.08	2.28	2.47	2.66	2.86	3.05
ζ (rad)	0.90	0.97	1.03	1.08	1.12	1.16	1.19	1.21	1.23	1.25
STAGGER	51.44	55.73	59.16	61.97	64.30	66.27	67.96	69.42	70.70	71.82
CAMBER(0.5-0.31*(S/C)^(1/3))	27.85	22.05	18.30	15.91	14.42	13.58	13.22	13.22	13.52	14.10
β1=2θ+ζ	65.36	66.75	68.31	69.92	71.51	73.06	74.57	76.03	77.46	78.87
incidence i= (a1-β1)	-5.00	-4.05	-3.59	-3.44	-3.49	-3.68	-3.97	-4.36	-4.82	-5.36
β2=β1-θ	37.51	44.70	50.01	54.01	57.09	59.48	61.35	62.81	63.94	64.78
deviation δ=α2-β2	8.92	7.67	6.85	6.35	6.09	5.99	6.04	6.21	6.48	6.86
deflection e =a1-a2	13.93	10.33	7.86	6.12	4.85	3.91	3.20	2.65	2.22	1.88
am (rad) =	0.95	1.02	1.07	1.11	1.15	1.18	1.21	1.23	1.25	1.27
am (deg) =	54.54	58.27	61.28	63.75	65.83	67.59	69.11	70.43	71.60	72.63
Cl (from Osbourne) = 2*S/C*(tana1-tana2)*cosam	0.63	0.61	0.58	0.56	0.53	0.51	0.49	0.47	0.45	0.43
CHORD (mm)	0.155	0.145	0.138	0.133	0.129	0.125	0.122	0.120	0.118	0.116

Table 2 Stator Vane Design (Design2)

	HUB									TIP
DIAMETER	0.416	0.459	0.501	0.544	0.587	0.629	0.672	0.715	0.757	0.800
a3	35.23	32.64	30.37	28.37	26.60	25.03	23.62	22.35	21.20	20.17
a3 (rad)	0.61	0.57	0.53	0.50	0.46	0.44	0.41	0.39	0.37	0.35
a4	3.00	2.00	1.00	0.00	0.00	0.00	0.00	0.00	0.00	0.00
a4 (rad)	0.05	0.03	0.02	0.00	0.00	0.00	0.00	0.00	0.00	0.00
tanam= (tana3+tana4)/2	0.38	0.34	0.30	0.27	0.25	0.23	0.22	0.21	0.19	0.18
tanζ=tanam -0.15	0.23	0.19	0.15	0.12	0.10	0.08	0.07	0.06	0.04	0.03
ζ (rad)	0.23	0.19	0.15	0.12	0.10	0.08	0.07	0.06	0.04	0.03
STAGGER	12.92	10.63	8.63	6.84	5.73	4.77	3.92	3.18	2.52	1.93
CHORD	0.13	0.13	0.13	0.13	0.13	0.13	0.13	0.13	0.13	0.13
S=	0.10	0.11	0.12	0.13	0.14	0.15	0.16	0.17	0.18	0.19
S/C=	0.76	0.84	0.92	0.99	1.07	1.15	1.23	1.31	1.38	1.46
CAMBER	50.29	44.38	39.75	36.14	31.02	26.58	22.70	19.26	16.22	13.49
β1=ζ+θ/2	38.06	32.82	28.51	24.92	21.25	18.06	15.27	12.81	10.63	8.67
i=a3-β1	-2.83	-0.18	1.87	3.46	5.36	6.97	8.34	9.54	10.58	11.49

Table 3 Rotor data for Design2

SECTION	1.00	**2.00**	3.00	**4.00**	5.00	**6.00**	7.00	**8.00**	9.00	**10.00**
CAMBER	27.85	**22.05**	18.30	**15.91**	14.42	**13.58**	13.22	**13.22**	13.52	**14.10**
CHORD	0.155	**0.145**	0.138	**0.133**	0.129	**0.125**	0.122	**0.120**	0.118	**0.116**
DIAMETER	0.42	**0.46**	0.50	**0.54**	0.59	**0.63**	0.67	**0.71**	0.76	**0.80**
STAGGER	51.44	**55.73**	59.16	**61.97**	64.30	**66.27**	67.96	**69.42**	70.70	**71.82**

Table 4 Stator data for Design2

SECTION	1.00	**2.00**	3.00	**4.00**	5.00	**6.00**	7.00	**8.00**	9.00	**10.00**
CAMBER	-50.29	**-44.38**	-39.75	**-36.14**	-31.02	**-26.58**	-22.70	**-19.26**	-16.22	**-13.49**
CHORD	0.132	**0.132**	0.132	**0.132**	0.132	**0.132**	0.132	**0.132**	0.132	**0.132**
DIAMETER	0.416	**0.459**	0.501	**0.544**	0.587	**0.629**	0.672	**0.715**	0.757	**0.800**
STAGGER	-12.92	**-10.63**	-8.63	**-6.84**	-5.73	**-4.77**	-3.92	**-3.18**	-2.52	**-1.93**

Table 5 Final Stator Vane Design (Design2) (optimized)

	HUB									TIP
DIAMETER	0.416	0.459	0.501	0.544	0.587	0.629	0.672	0.715	0.757	0.800
a3	35.23	32.64	30.37	28.37	26.60	25.03	23.62	22.35	21.20	20.17
a3 (rad)	0.61	0.57	0.53	0.50	0.46	0.44	0.41	0.39	0.37	0.35
a4	3.00	2.00	1.00	0.00	0.00	0.00	0.00	0.00	0.00	0.00
a4 (rad)	0.05	0.03	0.02	0.00	0.00	0.00	0.00	0.00	0.00	0.00
tanam= (tana3+tana4)/2	0.38	0.34	0.30	0.27	0.25	0.23	0.22	0.21	0.19	0.18
tanζ=tanam -0.15	0.23	0.19	0.15	0.12	0.10	0.08	0.07	0.06	0.04	0.03
ζ (rad)	0.23	0.19	0.15	0.12	0.10	0.08	0.07	0.06	0.04	0.03
STAGGER	12.92	10.63	8.83	7.44	6.83	6.27	5.82	5.48	5.12	4.73
CHORD	0.13	0.13	0.13	0.13	0.13	0.13	0.13	0.13	0.13	0.13
S=	0.10	0.11	0.12	0.13	0.14	0.15	0.16	0.17	0.18	0.19
S/C=	0.76	0.84	0.92	0.99	1.07	1.15	1.23	1.31	1.38	1.46
CAMBER	50.29	44.38	40.67	38.91	36.09	33.49	31.44	29.86	28.19	26.39
β1=ζ+θ/2	38.06	32.82	29.17	26.90	24.88	23.01	21.55	20.41	19.21	17.92
i=a3-β1	-2.83	-0.18	1.21	1.47	1.72	2.01	2.07	1.94	1.99	2.25

Table 6 Verification of Design2

Rotor mesh (thousands elements)	Stator mesh size (thousands elements)	Total Pressure Rise (Pa)
56.5	58.7	**526**
113.8	117.3	**530**
236.9	238.2	**532**
461.6	463.5	**534**

APPENDIX "B". Design3 Data

Table 1 Final Rotor Blade Design (Design3)

	HUB									TIP
DIAMETER	**0.384**	**0.430**	**0.476**	**0.523**	**0.569**	**0.615**	**0.661**	**0.708**	**0.754**	**0.800**
S/C	0.65	0.77	0.90	1.03	1.16	1.28	1.41	1.54	1.67	1.79
a1	58.92	61.72	64.09	66.12	67.86	69.38	70.71	71.89	72.93	73.87
a2	42.67	50.21	55.67	59.78	62.97	65.53	67.63	69.38	70.86	72.14
tanam= (tana1+tana2)/2	1.29	1.53	1.76	1.99	2.21	2.43	2.64	2.86	3.07	3.28
tanζ=tanam -**0.15**	1.14	1.38	1.61	1.84	2.06	2.28	2.49	2.71	2.92	3.13
ζ (rad)	0.85	0.94	1.02	1.07	1.12	1.16	1.19	1.22	1.24	1.26
STAGGER	**48.76**	**54.07**	**58.18**	**61.44**	**64.10**	**66.30**	**68.15**	**69.73**	**71.09**	**72.28**
CAMBER	**30.34**	**22.59**	**17.81**	**14.85**	**13.06**	**12.03**	**11.52**	**11.41**	**11.59**	**12.01**
(0.5-0.31*(S/C)^(1/3))										
β1=2θ+ζ	63.92	65.37	67.08	68.87	70.63	72.31	73.91	75.43	76.89	78.29
incidence i= (a1-β1)	-5.00	-3.64	-2.99	-2.75	-2.76	-2.93	-3.20	-3.54	-3.95	-4.42
β2=β1-θ	33.59	42.77	49.28	54.02	57.57	60.28	62.39	64.02	65.30	66.27
deviation δ=α2-β2	9.08	7.44	6.39	5.76	5.40	5.25	5.24	5.35	5.56	5.86
deflection e =a1-a2	16.25	11.51	8.42	6.34	4.89	3.85	3.09	2.51	2.07	1.73
am (rad) =	0.91	0.99	1.05	1.10	1.15	1.18	1.21	1.23	1.26	1.27
am (deg) =	52.23	56.83	60.42	63.29	65.65	67.61	69.28	70.71	71.95	73.04
Cl (from Osbourne) = 2*S/C*(tana1-tana2)*cosam	0.58	0.56	0.53	0.50	0.47	0.45	0.43	0.41	0.39	0.37
CHORD	**0.170**	**0.159**	**0.151**	**0.145**	**0.140**	**0.137**	**0.134**	**0.131**	**0.129**	**0.127**

Table 2 Final Stator Vane Design (Design3)

	HUB									TIP
DIAMETER	0.384	0.430	0.476	0.523	0.569	0.615	0.661	0.708	0.754	0.800
a3	36.41	33.36	30.73	28.45	26.47	24.72	23.18	21.81	20.59	19.49
a3 (rad)	0.64	0.58	0.54	0.50	0.46	0.43	0.40	0.38	0.36	0.34
a4	3.00	2.00	1.00	0.00	0.00	0.00	0.00	0.00	0.00	0.00
a4 (rad)	0.05	0.03	0.02	0.00	0.00	0.00	0.00	0.00	0.00	0.00
tanam= (tana3+tana4)/2	0.39	0.35	0.31	0.27	0.25	0.23	0.21	0.20	0.19	0.18
tanζ=tanam -0.15	0.24	0.20	0.16	0.12	0.10	0.08	0.06	0.05	0.04	0.03
ζ (rad)	0.24	0.19	0.15	0.12	0.10	0.08	0.06	0.05	0.04	0.03
STAGGER	13.76	11.12	9.26	7.70	7.05	6.49	5.97	5.57	5.17	4.75
CHORD	0.139	0.139	0.139	0.139	0.139	0.139	0.139	0.139	0.139	0.139
S=	0.13	0.15	0.16	0.18	0.19	0.21	0.22	0.24	0.25	0.27
S/C=	0.94	1.05	1.16	1.27	1.39	1.50	1.61	1.72	1.84	1.95
CAMBER	51.25	44.08	40.32	37.84	35.02	32.55	30.29	28.55	26.79	24.95
β1=ζ+θ/2	39.39	33.16	29.42	26.61	24.56	22.76	21.12	19.85	18.57	17.22
i=a3-β1	-2.98	0.19	1.30	1.84	1.91	1.96	2.07	1.97	2.03	2.27

Table 3 Rotor data for Design3

SECTION	1	**2**	3	**4**	5	**6**	7	**8**	9	**10**
CAMBER	30.34	**22.59**	17.81	**14.85**	13.06	**12.03**	11.52	**11.41**	11.59	**12.01**
CHORD	0.170	**0.159**	0.151	**0.145**	0.140	**0.137**	0.134	**0.131**	0.129	**0.127**
DIAMETER	0.384	**0.430**	0.476	**0.523**	0.569	**0.615**	0.661	**0.708**	0.754	**0.800**
STAGGER	48.76	**54.07**	58.18	**61.44**	64.10	**66.30**	68.15	**69.73**	71.09	**72.28**

Table 4 Stator data for Design3

SECTION	1	**2**	3	**4**	5	**6**	7	**8**	9	**10**
CAMBER	-51.25	**-44.08**	-40.32	**-37.84**	-35.02	**-32.55**	-30.29	**-28.55**	-26.79	**-24.95**
CHORD	0.139	**0.139**	0.139	**0.139**	0.139	**0.139**	0.139	**0.139**	0.139	**0.139**
DIAMETER	0.384	**0.430**	0.476	**0.523**	0.569	**0.615**	0.661	**0.708**	0.754	**0.800**
STAGGER	-13.76	**-11.12**	-9.26	**-7.70**	-7.05	**-6.49**	-5.97	**-5.57**	-5.17	**-4.75**

APPENDIX “C”, Tip Clearance Effect

Performance comparison of new Designs with nominal tip clearance (1.5%) and high tip clearance (3%)

Tip Clearance effect for Design1

Volume Flow vs Efficiency

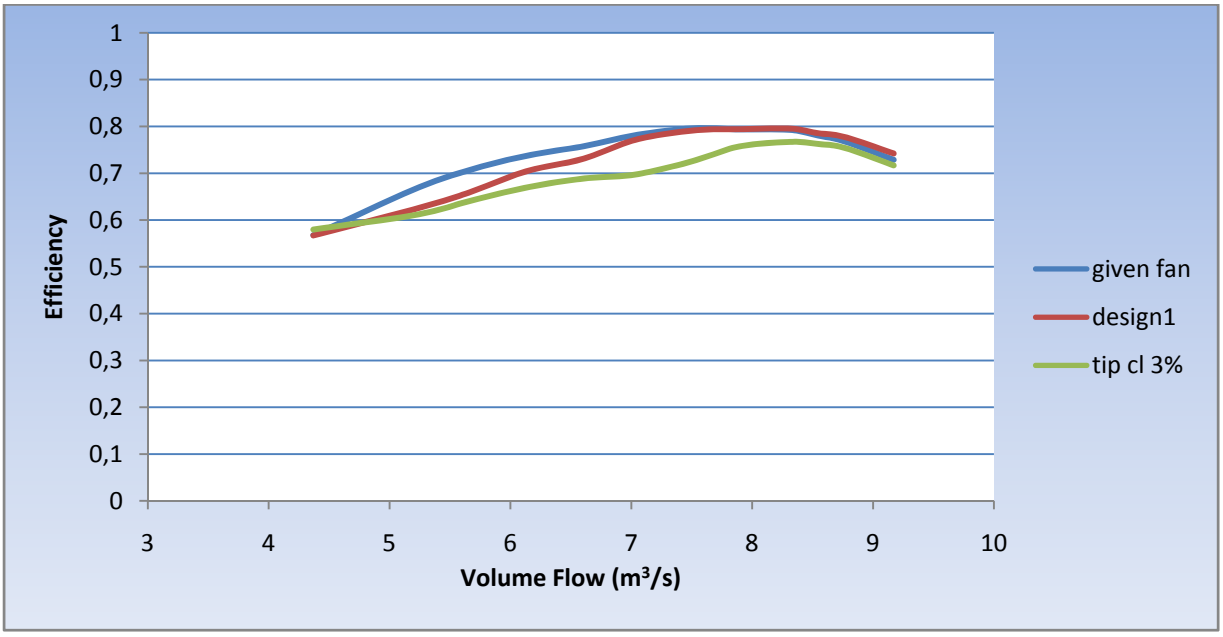

Volume Flow vs Total Pressure rise

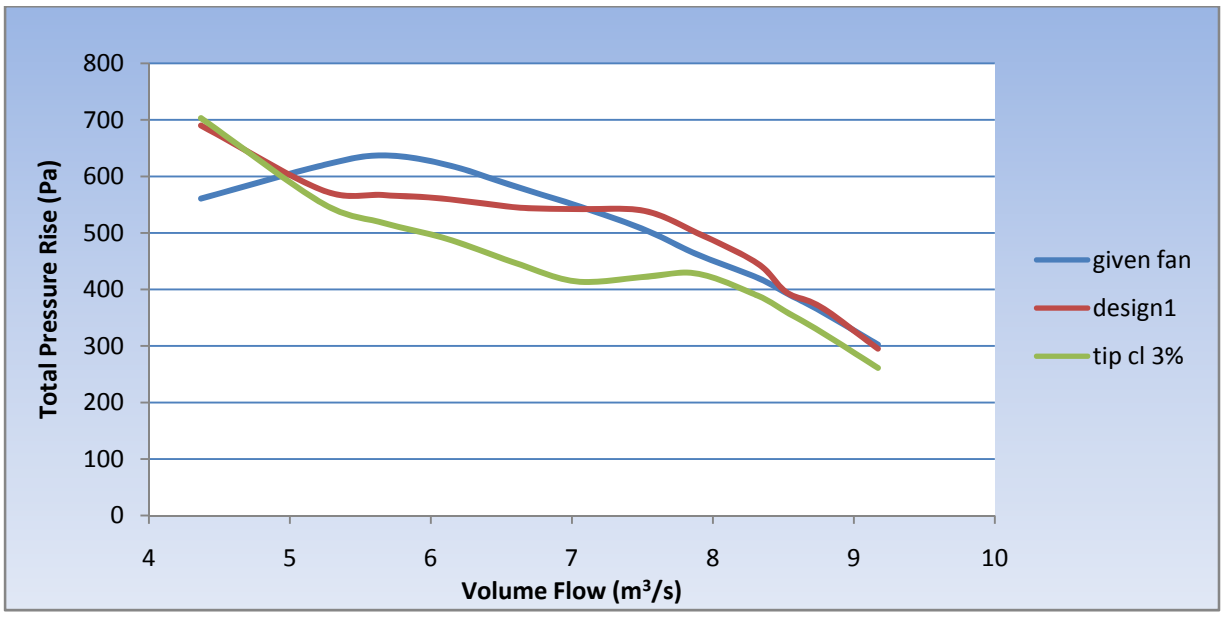

Tip Clearance effect for Design 2

Volume Flow vs Efficiency

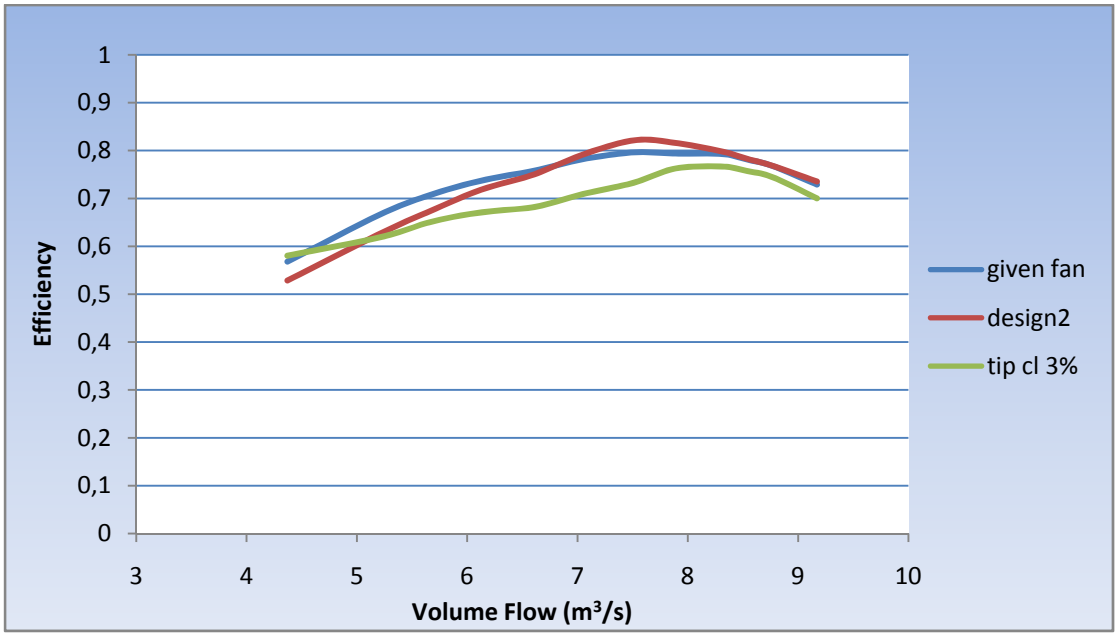

Volume Flow vs Total Pressure rise

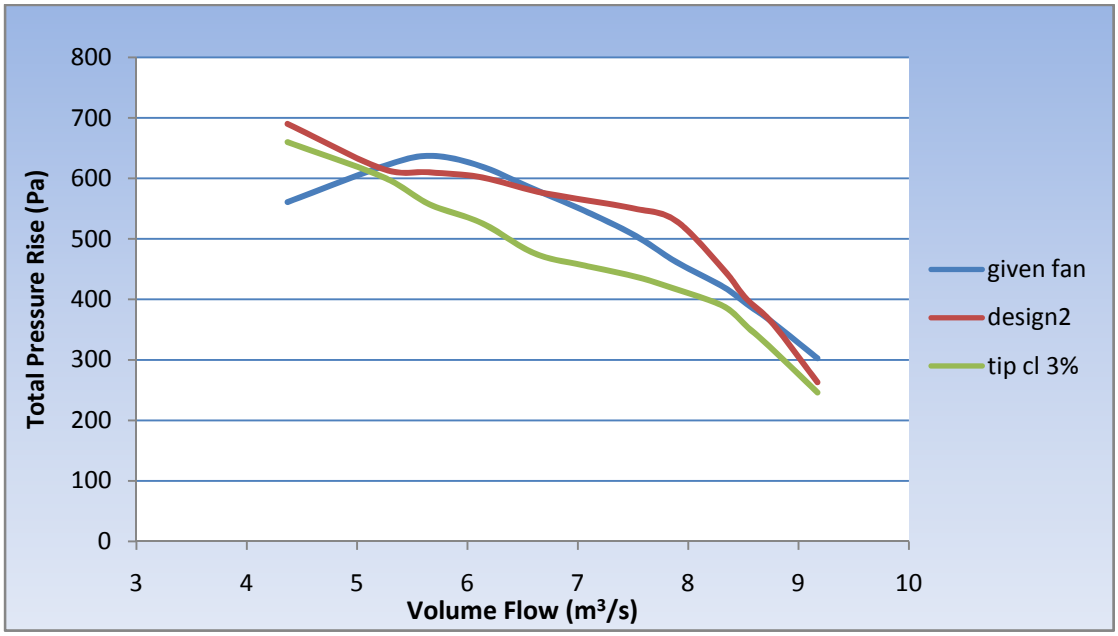

Tip Clearance effect for Design3

Volume Flow vs Efficiency

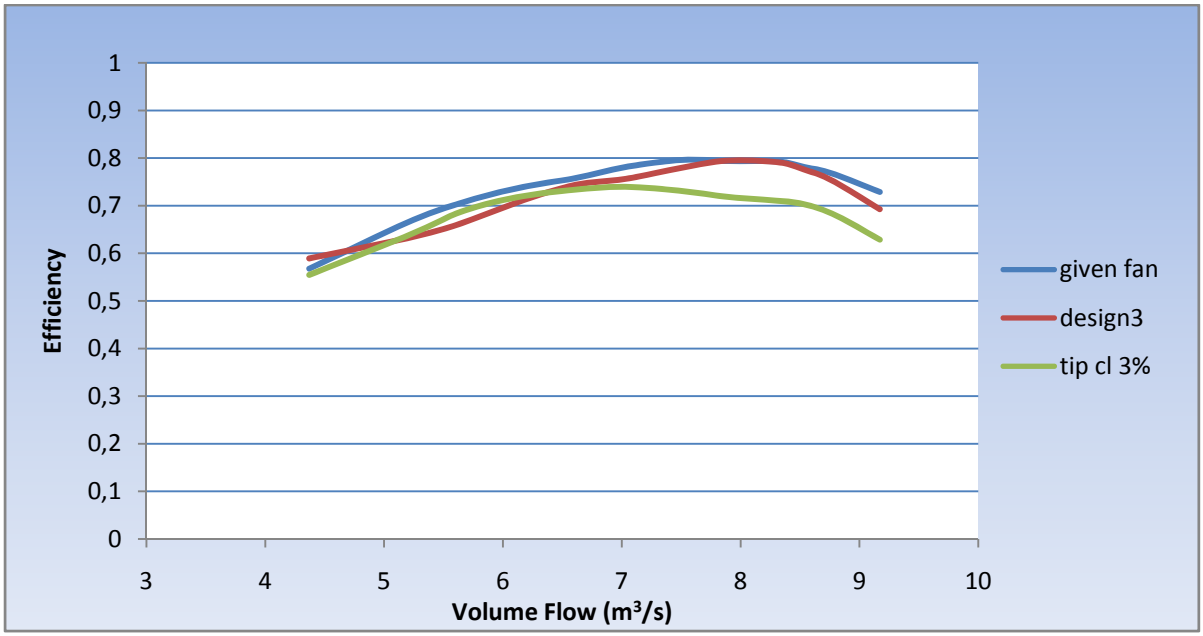

Volume Flow vs Total Pressure rise